Control of a Hydraulically Actuated Mechanism Using a Proportional Valve and a Linearizing Feedforward Controller

A Thesis Submitted to the
College of Graduate Studies and Research
in Partial Fulfillment of the Requirements
for the Degree of Doctor of Philosophy
in the Department of Mechanical Engineering,
University of Saskatchewan, Saskatoon
Canada

By
Jeffery William Dobchuk
August 2004

Permission to Use

In presenting this thesis in partial fulfillment of the requirements for a Postgraduate degree from the University of Saskatchewan, I agree that the Libraries of this University may make it freely available for inspection. I further agree that the permission for copying this thesis in any manner, in whole or in part for scholarly purposes, may be granted by the professors who supervised my work or, in their absence, by the Head of the Department or Dean of the College in which my thesis work was conducted. It is understood that any copying or publication or use of this thesis or parts thereof for financial gain shall not be allowed without my written permission. It is also understood that due recognition shall be given to me and to the University of Saskatchewan in any scholarly use which may be made of any material in my thesis.

Requests for permission to copy or to make other use of material in this thesis, in whole or part, should be addressed to:

Head, Department of Mechanical Engineering
University of Saskatchewan
College of Engineering
57 Campus Drive
Saskatoon, Saskatchewan, S7N 5A9
Canada

Acknowledgements

I would like to acknowledge the invaluable contributions, both technical and financial, of my supervisors, Dr. R.T. Burton and Dr. P.N. Nikiforuk. The technical assistance of Mr. D.V. Bitner is also gratefully acknowledged.

I would also like to acknowledge the financial contribuations made by the Department in the form of Graduate Teaching Fellowships.

The love and support of my parents, Jim and Bonnie, was a vital component in the completion of this thesis. So too was the advice and friendship of all who passed through the Fluid Power Lab. A short message to you all:
Thanks

Dedication

I would like to dedicate this thesis to my wife Bonnie. Without her support none of this would have been possible. She has my eternal love, gratitude and admiration.

Abstract

A common problem encountered in mobile hydraulics is the desire to automate motion control functions in a restricted-cost and restricted-sensor environment. In this thesis a solution to this problem is presented. A velocity control scheme based on a novel single component pressure compensated flow controller was developed and evaluated.

The development of the controller involved solving several distinct technical challenges. First, a model reference control scheme was developed to provide control of the valve spool displacement for a particular electrohydraulic proportional valve. The control scheme had the effect of desensitizing the transient behaviour of the valve dynamics to changes in operating condition. Next, the pressure/flow relationship of the same valve was examined. A general approach for the mathematical characterization of this relationship was developed. This method was based on a modification of the so-called turbulent orifice equation. The general approach included a self-tuning algorithm. Next, the modified turbulent orifice equation was applied in conjunction with the model reference valve controller to create a single component pressure compensated flow control device. This required an inverse solution to the modified orifice equation. Finally, the kinematics of a specific single link hydraulically actuated mechanism were solved. Integration of the kinematic solution with the flow control device allowed for predictive velocity control of the single link mechanism.

Contents

List of Figures

Chapter 1

Introduction and Thesis Research Goals

1.1 Electrohydraulic Control of Mobile Hydraulic Applications

The mobile hydraulic equipment industry strives to deliver more features at low cost and with maximum reliability. A major marketing coup in this industry is to deliver features found in more expensive machines in a lower cost model. As an example, consider the John Deere (JD) model 410G front-end loader shown in the photograph in Figure 1.1 and the simplified functional schematic of the same in Figure 1.2.

This implement, and equipment of similar physical configuration (cranes, logging equipment, backhoes, etc.), are referred to collectively hereafter as mobile equipment. For the implement shown in Figures 1.1 and 1.2 it is necessary that the operator have control of the boom and bucket angles, θ_A and θ_B, respectively, through visual feedback. To facilitate this, it is also necessary that the rate of change of these variables, $\dot{\theta}_A$ and $\dot{\theta}_B$, be proportional to an input signal supplied by the operator and that their magnitudes remain invariable in the face of changing operating conditions (load, temperature, and spatial displacement). This requirement is necessary to

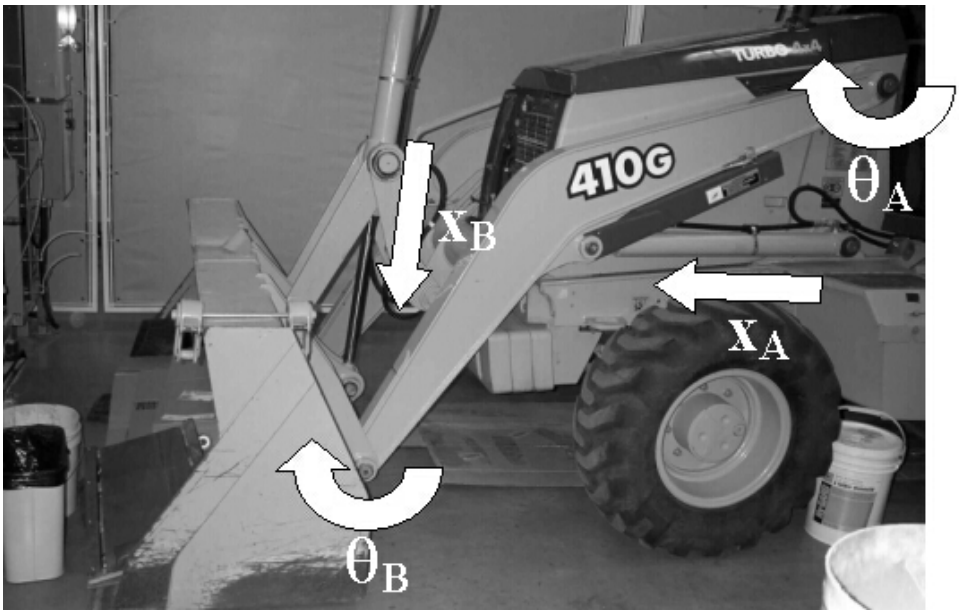

Figure 1.1: Front-end loader implement mounted on a JD 410G.

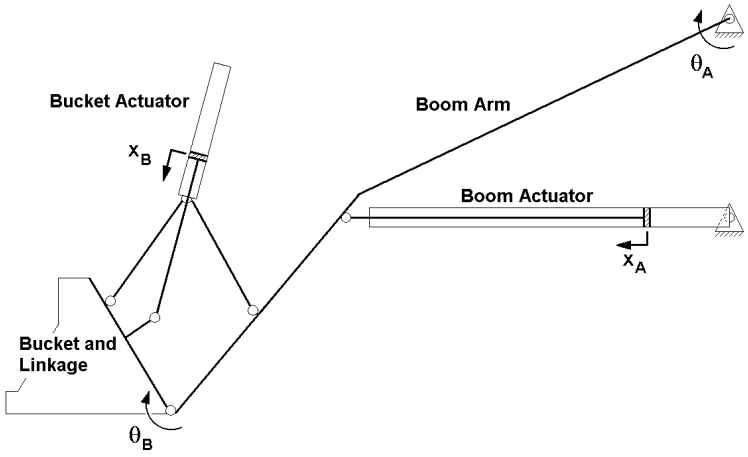

Figure 1.2: Boom arm function for a front-end loader.

produce consistent "feel" for the operator thereby reducing fatigue and improving smoothness of operation.

Currently, these performance requirements are achieved using mechanical feedback. Invariance of the boom and bucket velocities in the face of changing operating conditions is achieved through a combination of linkage design and manually operated, pressure compensated flow control to the actuator. The present system works quite

well with an operator in the loop but the manually operated valves offer little opportunity for function automation.

To understand the problems generated by attempting to introduce automatic functions in the current system, consider the task of *load levelling*. Load levelling is a function in which the bucket angle, θ_B, is automatically reduced so as to keep the load level for large values of boom angle, θ_A. The purpose of this is to prevent the bucket from tipping material onto the hood of the tractor. This is currently accomplished on the JD 410G through a mechanical feedback mechanism which interacts directly with the manually operated valve. The external portion of the feedback system is shown in Figure 1.3.

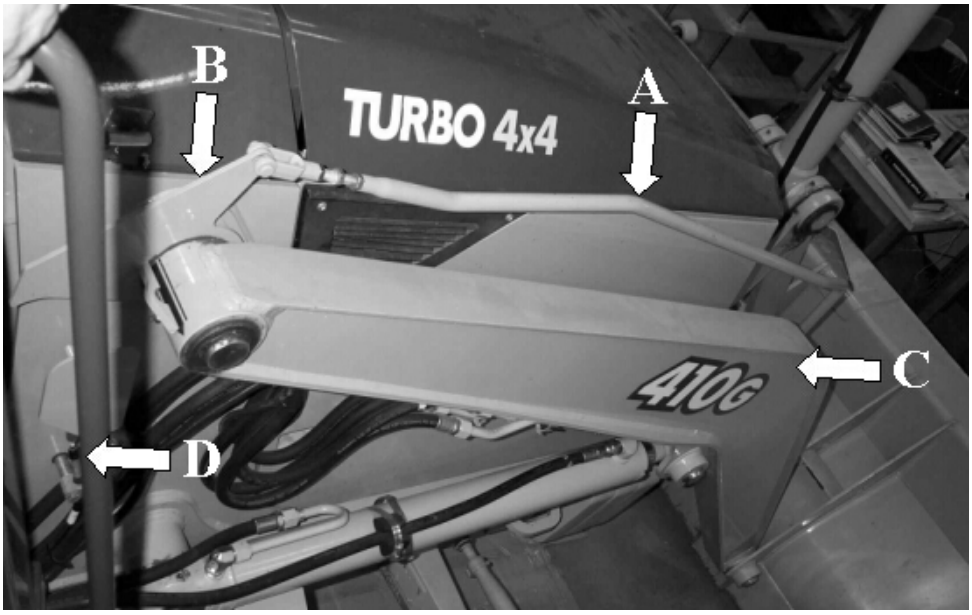

Figure 1.3: Load levelling system on a JD 410G.

In this mechanism a feedback linkage (A) is connected to a cam at B and the bucket linkage at a point hidden behind the boom arm in Figure 1.3 at a position approximated by C. As the boom angle increases (θ_A in Figure 1.1) the cam rotates on its mounting pin. At some fixed angle the cam engages a cable system, the initial portion of which is indicated by D in Figure 1.3. This cable system is attached through a spring to the manually operated control "stick" located in the cab of the

tractor through which it actuates a control valve in order to decrease the angle of the bucket.

During a typical load levelling operation, several key functions are performed. The angular velocity of the boom arms is maintained relative to an operator input by a pressure compensated flow control valve. The relative angular positions of the boom and bucket are sensed by the mechanical feedback system. The angle of the bucket is adjusted by the feedback linkage acting on the bucket tilt manual valve.

This system illustrates the mechanical complexity required for a single automated feature through use of direct mechanical feedback. Ideally, other functions such as "return to dig", task memory, and function planning for minimum energy use would also be available to the consumer. As illustrated by the load levelling example, this is not practical in the current configuration. Although this loader was not used directly in this study, the challenges associated with control of the loader provided the motivation for this project and provided a reference to which the research work could be continuously related.

If it were made practical to automate motion of a system similar to the boom and bucket on the JD410G, then features of more expensive machines could be readily incorporated in lower cost models. To do this requires two very important requirements:

1. The ability to control the flow rate of oil to the hydraulic actuator (and hence the actuator velocity) in the presence of changing loads.

2. Knowledge of the position of the components.

Motion control using an electrohydraulic valve would be an ideal solution to meeting these requirements providing that the additional costs could be kept small and the reliability high. This would require the implementation of electrohydraulic valves and feedback elements relating to the spatial variables and the development of an appropriate control algorithm to achieve the desired function.

To determine the state of research in this area, a detailed literature review on these topics was conducted and the results of this review are presented in the next section.

1.2 Literature Review

The survey of the literature began with an examination of the reported research specific to the automation of mobile equipment similar to that considered in this thesis. The review was made progressively more specific, addressing the research challenges which applied directly to the proposed application. This literature survey was used to compile techniques which were deemed to be useful and to highlight deficiencies in the current body of research as addressed in the research goals presented later in this chapter.

In the remainder of this section, publications from the following general categories are discussed:

1. The velocity and position control of hydraulically actuated mobile equipment (loaders, backhoes, and logging equipment) using electrohydraulic valves.
2. Electrohydraulic control of linkages in non-mobile applications.
3. Modelling and control of electrohydraulic spool valves.
4. Mathematical representations of orifice pressure/flow relationships for spool valves.

1.2.1 Motion Control of Mobile Hydraulically Actuated Systems

There are many examples of the application of electrohydraulic control to mobile hydraulic equipment. One of the most thorough studies was performed by Cobo et al. [1]. They presented a kinematic model of a loader linkage, a dynamic model

for the hydraulic system on a particular loader, and experimental evaluation of the dynamic response of a loader employing their real-time control algorithm.

The hydraulic system on their implement was supplied by a fixed displacement pump and employed open center control valves without pressure compensation. This meant that the angular velocity of the boom arms was a function of the load, valve displacement, and pump flow rate. The authors maintained proportional velocity control with a variable gain PI controller and a "dynamic valve transform" to account for the variation in valve flow due to load changes and engine speed. Their system is illustrated in Figure 1.4.

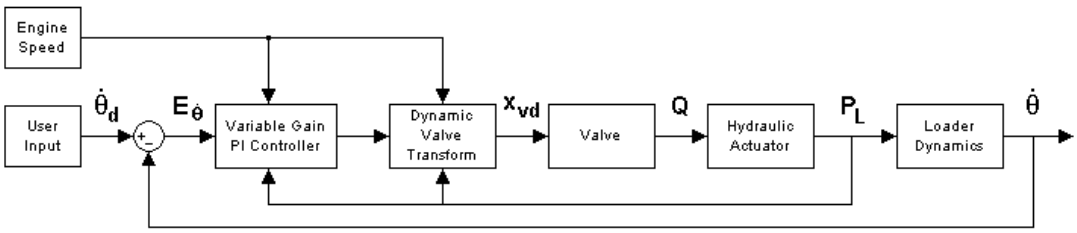

Figure 1.4: Block diagram of the control system investigated by Cobo et al..

The dynamic valve transform was a look-up table generated from experimental data and was used to linearize the steady state characteristics of the valve and actuator for a given operating condition. The valve spool position was operated in the open loop with velocity feedback control in an outer loop. This system required the direct measurement of the velocity of the boom arms. Two of the authors, Cobo and Ingram, performed the work while employed with Caterpillar, Inc. and as a result provided some industry driven guidelines for the performance requirements of mobile equipment.

A second, more straightforward approach was employed by Chen et al. [2]. Their work was based on the supposition that the manually-operated, hydraulically-piloted, proportional control valves currently installed on a particular loader worked quite well for constant velocity control. Their approach was to simply replace the manually-operated pilot stages with electrohydraulic two-way valves. The system

could then be operated remotely by activating the two-way valves using a radio transmitter/receiver. Their system incorporated no feedback control as the system would be operated with visual operator feedback only. This approach was an example of an "add-on" solution. The introduction of the two-way components without replacement of the existing control valve would increase the manufacturing cost, increase the number of components and reduce the reliability.

A study that proved most relevant to the research described in this thesis was that published by Sepehri et al. [3]. This work involved the electrohydraulic control of an excavator and took into account the special considerations encountered in many mobile hydraulic applications. Specifically, the authors addressed velocity control in the presence of variable load and supply pressures. The pressure compensation technique employed calculated the optimum valve spool displacement to achieve a desired flow rate by solving the turbulent orifice equation ("dynamic inversion model") using measurements of the differential pressure across the valve. As with Cobo et al. [1], measurement of the angular velocity was required to achieve closed loop control. Their system is shown in Figure 1.5.

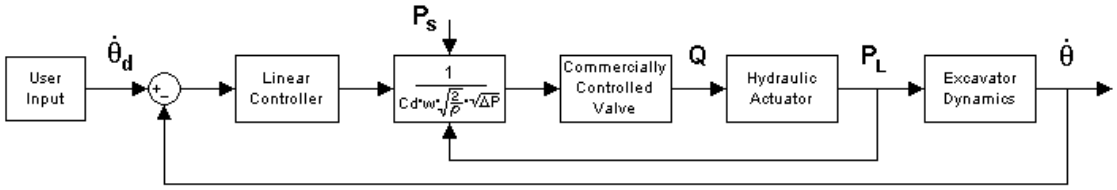

Figure 1.5: Block diagram of the control system introduced by Sepehri et al. [3].

While this technique proved relatively successful, results indicated limited repeatability for changing load conditions. A possible explanation for this was error in the dynamic inversion model, specifically in the simplified valve coefficient modifier used in the turbulent orifice equation. In the opinion of the author of this thesis, this method could be improved with a more accurate approach to modelling the pressure/flow relationship for the valve orifice. Also, the valve in their system was driven by a commercially supplied electronics package. In their paper the design of the con-

troller was not stated, however, if this electronics package used a linear controller for valve displacement (most often the case), some operating condition performance dependencies would inevitably exist. Furthermore, this system was operated in the closed loop with respect to position and velocity. Although not clear in their paper, it was assumed by the author of this thesis that the pressure compensation was designed to linearize the behaviour of the valve rather than produce predictive velocity control as the open loop performance, and hence the accuracy of the turbulent orifice equation linearizing function, was not examined in detail.

All three of the aforementioned research works relied on a combination of linearizing equations in the feedforward path and closed loop velocity feedback control. The matter of velocity feedback is a technical hurdle in the introduction of electrohydraulic motion control to mainstream equipment manufacture due to working conditions which are not conducive to instrumentation. The promising experimental results achieved using linearizing feedforward elements suggested that this type of approach would be appropriate for the system studied for this thesis.

1.2.2 Motion Control of Non-mobile Hydraulically Actuated Systems

Algorithm development and its full integration on a piece of mobile equipment can be a daunting task due to cost, instrumentation, and safety issues. It is more common to perform the research and development in a stationary environment where operating conditions can be more closely monitored. This section summarizes literature pertaining to the control of hydraulically actuated linkages in non-mobile applications.

Gholamreza and Donath [4] recognized that a hydraulically actuated system contains a host of nonlinear elements, thereby making a linear controller ineffective. Furthermore, the authors showed that linearization of the dynamic equations over a small operating range and the design of an appropriate controller for each condition

had limitations in the face of changes to time-variable parameters. Their solution involved the development of a so-called "linearizing feedback controller". A block diagram of this type of controller is shown in Figure 1.6.

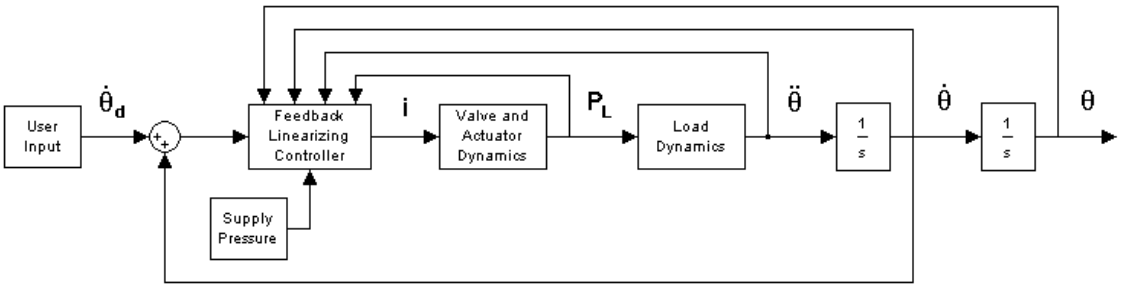

Figure 1.6: Block diagram of the linearizing feedback control strategy investigated by Gholamreza and Donath [4].

The premise was that the linearizing feedback controller prefiltered the operator command signal in such a way as to negate nonlinearities in the parameter variations, geometric relationships, and pressure/flow relations. It was noted by these authors that if the actuator dynamics in this system were much faster than the load dynamics then the derivatives of the angular position, $\dot{\theta}$ and $\ddot{\theta}$, were not necessary for effective control. The portion of the linearizing controller associated with the valve orifice was modelled with the turbulent orifice equation using approximations for coefficients with inherent assumptions based on geometry and flow regime. A limitation of this method was that when the system was operated in the open loop the accuracy was entirely dependent on the accuracy of the linearizing feedback functions within the controller. The authors ultimately compensated for errors in these functions by using another linear controller with velocity feedback in series with the linearizing feedback controller to achieve velocity control. In this configuration the dynamics of the system were dependent on the error between the linearizing model and the actual system as well as the dynamics of the linear controller. Other, more complicated control schemes were suggested, but not tested. The technique was not meant to be used as a predictive method in the absence of feedback, but as an augmentation to a conventional linear full state feedback system.

The approach of Gholamreza and Donath [4] is very similar to that employed by Sepehri et al. [3] which was discussed earlier in this section. Performance in both cases was evaluated with full state feedback so the effectiveness of their linearizing feedforward function was not explicitly evaluated. In particular, the conclusion of Gholamreza and Donath [4], that the higher derivatives of position play a negligible role in the development of a linearizing controller for a large inertial load, was especially valuable to the development of the control strategy in this thesis.

A study of particular interest was that performed by Pietola and Vilenius [5] in which the performance of a model reference control approach (MRC) was compared to that of a proportional controller and a nonlinear proportional-integral-derivative (PID) based controller when applied to the same electrohydraulic system. They found that the MRC provided the most consistent performance in terms of rise time regardless of load. A disadvantage of this approach, however, was that a large amount of detail was required for the reference model. Extensive system identification was performed for their approach to achieve better results than a linear feedback control system. The requirement of an accurate real-time model is especially detrimental to operations where inertia or friction can be time variant. This is a useful approach when the parameters are well understood which is the case for control of the displacement of a valve spool.

The limitations of the approach taken by Pietola and Vilenius [5] arise from the fact that the dynamics of the system are governed by physical quantities which are unknown, uncertain, or time-variant. This type of problem can potentially be solved through the development of an adaptive robust controller. This was the approach taken by Bu and Yao [6],[7] which allowed for mathematical proof of the tracking convergence. Experimental results showed that, under certain operating conditions, using their inertial compensating algorithm resulted in less error for a given trajectory than that which occurred using a linear motion control algorithm. In [7] the authors recognized the role of variable flow gain and introduced a simplified pressure and displacement dependant flow relationship to compensate for this variability when developing their nonlinear model. A disadvantage of the approach reported

in both papers was that synthesizing the control law and calculating the parameter update algorithm were computationally intense. In terms of controller performance, their experimental data did not address the behaviour of their controller in a fast trajectory under high load, a case where the adapted parameters would dominate. As a final note, although their system was designed to compensate for variable inertia, this did not represent the addition or removal of a load during a system cycle. Rather, the system was only meant to compensate for the variation in the equivalent load seen by the hydraulic actuator due to changing gravitational loading of the system over the system stroke. The result was a smooth nonlinearity which was relatively "slow" in the dynamic sense. Stability issues regarding the system behaviour when subject to "fast" operating condition changes were not addressed.

An adaptive control approach was also studied by Guenther et al. [8]. Their work included theoretical and experimental developments, and proof of the stability of their approach using Lyapunov methods. The limitation of their approach, as with most adaptive control strategies, was the dependence on continuous noise-free state feedback.

Motion control of electrohydraulically controlled linkages, in the sense of trajectory tracking, was investigated by Tafazoli et al. [9]. The goal of their study was to reduce disturbance caused by nonlinear friction in the actuators controlled by linear feedback techniques. They designed a nonlinear friction observer which was then used in a nonlinear controller. The method was very useful for decreasing tracking error and "smoothing" response. This method required continuous state feedback in order to compensate for the friction disturbance.

In the first part of the two part study conducted by Edge and de Almeida [10], the control of a system in a dynamically coupled environment was examined. They examined a multiple degree-of-freedom system where more than one actuator was operated from the same supply. Their approach incorporated an adaptive model reference controller as an internal velocity control loop. Variable structure system theory was used to develop the adaptation laws. In the second part of the study,

experimental results employing the developed controller were presented. Some general guidelines on appropriate pole placement for model reference controllers were determined and presented. They also included the development of a dynamic model for electrohydraulic spool valves of a type similar to that used in the research described in this thesis; however, their control system response suffered from variable performance with varying load especially with respect to rise time. The authors claimed that their algorithm should compensate for varying load; therefore, it would be reasonable to assume that the change in response was due to variable valve pressure/flow characteristics. A very useful result from this paper was the theoretical justification for the concept of designing a well controlled velocity inner loop with a simple proportional position control outer loop.

An example of using differential pressure measurements across a valve orifice to achieve pressure compensated flow control in an electrohydraulic system was suggested by Wang et al. [11]. This work was of particular interest as their system was designed to be used on an excavator whose geometry and operating conditions were similar to those of the JD 410G described earlier in this chapter. No information was presented with respect to the function used to relate the flow rate through the valve to the differential pressure measurements across it. Experimental results showed that this approach had the capability of producing smooth performance in the presence of large inertial loads. Flow control was achieved by using two separate valves for the meter-in and meter-out operations. The switching between meter-in and meter-out was controlled by software. The same functionality could be achieved with a single four-way valve performing both the meter-in and meter-out operations.

A more conventional approach was taken by Cheng [12]. For a wood panel pressing operation, the author required the physical robustness offered by a proportional valve as opposed to that of a servovalve. Velocity control in the presence of changing load was also a requirement. The approach employed a proportional flow control valve which had an integrated hydrostat for pressure compensation. The valve suggested by Cheng increases cost and reduces reliability relative to a non-compensated valve. It was shown by Dobchuk et al. [13] that a single orifice whose area is controlled

through use of pressure transducer feedback can perform the same task with software compensation without the need for mechanical compensation in the form of an integrated hydrostat.

The most economical approach to electrohydraulic control encountered in the literature was suggested by Hu and Zhang [14]. They used an array of proportional two-way solenoid valves to achieve position control under several mock system scenarios (open-center or closed-center). While an interesting possibility, the authors only explored position control with a potentiometer in the loop. They did not investigate pressure compensation issues.

Inherent to all the work discussed in this section was some type of kinematic analysis of the linkage to be controlled. The difficulty is that all of these systems contained an actuator which is a translational element and the desired output was a rotation of the linkage. It was therefore necessary to solve the governing geometry so that the two may be related. Hermani and Daneshmend [15] presented a simple yet thorough investigation of the kinematics governing a system which was very similar to that analyzed by the author of this thesis. This paper was used as a model for the development of the kinematic equations presented in this thesis.

Most of the recent work performed on hydraulically actuated linkages has focused on developing some type of adaptive controller. These controllers are meant to compensate in real-time for nonlinear elements such as friction and smooth time-variant load changes. These methods rely on continuous noise-free feedback and are generally computationally intense making them non-ideal for application to low cost mobile equipment. The exception was the work of Gholamreza and Donath [4] who employed a linearizing feedforward element to compensate for nonlinear valve behaviour. This approach does not require the real-time solution of system parameters for synthesis of a control law. The method was similar to several approaches discussed in the previous section, all of which produced encouraging results. All of these approaches, however, relied on closed loop velocity feedback to compensate for errors in the linearizing feedforward elements. Dependence on velocity feedback

could be reduced if sufficient analysis was performed on these linearizing functions to ensure their accuracy. The two main components of the linearizing functions are the valve dynamics and the valve orifice pressure/flow relationship. These two topics are discussed in the following sections.

1.2.3 Modelling and Control of Electrohydraulic Spool Valves

The linear motion control techniques (PID or its derivatives) and adaptive control techniques discussed in the previous section share a common drawback: they all strongly depend on full state feedback. In order to remove this dependence in a system employing a linear feedforward compensator, the linearizing function must be sufficiently accurate to ensure that the system can operate in the absence of feedback for extended durations. This requirement demands the accurate and fast control of the spool motion of the hydraulic valve as well. Material available on the dynamic modelling and control of electrohydraulic valves is extensive. Rather than a comprehensive review of the literature (which would be impractically large) this section highlights works which either:

1. Contain methods or results of particular significance to this thesis.
2. Reflect analysis of commercially available valve controllers.

Lai and Chen [16] developed a method for a self tuning pressure compensating flow controller using a reference model as a predictor of the flow rate. The authors based their adaptive update algorithm on feedback from a flow meter in the loop. Their method was prone to instability and the introduction of a flow meter limited the reliability and system simplicity for mobile applications.

Gholamreza and Donath [4] showed the importance of accurate determination of physical parameters in the modelling of a valve if that model is to be used to investi-

gate dynamic performance. The effect of variations in parameters on the frequency characteristics of the valve were tested using simulation and verified experimentally.

Zavarehi et al. [17] also produced a detailed mathematical model of a spool type valve. The valve used in their study had a solenoid actuated spool primary. The governing equations of motion for the main stage included nonlinear friction and flow force terms. The pilot spool and solenoid were carefully modelled as these were deemed vital to capturing the dynamic characteristics of the valve. Simulation and experimental frequency and step response results were used to validate the model. Their results showed a dependence of the main stage spool response on temperature. This was directly correlated to increased viscosity and a resulting decreased activation pressure from the main stage. This implied that a simple linear controller in the valve spool displacement control loop would not produce repeatable motion control in the presence of variable temperature. The work of Zavarehi et al. [17] highlighted the importance of accurate modelling of the primary stage of a two-stage valve to the overall accuracy of a full valve model.

The research performed by Henri et al. [18] provided a thorough investigation of a primary stage similar in configuration to that on the valve used in the research presented in this thesis. Although their work was based on a pneumatic valve, the underlying principles are equally applicable to hydraulic valves. Their analysis included parameter determination, mathematical modelling and experimental verification of the dynamic performance of a primary stage. Furthermore, methods were introduced for using feed forward control to overcome system nonlinearities, which tend to be exaggerated in pneumatic systems. This paper also contained an excellent summary of the relative contribution of subsystem (primary stage, main stage, and actuator) poles to the overall system dynamics.

A commercially available solution for controlling flow in the presence of variable pressure was introduced by Prasetiawan et al. [19]. They used a valve which is sold under the tradename “valvistor”. This is essentially a two stage pressure compensated poppet style flow control valve. They investigated the performance limitations

of the valve in simulation. The simulation study required the development of a pressure/flow model which was built on the turbulent orifice equation. The limitation of a commercial solution such as this in a design sense is the dependence on a particular valve with resulting loss in flexibility of system design, performance and manufacture.

It has been shown in the literature that fast, accurate control of an electrohydraulic valve is critical to overall dynamic performance of a system. Despite this, an approach to control of a valve spool position is not available which remains portable from manufacturer to manufacturer without extensive analysis of the particular valve and still provides repeatable performance independent of operating condition. Development of such an approach would be a valuable contribution to the field of electrohydraulic motion control.

1.2.4 Orifice Pressure/Flow Relationships for Spool Valves

It was evident from experimental results presented in some of the application oriented works already discussed in this chapter, that along with valve dynamics, a limiting factor on obtaining flow control using differential pressure measurements was the pressure/flow relationship used to determine the valve spool position for a given operating condition. In most cases the relationship used was the turbulent orifice equation.

It has been shown by Viall and Zhang [20] that the turbulent orifice equation employing fixed discharge coefficients may be insufficient. In an experimental method, which shared many traits with that presented by Dobchuk et al. [13], Viall and Zhang [20] showed the variability in the discharge coefficient that can occur with changing geometry and flow regime (laminar or turbulent).

The same conclusion was arrived at by Merritt [21] who developed a Reynolds number dependent discharge coefficient for the turbulent orifice equation. A detailed analysis of the equations governing these types of flows was also conducted by Wu

et al. [22]. They developed a correction factor which, when applied to the turbulent orifice equation, allowed this equation to be extended into the laminar region.

The literature review showed that the characterization of the pressure/flow relationship for an orifice is developed in one of three ways, each of which has its disadvantages. The first method is to apply the turbulent orifice equation without concern for applicability. The second method is to lump the flow characteristics as a nonlinear gain. In the third method, the relationships are developed through detailed and extensive analysis based on careful measurements of orifice geometry. It was concluded by the author of this thesis that development of a straightforward empirical approach to characterizing the pressure/flow relationship for an orifice in a mathematically and numerically compact fashion would be a significant contribution to this field of research.

1.3 Outline of Research Scope

As indicated in the previous sections, Cobo et al. [1], Sepehri et al. [3], and Gholamreza and Donath [4], have had success using a linearizing feedforward controller as part of an electrohydraulic velocity control system. Each of these studies, however, took into account the fact that the linearizing elements used had some degree of error and in each case a linear controller employing velocity feedback was also used to compensate for this error. The requirement for this type of feedback must be removed before the linearizing feedforward approach can be applied to mobile equipment as a harsh working environment does not allow for the addition of external transducers. It is clear as well that some form of feedback would be required to compensate for drift, but a system which could operate under open loop velocity control for extended durations would increase the options for practical indirect instrumentation.

The literature review also indicated that a proportional valve is an appropriate choice for the electrohydraulic velocity control of mobile equipment; however, control of

the valve spool position is critical to the overall system performance. A generic description of the pressure/flow characteristics of the orifice is also desirable such that valves of different configuration could be used interchangeably without *a priori* knowledge of the valve orifice geometry.

Given the above considerations, the approach which was selected for the study reported in this thesis is summarized in Figure 1.7. The parameter to be controlled was the angular velocity, $\dot{\theta}_d$, of a hydraulically actuated arm. Since the relationship between the arm angular velocity and the flow rate to the hydraulic actuator could be determined analytically, the desired angular arm velocity may be transformed into a desired actuator flow rate, Q_d. This desired flow rate, combined with load pressure measurements were "mapped" to a desired valve spool position, x_{vd}. An appropriate closed loop valve spool position controller with the electrohydraulic valve in the loop achieved the desired spool position. The resulting valve spool position created an orifice area which was subject to the load and supply pressures, $P_{1,2}$ and P_s, respectively, resulting in the flow rate, Q, through the valve. The flow rate resulted in an actuator linear velocity that was translated, through the arm kinematics, to an output arm angular velocity. Collectively, the components created a novel linearizing feedforward velocity control system.

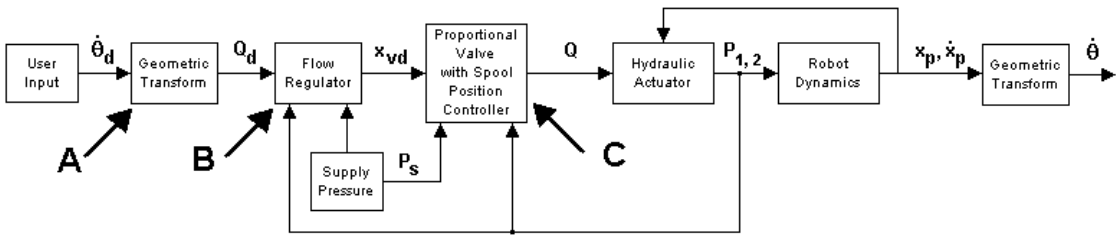

Figure 1.7: Block diagram of a predictive velocity control system.

Critical to the implementation of this velocity control system are:

A. A kinematic relationship between $\dot{\theta}_d$ and Q_d.

B. An accurate relationship between the desired flow rate, the valve spool position,

the supply and load pressure, and the various nonlinear and operating point dependent valve coefficients.

C. A robust controller for the nonlinear proportional valve system to ensure accurate control of the spool position.

As mentioned earlier in the literature review, the feasibility of new control schemes such as that proposed in this thesis, must be established in a controlled environment. Thus, in order to evaluate the performance of the proposed velocity control system, the experimental verification was performed on a laboratory robot shown in Figure 1.8. The robot had similar geometry to that of the JD 410G as can be seen by comparison of Figure 1.8 and Figure 1.1 with the added advantage of tighter control of the operating conditions. The apparatus allowed the load and supply pressure conditions to be tailored to mimic different operational scenarios and provided greater flexibility for instrumentation.

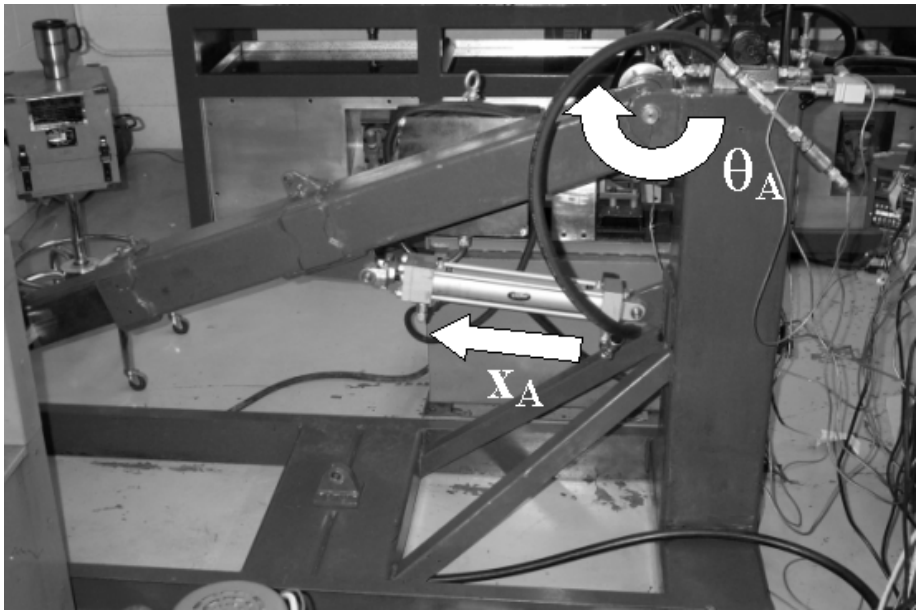

Figure 1.8: The laboratory robot used for development and evaluation.

It was decided that the first stage of the research project was to develop a unique single component pressure compensating flow regulator using a proportional valve.

The development of such a flow regulator would be a major contribution to the advancement of velocity control of such systems as previously discussed and would be one of the original contributions of this study. In the second stage of this research project, the flow regulator was to be coupled to a hydraulically actuated single link mechanism for the purpose of developing a novel open loop linearizing velocity control system.

The next section outlines the specific research goals and steps required to develop a working prototype of the system and to evaluate its performance.

1.4 Research Goals

The objective of this research project was to develop and evaluate a control scheme for the open loop predictive velocity control of a hydraulically actuated single link mechanism. The overall strategy is shown in Figure 1.7. Practical considerations coupled with a review of the literature related to the research project necessitated that the proposed project be divided into the following specific goals representing areas of particular academic interest.

1. Compile a review of literature relevant to the various aspects of the research project.

2. Determine the dynamic characteristics of a two-stage proportional valve with the intent of using this information to develop an accurate and repeatable closed loop valve spool position control scheme.

3. Design a methodology to determine a mathematical relationship which describes the pressure/flow characteristics of a spool valve.

4. Utilize the new equation and the spool position controller to realize a novel single component pressure compensated flow controller and to implement it on a laboratory robot.

5. Develop the kinematics of a single link hydraulically actuated mechanism in order that the developed flow controller may be implemented as an open loop velocity controller.

6. Develop a linearizing feedforward controller and evaluate its performance limitations when used to achieve open loop velocity control of the hydraulically actuated mechanism.

1.5 Organization of this Thesis

The remainder of this thesis is organized into six chapters.

Presented in Chapter 2 is material pertaining to Research Goal #2. Several system identification techniques were employed to determine a model for the dynamic behaviour of a particular proportional valve. A model reference spool position controller based on the system identification was designed and tested.

Chapter 3 contains a description of the work performed in order to achieve Research Goals # 3 and 4. Experimental procedures and apparatus were developed to generate representative pressure/flow/displacement data for the valve. A new empirical form of the the turbulent orifice equation was developed from these data. An optimization routine was employed to reduce the error in the empirical coefficients. The optimized pressure/flow relationship, called the "valve map", was used to predict the flow rate in an environment with variable operating conditions.

The work done to achieve Research Goal #5 is addressed in Chapter 4. It contains the development of the kinematics of the single link mechanism necessary to use the newly developed flow control strategy for the angular velocity control of the mechanism. A mathematical model of the mechanism is presented.

In Chapter 5 the analysis associated with Research Goal #6 is presented. It is a summary of experimental results indicating the performance limitations of the linearizing feedforward velocity control system. The effect of compounding error in

velocity tracking on the prediction of the angular displacement of the robotic arm is also discussed.

Chapter 6 consists of the concluding remarks. It includes a summary of how the Research Goals were achieved and highlights the author's original contributions. Conclusions on the performance of the system are given and the feasibility of using this control approach on mobile equipment is discussed. Finally, comments are made regarding areas which appear promising for future work.

Chapter 2

Physical Description, Operating Characteristics, and Control of a Two-Stage Proportional Valve

Before a motion control system for a hydraulically actuated single link mechanism can be discussed, it is imperative to understand the physical construction and dynamic behaviour of the component which will be acting as the electrohydraulic interface. In the introduction to this thesis the desire to incorporate electrohydraulic control in a cost effective manner was discussed. For this reason the type of valve chosen to be the hydraulic control element in the experimental system discussed in this thesis was a two-stage proportional valve. Among its desirable characteristics are the following:

1. Relatively low cost (compared to servo-valves),
2. Simplicity (no internal mechanical or hydraulic feedback),
3. Relatively low input power requirements,
4. Good bandwidth (>20 Hz),
5. Good linearity (± 5%).

These valves are designed to create a valve spool displacement proportional to the magnitude of an input signal. Control of the valve spool position is often optimized to provide the fastest stable transient response in order to obtain the greatest bandwidth. Linear controllers of this type tend to be sensitive to disturbance inputs generated by the operating conditions of the valve. This variable response is detrimental to a linearizing control strategy where the goal is make the dynamic response of the overall system independent of operating condition. The material discussed in the remainder of this chapter examines the dynamic characteristics of a particular spool valve and uses this information to develop a general valve spool position control system which can be readily adapted to any spool valve. The controller was designed to produce acceptable dynamic response and insensitivity to variable operating conditions such as supply pressure and temperature.

This chapter is organized into four sections. Section 2.1 presents an overview of the physical configuration and function of a two-stage proportional valve and its components. Experimental and simulation analysis leading toward the development and verification of a mathematical model of the valve are presented in Section 2.2. Section 2.3 contains the development of a valve spool displacement control system based on the valve model. Experimental results of the control system are also presented. Section 2.4 is a discussion of the results and conclusions based on material in this chapter.

2.1 Physical Configuration of a Two-Stage Proportional Valve

Control of any electrohydraulic system is made difficult by the inherent complexity of the individual components which make up that system. An electrohydraulic spool valve is no exception. In order to develop a general strategy for valve spool displacement control, a specific valve is examined in detail so that the phenomena affecting spool valve dynamic behaviour can be identified and quantified. Based on

such an analysis, an appropriate general compensator design for spool valves can be developed. The first step in developing an understanding of the dynamic behaviour is to identify the function of each of the major components within the valve used in this study.

The valve is shown schematically in Figure 2.1. The valve is supplied with oil at a supply pressure, P_s. The supply pressure is regulated in the primary stage to a fixed value, P_{ps}, which is used by the primary stage to create a differential pressure $(P_1 - P_2)$ which drives the main stage. The main stage meters flow to and from the rod side and blank side of the hydraulic actuator (not shown), with the return oil directed to the reservoir at atmospheric pressure, P_t.

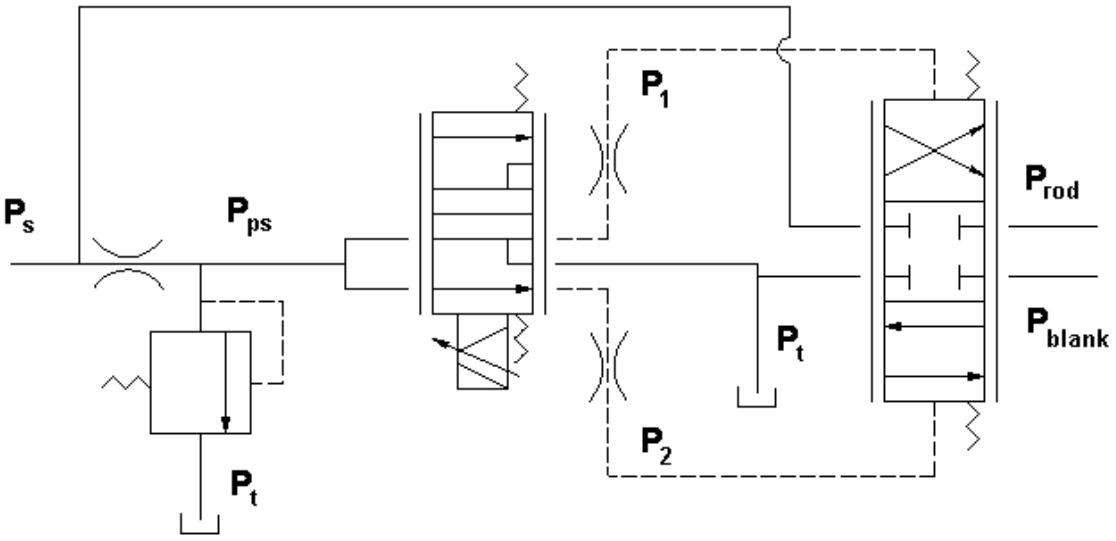

Figure 2.1: Symbolic representation of the components of a two-stage valve.

This valve is termed a "proportional valve" which is a colloquialism for a broad class of electrohydraulic valves with a variety of configurations. The physical configuration of the specific valve used in this research requires the addition of the following descriptors:

1. Spool Type

2. Directional

3. Proportional

4. Two-Stage

5. Electrohydraulic.

The implication of these descriptors with respect to the valve configuration will now be addressed.

2.1.1 Spool Type

The term "spool valve" refers to the shape of the mechanical component which creates the orifice inside the main stage of the valve. The main stage of the valve is that part of the valve which interacts with the overall hydraulic system through a port plate. The location of the valve spool is indicated in Figure 2.2.

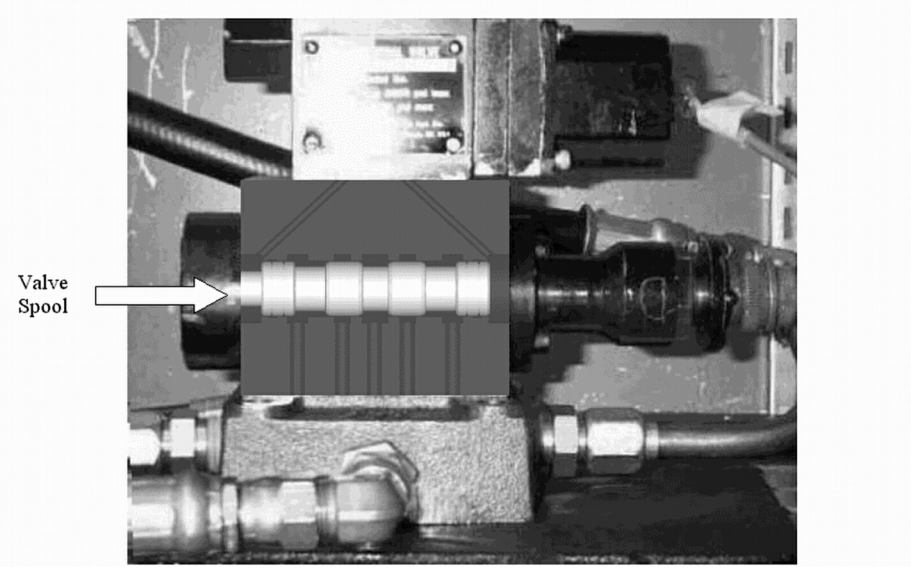

Figure 2.2: Cutaway view of the main stage to show location of valve spool.

It is the purpose of the valve spool to create a metering orifice in the valve. The orifice is created by the clearance between the valve lands (wide parts) and the valve body. This is illustrated by the close-in view of a single land and its position relative to a port machined in the valve body shown in Figure 2.3.

It can be seen in Figure 2.3 that as the spool moves laterally relative to the valve body the area of the annular orifice changes. The mathematical relationship between the orifice size and the lateral spool motion is discussed later in this thesis. The spool is free to slide within the valve body. It is contained at either end by a "return spring", so named because these springs return the spool to the neutral position in the absence of a control signal.

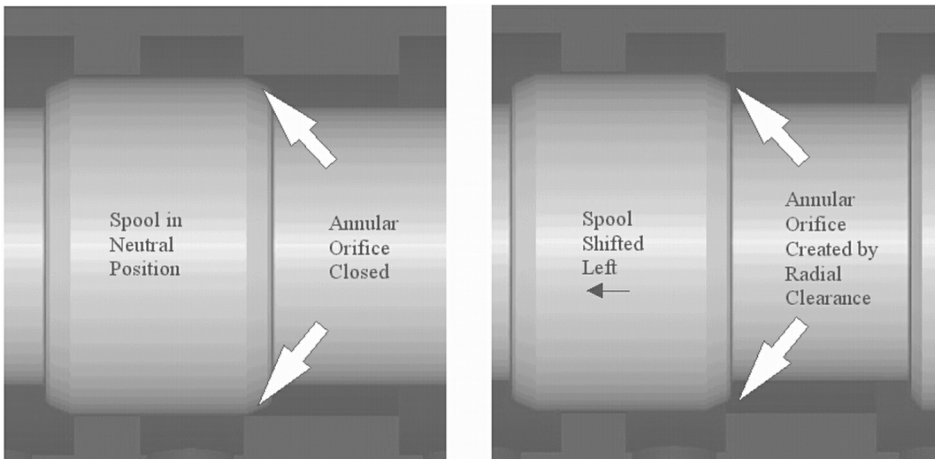

Figure 2.3: Illustration of the metering orifice created by the radial clearance between the spool and the valve body.

The lateral motion of the spool (left or right in Figure 2.2) determines the directional control of the hydraulic system in which the valve is installed.

2.1.2 Directional Control Valve

In Figure 2.3 it is illustrated how the clearance between a single spool land and the valve body creates a metering orifice. A directional control spool valve has multiple lands capable of creating multiple metering orifices. The multiple orifices are arranged to allow for the directional control as illustrated in Figure 2.4

How the spool is moved in the positive or negative direction (orientation is arbitrary and interchangeable) is the subject of the next section.

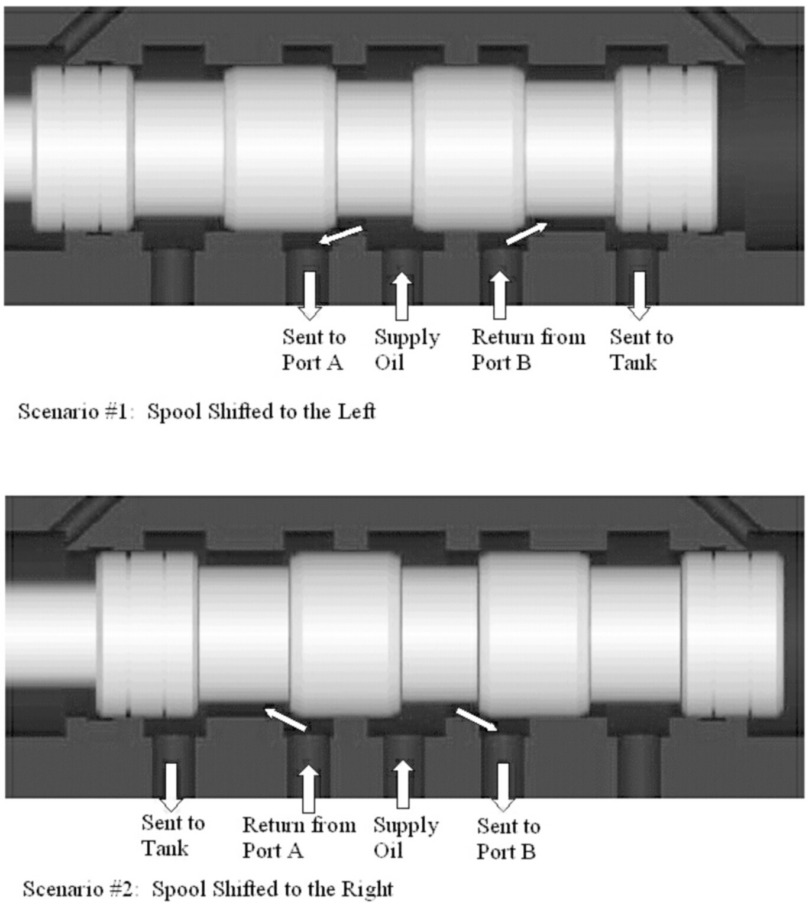

Figure 2.4: Directional control with a spool valve arrangement.

2.1.3 Proportional Valve

Displacement of the valve spool is achieved by applying control forces to the ends of the valve spool which is referred to in this thesis as a differential activation force. The magnitude of the force required to achieve a desired displacement varies with operating condition. Friction, flow forces, and the spring reaction forces must all be overcome before a desired displacement can be achieved.

The term "proportional valve" is applied to valves which achieve a linearly proportional relationship between an input signal and the valve spool displacement. This proportionality is easier to achieve if disturbance forces such as flow forces or friction are negligibly small relative to the return spring forces. In this case, the displacement of the spool in the steady state is governed by the reaction force of the return

springs which increases linearly with the displacement. The various forces acting on the valve spool and their relative amplitudes are discussed in detail in Appendix A and addressed briefly in the next section.

If the force required to displace the valve spool increases linearly with its displacement, then any device capable of linearly transforming a user input to a differential activation force will result in a "proportional valve". This device may be a manually operated lever, a proportional solenoid, or in the case of the valve used in this research, a separate hydraulic system which is termed a "primary stage". The configuration of the primary stage is the subject of the next section.

2.1.4 Two-Stage Valve

Employing a primary stage on a hydraulic valve addresses two issues relating to the valve dynamics. The first is the need for large amplitude activation forces to overcome dynamic disturbance forces. The following phenomena lead to the necessity of large amplitude activation forces in the dynamic sense:

a) Flow forces.

b) Forces arising from accelerating the spool.

The flow forces behave as a nonlinear spring whose spring rate varies with operating condition [21]. Details of the characteristics of flow forces may be found in Appendix A. To combat this, valve manufacturers routinely make the return springs relatively stiff [21]. The prevailing assumption is that the force disturbance introduced by the flow forces will not be dominant when compared to the activation force required to move the spool against the spring. The direct result is that large activation forces are required to work against the return springs which often increases the force requirements out of the range of proportional solenoids for high flow valves.

Large forces arising from the acceleration of the spool are based on the desirability to maintain high bandwidth. The required bandwidth to control hydraulic systems

can exceed 20 Hz [21]. Maintaining this bandwidth is complicated by practical considerations introduced by the physical construction of the valve. That is, in order to achieve physical robustness and appropriate geometry to accommodate large flows, the valve spool is typically quite massive ($\sim$0.3 kg). As a result, the force required to accelerate the spool to achieve reasonable bandwidth is large.

In addition to the need for large amplitude activation forces, a second issue that a two-stage system addresses is force coupling between the driving element (primary stage) and the driven element (main stage). From a control standpoint, it is desirable to impart a force control signal on the spool. If a primary stage device is directly coupled to the main stage, any disturbance force on the main stage will be fed back as a disturbance input to the force control system of the primary for which compensation must be made. In the case of the valve used in this thesis, the solution was to use a force transmission element that was "uni-directional". An analogy to this situation is two components attached by a string. Disturbance forces in compression are not allowed because the the string only transmits force in tension. The device used to implement this uni-directional force transmission was the hydraulic jet primary stage.

The hydraulic jet primary stage employs two fluid jets aimed at two corresponding receiving ports. One such "supply jet/receiving port" pair is illustrated in Figure 2.5.

The linear momentum carried by the fluid passing through the jet becomes a force transmission mechanism. The system is similar to a jet interacting with a fixed surface as discussed by White [24]. In that solution the force applied by an impinging jet for an angle of impingement of 90° is equal to the linear momentum flux of the jet. If the solid surface in the solution of White [24] is replaced by a receiving port, as illustrated in Figure 2.5, then the result is a static pressure at the entrance to the receiving port when mixing effects are neglected.

The hydraulic jet concept illustrated in Figure 2.5 can be employed as a variable force transmission element by the introduction of a diverter to the fluid jet. Since the

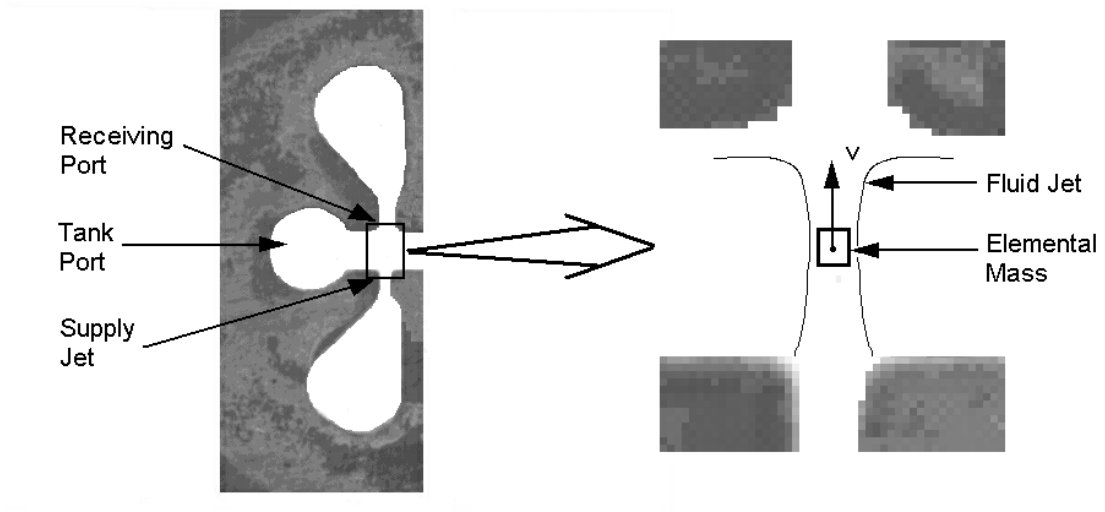

Figure 2.5: Supply jet/receiving port pair.

reactionary force (or static pressure since the receiving port is of constant area) at the receiving port is a function only of the momentum carried by the fluid jet, diverting a portion of the jet will reduce the static pressure by a proportional amount. By adding two jets and two receiving ports, with a single diverter, it is possible to obtain a pressure differential between the two receiving ports that shares a relationship to the diverter displacement. This arrangement is illustrated by the picture of the primary stage port plate shown in Figure 2.6. The notation is the same as that used in Figure 2.1. The pressures, P_1 and P_2, are then ported to either end of the main stage valve spool to produce a differential activation pressure. Diverted jet flow is allowed to leak to tank pressure, P_t.

If the relationship happens to be linear then the hydraulic jet primary stage is a linear device in the sense that output (pressure) is directly proportional to the input (diverter displacement). The means by which the diverter is actuated is the subject of the next section.

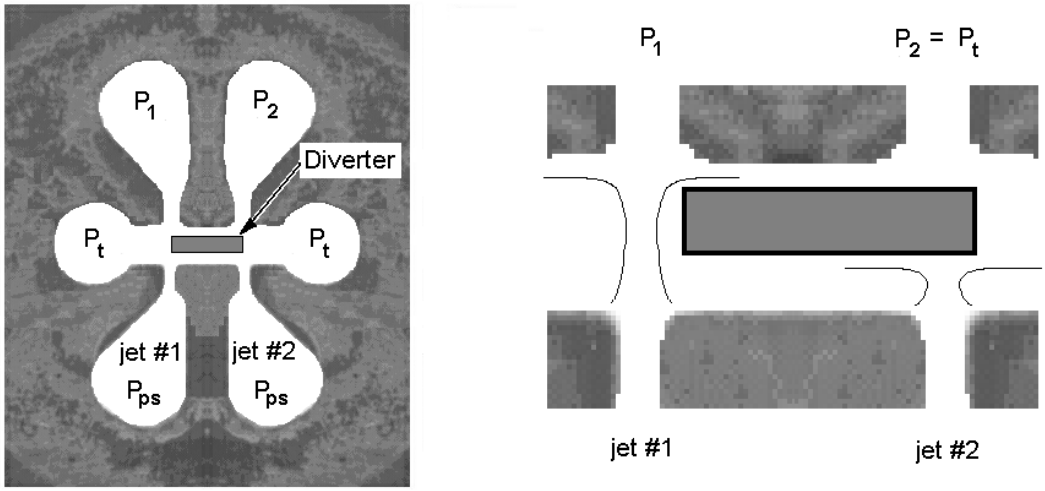

Figure 2.6: (Left) Primary stage with diverter location. (Right) Impingement scenario with diverter shifted fully to the right.

2.1.5 Electrohydraulic Valve

In order to accommodate a hydraulic valve in an electronic control system, the valve must have an electrohydraulic interface. In the valve used in this project that interface is a torque motor that operates the diverter discussed in the previous section. The torque motor assembly is illustrated in Figure 2.7.

The torque motor is a simple electromagnet with a ferrous cantilever as a core. This combination is referred to hereafter as the electromagnetic actuator or "EMA". As the cantilever rotates about the axis shown in Figure 2.7, the result is a linear translation ($tan(\theta) = \theta$ for small angles) at the cantilever tip, x_{ps}. The cantilever mount acts as a spring, and if linear spring properties are assumed, then the tip displacement is proportional to the torque applied by the electromagnet. The torque is linearly related to the strength of the magnetic field created by the magnet and the magnetic field is in turn linearly related to the current through the magnet winding. If the resistance of the coil is constant then it follows that the current is proportional to an applied voltage. The tip displacement is then proportional to the applied voltage and the primary stage satisfies the description of a linear force transmission device.

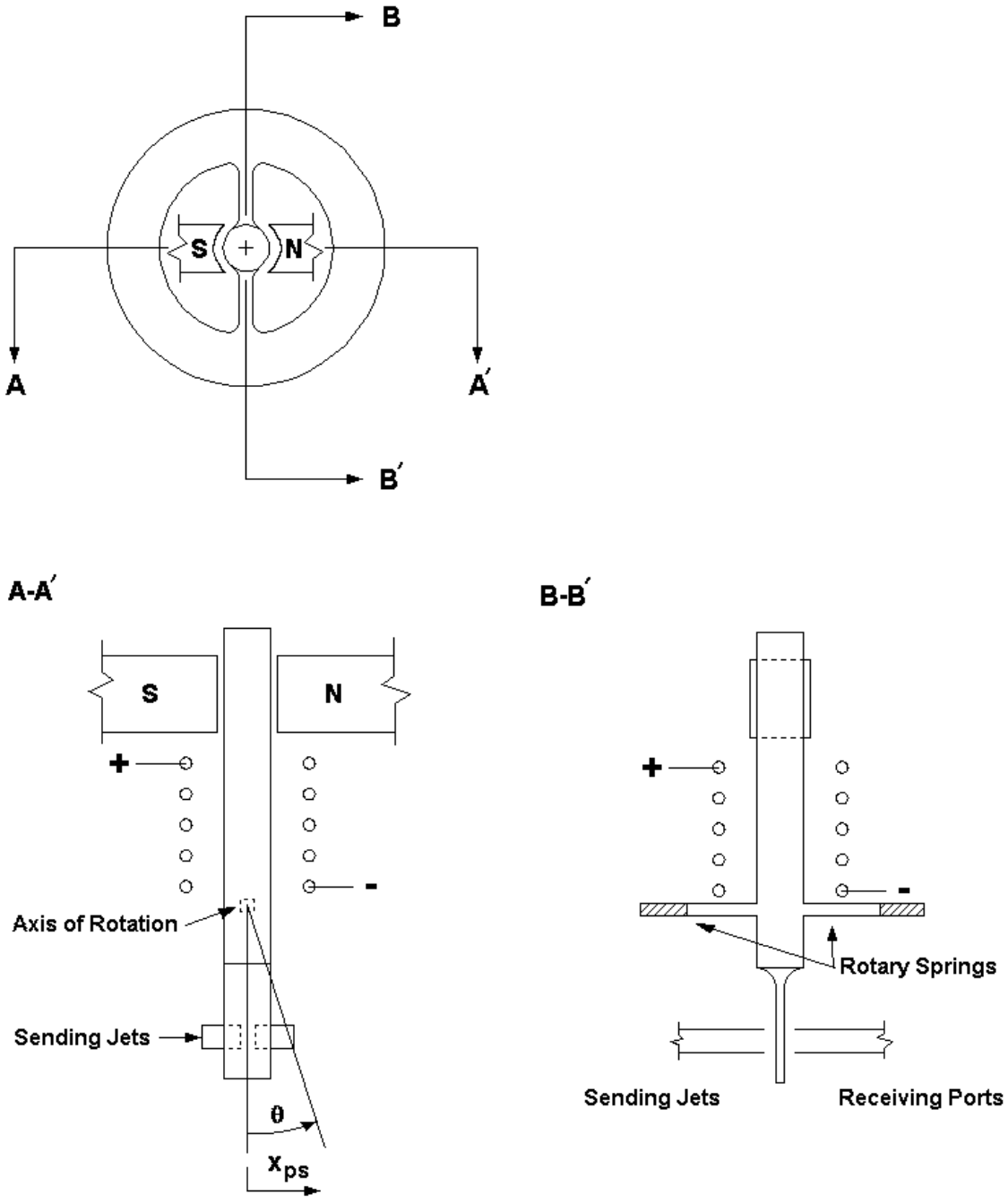

Figure 2.7: Primary stage diverter, electromagnetic torque motor, and rotary spring.

In the next section the operating characteristics of this spool type, directional, proportional, two-stage, electrohydraulic valve will be discussed.

2.2 Operating Characteristics of the Two-Stage Proportional Valve

In the previous section, the physical configuration of an electrohydraulic spool valve was introduced. The function of the components was qualitatively described, and no numerical analysis of their behaviour under operating conditions was presented. This section presents the theoretical background and experimental results which define the operating characteristics of the particular valve used in this research (Parker Model # EHD31VJ1C111 GT) including the:

1. Static behaviour of the primary stage,
2. Dynamic behaviour of the primary stage,
3. Dynamic behaviour of the main stage.

These operating characteristics were used to identify a mathematical model for the valve. This model was necessary for the development of an appropriate controller for the valve. In particular, nonlinearities in the dynamics of the valve were identified and quantified. For the system identification a physical model based approach was taken. In this approach, the physical relationships of the system components were examined, modelled, and then compared to the experimental data to ensure the accuracy of both the model structure and the model parameters. This differs from a "black box" system identification where the input/output relationship of a complex system is analyzed without regard for the underlying physical structure of the system. While the method of physical modelling can be more time consuming, it offers insight into potential control problems and limitations in the final system integration. When developing a physical model of a complex system, it is useful to

examine and characterize individual components and then to assemble a model from these parts. This was the approach used in this research as the primary and main stages were examined separately.

2.2.1 The Static Behaviour of the Primary Stage

The primary stage is intended to be an ideal electrohydraulic interface, accepting an electrical input signal and producing a corresponding hydraulic force on the main stage valve spool. Three experimental procedures were performed to determine the static operating characteristics of the primary stage and to verify the theoretical analysis of the force transfer mechanism of the primary stage. The characteristics of interest were:

a) Force vs. deflector displacement (Static),

b) Voltage vs. deflector displacement (Static) and,

c) Voltage vs. differential activation pressure.

2.2.1.1 Force vs. Deflector Displacement (Static)

As outlined in Section 2.1.4, the primary stage contains a diverter whose purpose is to deflect a portion of the jet from impinging on a receiving port. Thus, a physical relationship of great importance is how the deflector moves laterally for a given input. The torque motor that actuates the diverter is an electrical system whose properties are analyzed in the next section. In this section, only the mechanical properties of the diverter are discussed. To facilitate the analysis of these properties, the diverter was removed from the primary stage and placed in an apparatus capable of the simultaneous measurement of force and displacement. This arrangement is shown schematically in Figure 2.8.

The probe on the test apparatus was built to ensure a point load on the diverter top end. A force was applied to the top end of the diverter and the force and resulting

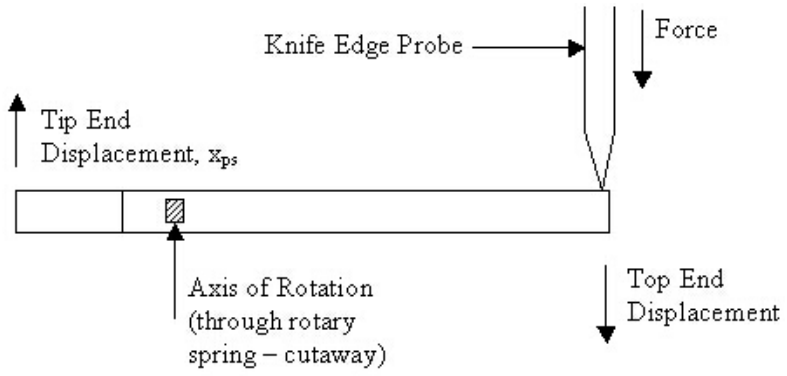

Figure 2.8: Rotary spring test apparatus.

displacement were recorded. During this procedure the velocity of the probe was kept to 0.1 $\frac{mm}{s}$ so as not to excite any system dynamics; hence, the test was considered "static". In addition the displacement of the probe was limited to $\pm$ 1 mm so that the displacement could be considered to be solely in the vertical plane. The results, compiled over three tests, are shown in Figure 2.9. To obtain measurements in the negative direction, the orientation of the rotary spring was reversed. The tip end displacement was calculated using the ratio of the relative distances from the tip and top ends to the axis of rotation.

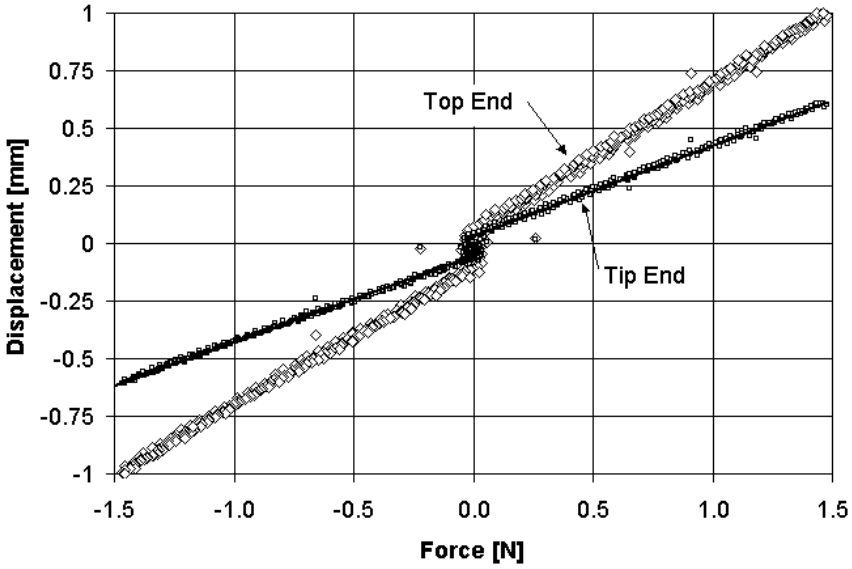

Figure 2.9: Primary stage rotary spring displacement.

The experimental data in Figure 2.9 indicated a linear relationship between the applied force and the cantilever lateral displacement. The offset that exists at zero force was a characteristic of the testing procedure and apparatus control software. Each test was started with the probe manually positioned some small distance from the point of contact with the diverter. Thus, a force threshold was required by the test apparatus control software in order to determine the point of contact and the start of a testing cycle. This threshold was set at the minimum value allowed by the control software at 0.1 N. Thus, displacement was recorded prior to contact, however, the recorded force was zero until the threshold was reached. The bias was removed in the post processing of the data and a linear regression was performed to determine the force/displacement relationship described by:

$$\frac{F}{x_{ps}} = K_p \left[\frac{N}{m}\right], \tag{2.1}$$

where the value of the spring constant, K_p, was 2534 $\frac{N}{m}$ with an R^2 of 0.9918 in the positive direction and 2658 $\frac{N}{m}$ with an R^2 of 0.9888 in the negative direction. The identical value was expected in both directions, however, it is conceivable that the operating history of the valve has resulted in a directionally dependent spring rate. The difference in the two was under 5% indicating a mean of the two was an acceptable assumption for the bi-directional spring constant.

2.2.1.2 Voltage vs. Deflector Displacement (Static)

With the mechanical components of the primary stage tested for linearity and the value of the spring constant determined, the electrical coil was added to the diverter and the static behaviour of the combined mechanism was examined. Of primary interest were the DC gain of the combined mechanism (EMA) and the linearity of the displacement output relative to a voltage input.

Three separate tests were used to verify these relationships. All three involved the input of a fixed voltage using a calibrated voltage source. The difference in the tests was the method used to measure the tip displacement. Initially, calipers were used as

a measuring device, but were found to have an intrusive effect on the measurements which led to uncertainty in the measurements of up to 0.1 mm. This problem arose as the measurements relied on an operator determining the point of contact between the caliper and the diverter tip. To minimize this effect, a micrometer was then employed in a similar fashion. This instrument reduced the uncertainty in the point of contact by half, but the error was still unacceptably large. Finally, a magnification projection table was used. This method was non-intrusive with the only sources of error being slight fuzziness of focus due to the components being out of plane with the light table. The width of the "fuzzy" region was measured and considered to be the margin of measurement error. The results of the three different measurement techniques are presented in Figure 2.10 with the estimated uncertainty indicated with error bars.

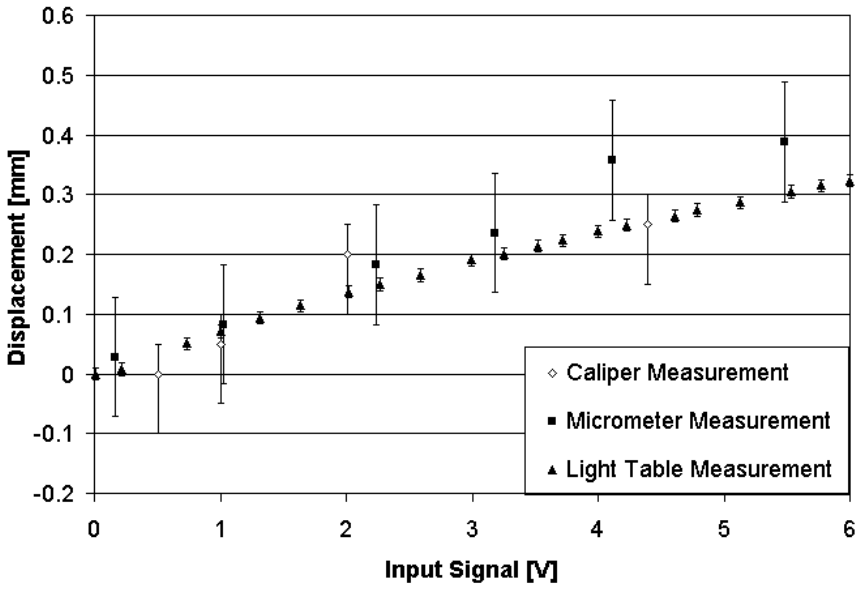

Figure 2.10: Diverter tip displacement versus voltage.

A linear regression was performed on the light table measurements shown in Figure 2.10 and a slope of 0.0578 $\frac{mm}{V}$ was determined with an R^2 value of 0.9802. Since the cantilever spring was found to exhibit linear behaviour (Figure 2.9), and the relation between the voltage and the displacement (Figure 2.10) was also linear, it was concluded that the EMA could be modelled as a fixed voltage-to-force gain,

K_{EMA}, for steady state conditions. The slopes of the regression curves for the data presented in Figure 2.9 and Figure 2.10 were used to determine an EMA gain, K_{EMA}, of 0.15 $\frac{N}{V}$.

It was noted, however, that the force generated by the EMA was related to the current passed through the coil rather than the voltage. The resistance of a copper coil would vary with temperature, so a test was performed to determine the extent of the change over the operating range of the valve. The results of that test are plotted in Figure 2.11 with maximum resolution for temperature and resistance indicated with error bars.

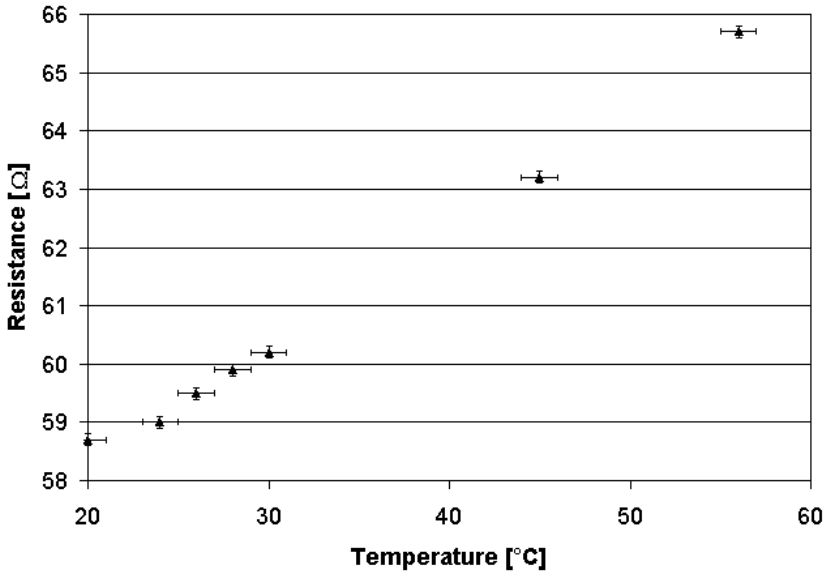

Figure 2.11: Primary stage actuator coil resistance as a function of coil temperature.

The resistance stated by the manufacturer was 60 Ω with no correction for temperature. A linear regression on the data in Figure 2.11 indicated that the temperature affected the resistance at a rate of approximately 0.2 $\frac{\Omega}{^{\circ}C}$ causing an increase of approximately 7 Ω or ∼12% in the range from 20°C to 60°C. While not insignificant, it was decided that it was simpler to compensate for the change in the resistance using the closed loop valve spool displacement control system developed later in this chapter than developing a temperature compensated current driver. In practice, fol-

lowing a brief warm up period, the temperature of the valve tended to be regulated by the oil temperature. Furthermore, as the oil temperature for the tests carried out over the course of the research did not exceed 36°C in the laboratory, the resulting variation in the coil resistance was less than 5%.

The following general observations were drawn from the static deflector displacement tests.

1. The diverter spring had a linear applied force-to-displacement characteristic.
2. The force applied by the electromagnetic actuator was linearly related to an applied voltage as long as the resistance of the coil could be assumed constant.
3. The resistance of the coil showed a ∼5% variance over the range of operating temperatures expected in the valve.
4. The voltage-to-displacement characteristic was linear with the exception of a temperature variance of ∼5% (linear elements in series).

2.2.1.3 Theoretical Analysis of the Diverted Jet Primary Stage

The results presented in Subsections 2.2.1.1 and 2.2.1.2 verified that a linear proportional relationship existed between the applied voltage signal and the tip displacement of the diverter for a wide range of operating conditions. This subsection presents a theoretical development of the fluid momentum transfer across the gap in the primary stage and shows how the diverter is instrumental in turning this momentum transfer into a linear force transfer mechanism by creating a differential activation pressure at the ends of the valve spool.

For the momentum analysis the supply jet/receiving port arrangement shown in Figure 2.5 was examined for the case of a constant primary stage supply pressure, P_{ps}. The supply jet was considered to be a long edged orifice venting to the tank pressure, P_t, which for this analysis was assumed to be 0.69 MPa (100 psi). The first step in the analysis was to determine the flow regime through the supply jet. This

was done by calculating the Reynolds number based on an equivalent orifice throat diameter, Re_d, as the actual jet orifice was rectangular. The Reynolds number based on throat diameter is described by White [24] as,

$$Re_d = \frac{V_t d}{\nu}, \tag{2.2}$$

where:

$$\begin{aligned} d &= \text{Equivalent throat diameter } [m], \\ \nu &= \text{Kinematic viscosity of the oil } \left[\frac{m^2}{s}\right], \end{aligned}$$

and the fluid velocity, V_t, is a function of the volumetric flow rate:

$$V_t = \frac{Q}{A_t}, \tag{2.3}$$

where:

$$\begin{aligned} A_t &= \text{Throat area } \left[m^2\right], \\ Q &= \text{Volumetric flow rate } \left[\frac{m^3}{s}\right]. \end{aligned}$$

Equations 2.2 and 2.3 present a circular argument in that the determination of the Reynolds number requires knowledge of the flow rate which is dependent on the flow regime. The flow regime, of course, is the property characterized by the Reynolds number. As a starting point, the flow was assumed laminar and evaluated using the correlation given by Merritt [21]:

$$Q = \frac{2\delta^2 D_h A_t}{\mu} \left(P_{ps} - P_t\right), \tag{2.4}$$

where:

$$\begin{aligned} D_h &= \text{Hydraulic diameter } [m], \\ \delta &= \text{Laminar flow coefficient } [dimensionless], \\ \mu &= \text{Absolute viscosity } \left[\frac{Ns}{m^2}\right]. \end{aligned}$$

The laminar flow coefficient depends upon the geometry of the orifice exit and was estimated to be 0.16 based on information given by Merritt [21]. By combining Equations 2.2, 2.3, and 2.4 and applying the physical properties of the oil used, Esso NUTO H68 [25], the Reynolds number was found to vary from 500 to 9150 depending on the temperature (viscosity) for a primary stage supply pressure of 2.76 MPa (400 psi). These results were compared to the transition Reynolds number of 15 as determined by Merritt [21]. Thus, the flow was assumed to be turbulent allowing the well known turbulent orifice equation for the flow (applying the notation used in White [24])to be used:

$$Q = \alpha A_t \sqrt{\frac{2}{\rho}} \sqrt{P_{ps} - P_t}, \tag{2.5}$$

where:

$$\begin{aligned} \rho &= \text{Density of the oil } \left[\frac{kg}{m^3}\right], \\ \alpha &= \text{Discharge coefficient } [dimensionless]. \end{aligned}$$

Given the orifice geometry, the discharge coefficient was assumed to be unity in accordance with the ISO recommended correlation listed in White [24]. The volumetric flow rate for a jet could be determined and, from this, the mass flow rate, $\dot{m}$, can be found:

$$\dot{m} = \rho Q. \tag{2.6}$$

When a control volume was placed around the jet, the momentum flux along the principal axis of the jet, $\dot{M}$, reduced to,

$$\dot{M} = \dot{m} V_t. \tag{2.7}$$

In one dimension, the conservation of momentum principle states that for a jet impinging on the static fluid in the receiving port, a force, F_{axis}, is imparted equal to the linear momentum flux of the fluid along the axis of the jet,

$$F_{axis} = \dot{M} = \dot{m} V_t. \tag{2.8}$$

When the jet is unobstructed, this force is applied across the entire receiving port area, A_p, creating an approximately uniform static pressure, P_j, across the port,

$$P_j = \frac{F_{axis}}{A_p}. \tag{2.9}$$

The function of the diverter is to obstruct a portion of the jet, and thus only a fraction of the jet and its total momentum flux reaches the receiving port. This is illustrated in Figure 2.12.

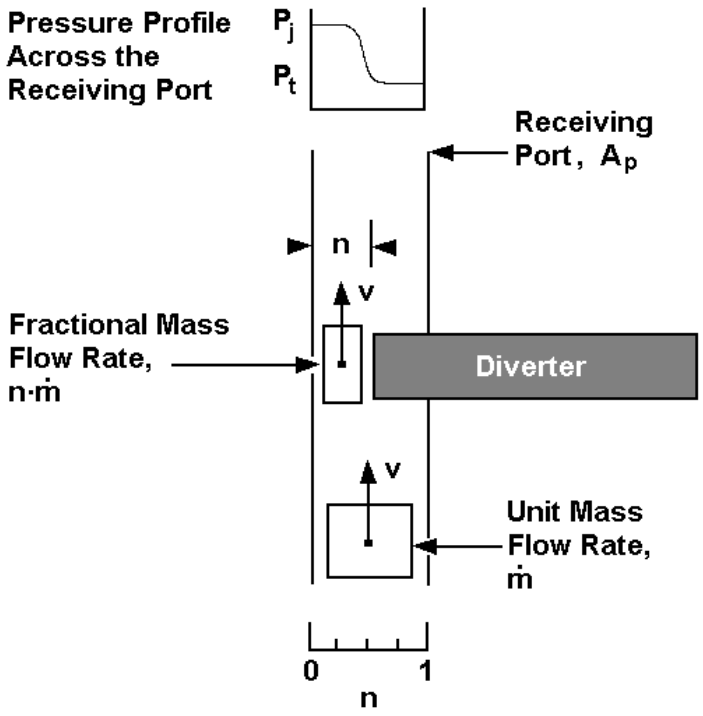

Figure 2.12: A partially diverted jet.

The fraction of the jet passing the diverter is represented by the variable, n, and thus, the force applied on the receiving port by a partially diverted jet is,

$$F_{axis} = n\dot{m}V_t. \tag{2.10}$$

The portion of the receiving port upon which this force is acting, however, is also reduced by the same fraction, n. The magnitude of the jet pressure remains unaffected by diverter displacement but the pressure profile across the receiving port is

no longer uniform. Substituting Equations 2.3, 2.5 and 2.6 into Equation 2.10 and dividing by the reduced receiving port area, nA_p, the pressure exerted by the jet on the unobstructed portion of the receiving port can be determined:

$$P_j = 2n\alpha^2 \frac{A_t}{A_p} \left(P_{ps} - P_t\right). \tag{2.11}$$

Mixing effects will average the pressure seen at the receiving port in the downstream chamber shown in Figure 2.6. Thus, the average of the pressure profile at the receiving port was considered to be a valid approximation of the activation pressure for a given port, (P_1 or P_2),

$$P_{1,2} = (1 - n)\, P_t + 2n\alpha^2 \frac{A_t}{A_p} \left(P_{ps} - P_t\right). \tag{2.12}$$

As mentioned earlier in this analysis, the discharge coefficient for the sending jet approaches unity and since properties were assumed uniform for a jet cross section, the ratio $\frac{A_t}{A_p}$, was also assumed unity. Under these conditions, Equation 2.12 reduced to,

$$P_{1,2} = (1 - 3n)\, P_t + 2nP_{ps}, \tag{2.13}$$

which describes the pressure seen at one receiving port given an opening ratio of, n. The quantity of interest was the difference in the pressure of the two receiving ports which was introduced earlier as the differential activation pressure, ΔP. An expression for this was found by relating the opening ratios of the two jets, n_1 and n_2, in terms of the common factor, n. The physical dimension of the diverter was such that, when one port was completely obstructed, a 16% obstruction remained on the other port. This was accounted for by the following relationship:

$$n_1 = n, \tag{2.14}$$

and,

$$n_2 = 0.84 - n, \tag{2.15}$$

The expressions in Equations 2.14 and 2.15 are valid for the range $0 < n < 0.84$. Substituting the relationships in Equations 2.14 and 2.15 into Equation 2.13 and subtracting the results yielded an expression for the differential activation pressure.

$$\Delta P = P_1 - P_2 = (2.52 - 6n)\, P_t + (-1.68 + 4n)\, P_{ps}. \tag{2.16}$$

The important observation in this analysis was that according to Equation 2.16, the differential activation pressure is a linear function of the receiving port opening ratio if the jet supply pressure and tank pressure are constant. It was shown in Section 2.2.1.2 that the diverter tip displacement is a linear function of voltage. It can be shown that for the tip deflections experienced over the operating range of the valve, linear tip displacement translates to linear blockage of the receiving port within 1%. Blockage of the receiving port results in a proportional diversion of the mass flow rate. Thus, the primary stage has been shown analytically to behave as a linear force transfer device within a set operating region. The next section presents an experimental verification of this.

2.2.1.4 Experimental Verification of the Force Transfer Mechanism

In order to verify the theoretical evaluation of the hydraulic jet force transfer mechanism an experimental apparatus was developed. The primary stage activation pressures could not be measured directly as they were routed internal to the valve body with no external ports. This made it necessary to remove the primary stage and to attach a port plate which allowed for insertion of pressure transducers into the pilot lines. A schematic of the test system is shown in Figure 2.13.

The test apparatus was designed such that the supply pressure could be externally controlled. It is noted that the supply pressure, P_s, is not equivalent to the jet supply pressure, P_{ps}, introduced earlier in this section. Rather, the primary stage has an internal relief valve which endeavours to keep P_{ps} constant regardless of the value of P_s. Examination of the internal relief valve revealed it to be of a single stage configuration which cannot maintain a constant pressure control for varying supply

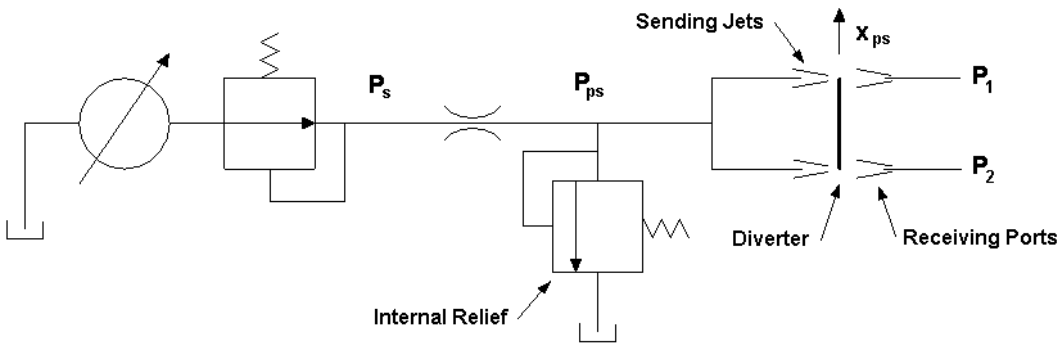

Figure 2.13: Schematic of the primary stage test system.

pressures. The effect of varying the supply pressure on the primary stage activation pressures is addressed later in this chapter.

Prior to beginning the tests described in this section, the system oil was forced to return to the tank over a relief valve until the reservoir temperature was sufficiently high to activate the oil cooling system. This ensured moderated oil temperatures over the duration of the tests and consistent oil properties for tests conducted non-consecutively. The set point of the oil cooling system was 38°C.

To measure the differential activation pressure as a function of input voltage and to verify the theoretical analysis of the force transfer mechanism, a "static step" procedure was employed. Following the warm-up period, the static step test involved applying a voltage to the primary stage which was increased from 0 to 2.5 V in 0.5 V increments every 5 seconds. Using this procedure it was found that the activation pressure did not overshoot and a sufficient number of data points were collected at each "steady-state step" such that a reasonable average value could be determined. A set of typical results is shown in Figure 2.14.

The null input results (input signal is zero) in Figure 2.14 provided an opportunity to indirectly determine the jet supply pressure, P_{ps}. With the diverter in the neutral position and the tank pressure constant at $\sim$0.72 MPa (105 psi), the pressure at both receiving ports was almost double the tank pressure. This indicated that the diverter did not completely cover the receiving ports in the neutral position and

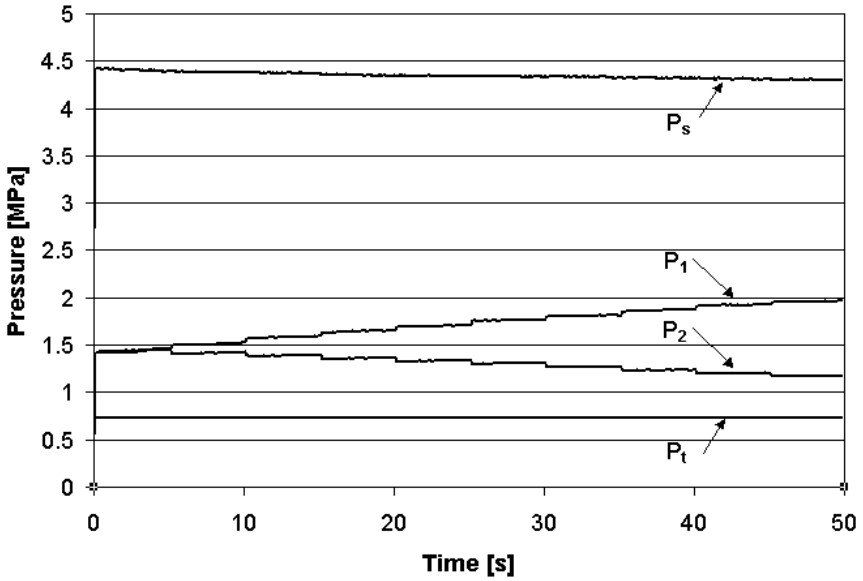

Figure 2.14: Typical pressure responses for a "static step" test.

the remaining open areas were equal. Additional measurements revealed that only 42.5% of each receiving port area was unobstructed when the input was zero, or, $n_{1,2} = .425$. By equation 2.13 a primary supply pressure of, $P_{ps} = 1.95\ MPa$ (283 psi) was calculated.

A second observation was drawn from the magnitude of the activation pressures at the final step shown in Figure 2.14. Data recorded during this test indicated that the input voltage at this step had a magnitude of 2.3 V when the system bias and gain were taken into account. From data summarized in Figure 2.10 it was deduced that the diverter deflection at this point was 0.16 mm. This corresponded to a value of $n = 0.78$. When this opening area ratio was applied to Equation 2.16 using the primary supply pressure calculated from the null position, a differential pressure of 0.8 MPa (116 psi) was calculated. Comparison to the data shown in Figure 2.10 showed agreement within 2% which was considered sufficiently accurate given that mixing effects due to the jets traversing an oil filled gap before impinging on the receiving port were neglected.

It was concluded that within reasonable error a linear uni-directional force ampli-

fier/transfer mechanism is an appropriate model for the primary stage EMA, diverter, and jet/receiving port arrangement.

2.2.1.5 Experimental Determination of the Primary Stage Gain

The diverted jet primary stage was shown in the previous section to be a linear force transfer device subject to several assumptions. The most important of these was that the jet supply pressure, P_{ps}, remained independent of the supply pressure, P_s. In this section, this assumption is examined experimentally. The results are used to develop a primary stage gain which relates the differential activation pressure to the input in the presence of changing supply pressures.

"Static step" tests were performed at various supply pressures using the procedure discussed in the previous section. The differential pressure, ΔP, was calculated for each step and plotted against the input voltage giving the results in Figure 2.15. Two tests were performed at a supply pressure of 3.45 MPa, two at 5.17 MPa, and two at 6.89 MPa. The supply pressure was set manually using a dial gauge for reference.

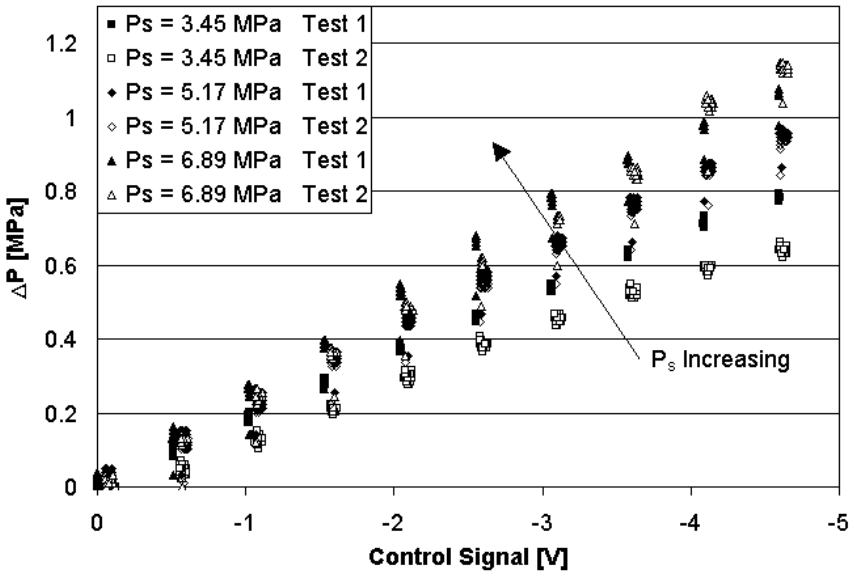

Figure 2.15: The differential activation pressure for several "static step" tests at varying supply pressures.

The data presented in Figure 2.15 showed a relationship between the supply pressure, P_s, and the *slope* of the differential pressure curve. It also gave an indication of the accuracy and repeatability of the differential pressure measurements. The spread in the ΔP-axis was taken as a reasonable approximation of error which was approximately 0.034 MPa (5 psi).

The 3.45 MPa, 5.17 MPa and 6.89 MPa runs plotted in Figure 2.15 were averaged and curve fitted with a linear regression. The supply pressure for these tests, which was recorded with a pressure transducer, was also averaged to provide a more accurate value for the supply pressure. The maximum data spread was considered as the measurement error and plotted as error bars in Figure 2.16. The regressions were not forced through null as some initial displacement in the diverter may have been present due to magnetic hysteresis in the EMA.

The slopes of the linear regression curves shown in Figure 2.16 were made positive for the purposes of maintaining a sign convention and plotted against the measured supply pressure for each run with the results shown in Figure 2.17.

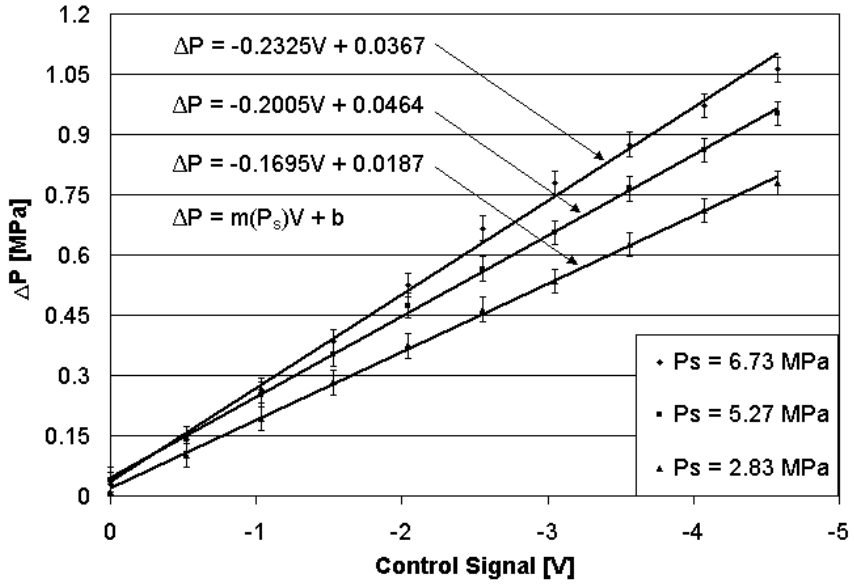

Figure 2.16: Averaged differential activation pressure for several supply pressures at varying voltages.

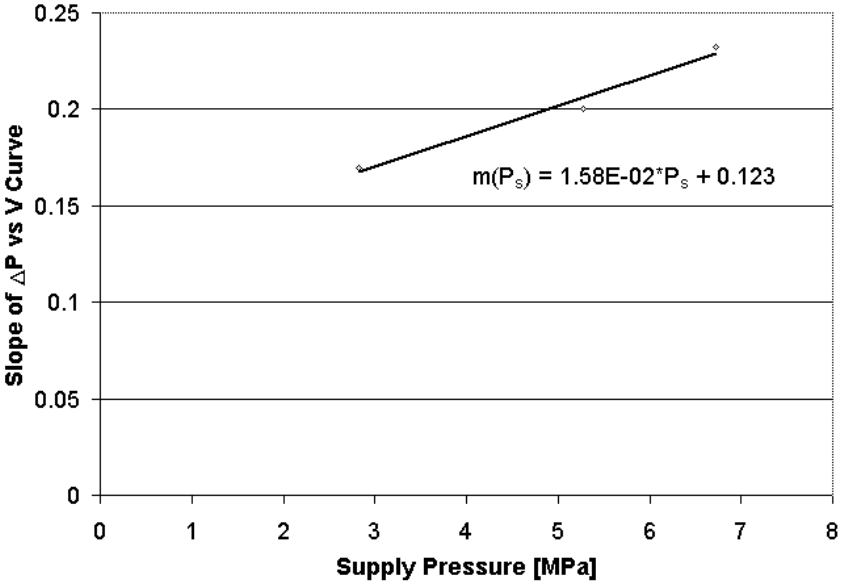

Figure 2.17: Slope of the differential pressure curve as a function of supply pressure.

The data in Figures 2.16 and 2.17 were used to determine a static gain for the primary stage based on the supply pressure. With the bias removed at $V = 0$, the

static gain was represented as follows:

$$\frac{\Delta P}{V} = 1.58 \times 10^{-2} P_s + 0.123. \quad \left[\frac{MPa}{V}\right]. \tag{2.17}$$

To ensure that the primary stage was bi-directional, and to test the system for hysteresis, a ramp test was also performed. In this test, the supply and tank pressures were held constant and the input voltage was varied linearly with time; first increasing to 5 V then decreasing to 0 V. The procedure was repeated with the voltage decreasing to -5 V then increasing to 0 V. Typical responses at a supply pressure of 5.17 MPa (750 psi) are shown in Figure 2.18.

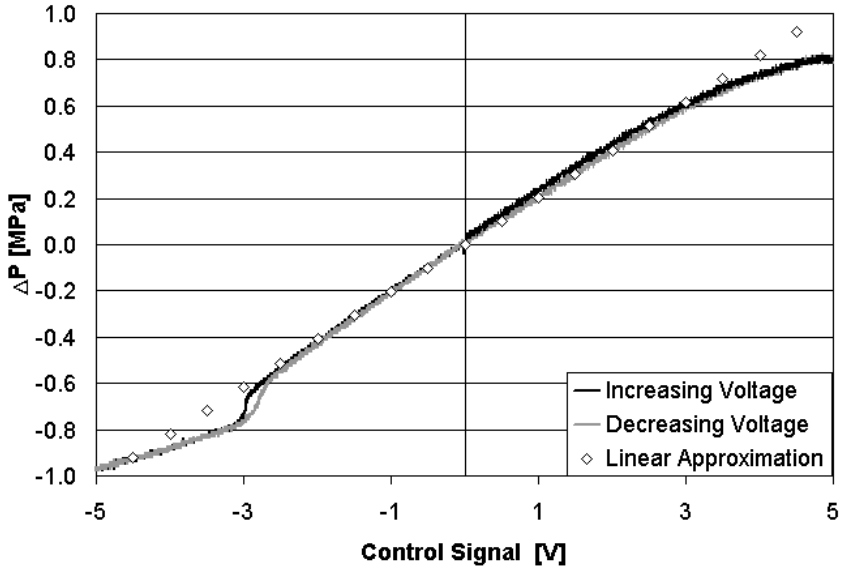

Figure 2.18: The differential activation pressure for a increasing/decreasing ramp input.

A "snap-through" phenomenon was present in the negative tests but not the positive. It was determined in later testing to be caused by contact between the diverter and the housing as a result of a plastic deformation of the primary stage. This was not particularly bothersome as it occurred outside the operating voltage range imparted by current limitation on the coil as set out by the manufacturer. Beyond this, the activation pressure showed excellent linearity for the operating range ± 3 V. The

hysteresis was smaller than expected (<2%) which added weight to the argument for use of these valves in an automated hydraulic control application.

From the preceding discussion, the following conclusions were drawn regarding the static relationship between the control signal input voltage and the differential pressure produced by the primary stage:

1. The differential pressure could be assumed to vary linearly with the input voltage between -3 V and 3 V.

2. The slope of the linear relationship was affected directly by Ps.

3. The relationship:

$$\frac{\Delta P}{V} = 1.58 \times 10^{-2} P_s + 0.123. \quad \left[\frac{MPa}{V}\right], \tag{2.18}$$

   was sufficient to approximate the differential pressure.

4. The activating force was linear throughout the operating range of the valve.

2.2.2 Dynamic Behaviour of the Primary Stage

It was shown in a previous section that steady state behaviour of the primary stage was linear within a specified input voltage range. The only exception of note was the dependence of the activation pressure on the supply pressure. It is the purpose of this section to present the analysis, both theoretical and experimental, which was employed to evaluate the linearity of the primary stage in a dynamic sense. That is, a linear Laplace domain model for the primary stage was sought which would agree well with the experimental results. This model would capture the transient behaviour of the primary stage which worked towards the goal of developing an overall dynamic model of the valve which could be used in design of an appropriate valve spool displacement controller.

This section is organized into two sub-sections. The first of these presents experimental step response results, an analysis of which was used to determine bulk system

parameters. The second section introduces the simulation of the primary stage and shows comparisons of experimental and simulated results.

2.2.2.1 Voltage vs Differential Activation Pressure $\left(\frac{\Delta P}{V}\right)$ Step Responses

Determination of the equations governing the dynamics of the primary stage and identification of the relevant parameters was made difficult by the physical construction of the valve. In particular, for the primary stage, the following presented challenges in making an estimate of the model structure:

1. The rotational inertia of the diverter was difficult to determine due to its non-homogeneous geometry and material properties.
2. The damping condition inside the diverter housing was not known and extremely difficult to determine.
3. The effect, if any, of axial forces arising from interaction with the jets was unknown.

For these reasons, it was decided that a brief departure from the physical modelling methodology was appropriate. Because of the number of parameters that could not be readily measured or estimated, it was more practical to apply an empirical transfer function estimation technique. To achieve this, differential activation pressure step responses were measured over a range of operating conditions and the results were examined for linearity and compared to the output of a transfer function of similar apparent order. Several responses to step inputs are plotted in Figure 2.19. These results are for tests carried out with a fixed supply pressure of $\sim$4.48 MPa (650 psi) with the temperature regulated by an oil cooler with a set point of 38°C.

Several points of interest arise from the data in Figure 2.19. The first of these is regarding the DC gain. The steady-state amplitude achieved after the transients have subsided should agree with the values determined in the "static step" tests described in the previous section. Solving for the steady-state pressure as described

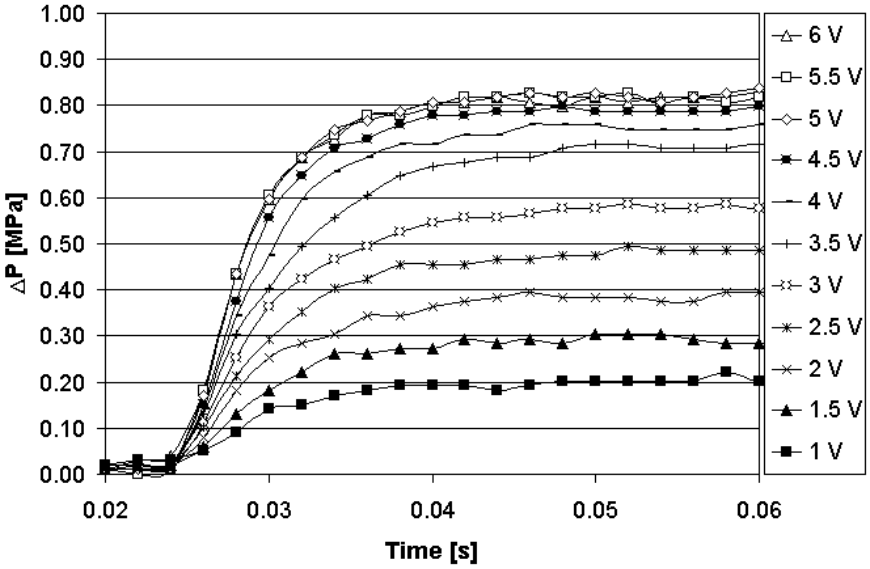

Figure 2.19: Differential activation pressure step responses to increasing input voltages.

by Equation 2.18 showed excellent agreement with the experimental data as will be shown later with simulation results. It should also be noted that the actual length of the data run was 0.1 s rather than the 0.06 s indicated in Figure 2.19. The the data set was truncated to emphasize the transient region. The run was sufficiently long to perform time averaging on the steady-state results to remove a 60 Hz noise signal barely evident in Figure 2.19.

Another observation was made regarding the apparent shape of the transient portion of the step response. The system was heavily overdamped as no overshoot occurred in the differential pressure. Thus, it was reasonable to assume that the system was of first order. Concern over the validity of the first order approximation was not based on the ability of the first order model to match step responses, but rather the associated phase shift which would become important for stability purposes should the system be operated beyond the lowest cutoff frequency. This concern was addressed by determining the estimated time constant that would be associated with a system exhibiting a step response similar to those shown in Figure 2.19. The

time constant was determined graphically to be $\sim 0.005\ s$ using both 99% and 63% magnitude criteria. This corresponded to a pole at -200 $\frac{rad}{s}$. Given that this was the dominant pole it is inconceivable that the valve would be operated beyond this cutoff frequency.

It was concluded, therefore, that the valve behaves as if it were linear and that the dynamic performance of the primary stage could be approximated by the linear transfer function,

$$G_p(s) = \frac{\Delta P}{V} = \frac{K_p}{\tau_p s + 1}. \tag{2.19}$$

2.2.2.2 Verification of Model Responses

In the analyses in the preceding sections, the emphasis was on distilling physical parameter values from experimental data. The focus in this section is on substituting the physical parameters into a simulation performed using the Matlab/Simulink® package in order to verify the dynamic behaviour of the system as described by Equation 2.19. The simulated results were compared to measured data from the experimental system to determine the model accuracy. The block diagram representation of the primary stage is shown in Figure 2.20.

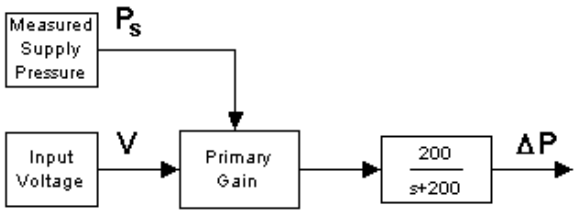

Figure 2.20: Block diagram representation of the primary stage.

The 0.5V, 1.5V, and 3V step responses were chosen for comparison as these input voltages represented the operating range expected in normal operation. The input voltage and supply pressure values recorded during the tests shown in Figure 2.19 were used as the inputs to the first order model shown in Figure 2.20. The results of the system tests and simulated tests are shown in Figure 2.21.

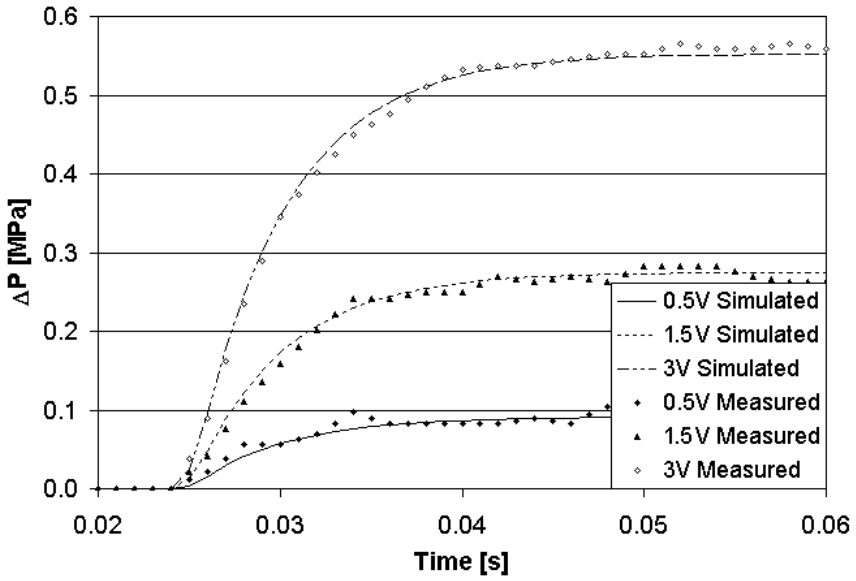

Figure 2.21: Experimental and simulated step responses for the primary stage.

Since two measured quantities were used as inputs to the model (supply pressure and voltage) there were both systematic errors due to model inaccuracy as well as measurement error due to resolution of the instrumentation present in the simulated results. For the purposes of comparison, a measurement error of $\pm 1.38 \times 10^{-2}\ MPa$ ($\pm 2\ psi$) was determined and plotted with the model error results in Figure 2.22.

It is evident from the data presented in Figure 2.22 that the model and experimental results were in agreement approaching the minimum measurement error. This was deemed verification of the primary stage dynamic model.

2.2.3 Dynamic Behaviour of the Main Stage

As was explained earlier,*a priori* knowledge of the configuration and operation of the valve was not available, and this made identification of the characteristics of the primary stage difficult. This was not the case with the main stage. The main stage consisted of a mass/spring/damper arrangement which is a well known system of second order. Further, a system identification analysis had already been performed by Rosa [26] with the main stage spool mass and the spring constants determined

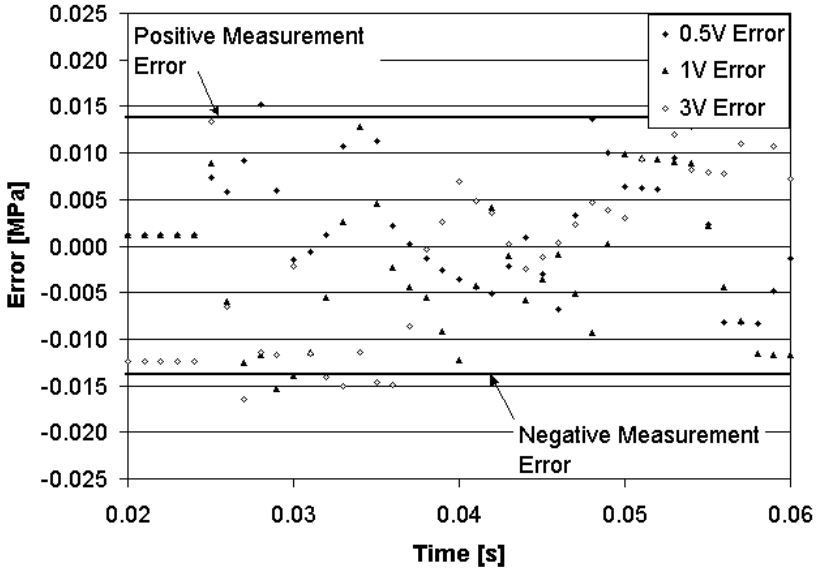

Figure 2.22: Error in differential pressure between simulated and measured step responses for the primary stage.

with acceptable accuracy. The parameter that remained to be determined was the valve spool damping which will be addressed in the next section.

2.2.3.1 Physical Model

Using data available from Rosa [26], it was possible to develop a physical model directly. It was assumed that the spool motion could be described by the linear second-order differential equation:

$$m\frac{d^2x_v}{dt^2} + \beta\frac{dx_v}{dt} + k_{eff}x_v = f\left(t\right). \tag{2.20}$$

where:

$$\begin{aligned} m &= \text{mass of the spool } [kg], \\ \beta &= \text{damping coefficient } \left[\frac{Ns}{m}\right], \\ k_{eff} &= \text{effective spring constant as outlined in Equation 2.26, and,} \\ x_v &= \text{axial displacement of the spool } [m]. \end{aligned}$$

Parameter values obtained by Rosa [26] were:

$$\begin{aligned} m &= 0.2174\,[kg]\,, \\ \beta &= 162\left[\frac{Ns}{m}\right], \text{and,} \\ k_{eff} &= 3720\left[\frac{N}{m}\right]. \end{aligned}$$

The flow reaction forces were not considered as they were determined to be negligibly small at steady state (see Appendix A). It is to be noted that the parameters in Equation 2.20 represented the "bulk" or "average" properties of the system. They were not specified as time variant or operating condition dependent. The operating condition and time have no effect on the mass, which was measured directly. Similarly, the spring constant was directly measured, and the operating environment had little effect on this value. The parameter of concern was the damping coefficient which was a lumped parameter characterizing several phenomena including friction on the spool and internal hydraulic losses. The effect of the operating condition on this parameter is discussed in detail later in this section. As a starting point for analysis, the Laplace transform of the differential equation in Equation 2.20 was performed:

$$\frac{X_v}{F} = \frac{1}{ms^2 + \beta s + k_{eff}}. \tag{2.21}$$

The remainder of this section examines the validity of the linear model with respect to experimental data.

2.2.3.2 Main Stage Dynamic Step Responses

Obtaining and interpreting the main stage step responses was slightly more involved than for the primary stage. The reason for this was that the input signal must pass through the primary stage that was shown in the previous section to contain dynamics of its own. A preliminary analysis was performed to ensure that the main stage dynamics could be distinguished from those of the primary stage.

The first step in the preliminary analysis was to establish the location of the dominant poles of each system in the s-plane. It was already determined that the primary stage was to be modelled as a first order system as it had a single dominant pole at $s = -200\ \frac{rad}{s}$. By substituting the parameter values found by Rosa [26] in Equation 2.21 two real roots at $s_1 = -23.7\ \frac{rad}{s}$ and $s_2 = -721.5\ \frac{rad}{s}$ were found. This indicated a heavily overdamped system.

A "rule of thumb" as described by Phillips and Harbour [27], is that a pole is considered to be dominant in the transient response if it is smaller than another by a factor of 5 to 10. By this criterion it was clear that the slowest pole of the main stage would be dominant and that the primary stage would have little effect on the transient behaviour of the main stage. This was assumed to be the case in the analysis of the main stage dynamic response.

A second consideration in the preliminary analysis was the amplitude of the input signal. In the testing of the primary stage, the limiting factor on the input voltage amplitude was the current in the EMA. Subsequent testing of the primary stage showed saturation in the differential activation pressure due to the geometric constraints which further limited the input amplitude to 3V in the open loop. The main stage was tested to determine if any similar constraints limited the allowable input voltage range.

Saturation was found to occur in the displacement of the spool at approximately $x_{max} = 4\ mm$ in the positive and negative directions. This saturation was found to occur when the force applied by the primary stage exceeded that applied by the return springs at maximum displacement. As a first step to analyzing this problem, it was recalled that the primary stage transfer function developed earlier in this chapter was given by,

$$\frac{\Delta P}{V} = \frac{K_p}{\tau s + 1} = \frac{(1.28 \times 10^{-2} P_s + 0.123)\, 200}{s + 200} \quad \left[\frac{MPa}{V}\right]. \tag{2.22}$$

For determination of force, differential pressure in units of Pascals was more appropriate. Therefore, given the supply pressure, P_s, also in Pascals, Equation 2.22

became,

$$\frac{\Delta P}{V} = \frac{K_p}{\tau s + 1} = \frac{\left(1.28 \times 10^{-2} P_s + 1.23 \times 10^5\right) 200}{s + 200} \quad \left[\frac{Pa}{V}\right]. \tag{2.23}$$

The input to the main stage as indicated by Equation 2.20 was not pressure, but force. The differential activation force was the product of differential activation pressure and the area on the ends of the spool,

$$\frac{\Delta F}{V} = \frac{\left(3.67 \times 10^{-6} P_s + 35.2\right) 200}{s + 200} \quad \left[\frac{N}{V}\right]. \tag{2.24}$$

At steady state, the magnitude of the force in Equation 2.24 reduced to,

$$\Delta F_{ss} = \left(3.67 \times 10^{-6} P_s + 35.2\right) V \quad [N]. \tag{2.25}$$

Equation 2.25 was then compared to the steady-state forces acting on the main stage of the spool at the null flow condition. The steady-state forces were those arising from the return springs, F_{ks}, as a result of the spool being displaced from equilibrium,

$$F_{ks} = k_{eff} x_v. \tag{2.26}$$

When F_{ks} in Equation 2.26 was substituted for ΔF_{ss} in Equation 2.25 and the physical values for the spring constant and a supply pressure 4.48 MPa (650 psi) were included, the following relationship for spool displacement in the steady-state was found:

$$\frac{x_v}{V} = 1.39 \times 10^{-2} \left[\frac{m}{V}\right]. \tag{2.27}$$

Substituting the saturation value, x_{max}, into Equation 2.27, determined the limiting input voltage to be $\sim 0.3\ V$ for the open loop testing. Results were unrepeatable at this input value due to effects discussed in the next section so a slightly higher input amplitude was used in testing.

To quantify the effect of temperature on system performance to a step input, output responses to a fixed amplitude step were recorded at varying temperatures. A thermocouple was placed on a metal pipe as near the valve as possible so as to determine the fluid temperature internal to the valve. The amplitude of the step input voltage was chosen to be 0.5 V with the results of several step responses plotted in Figure 2.23.

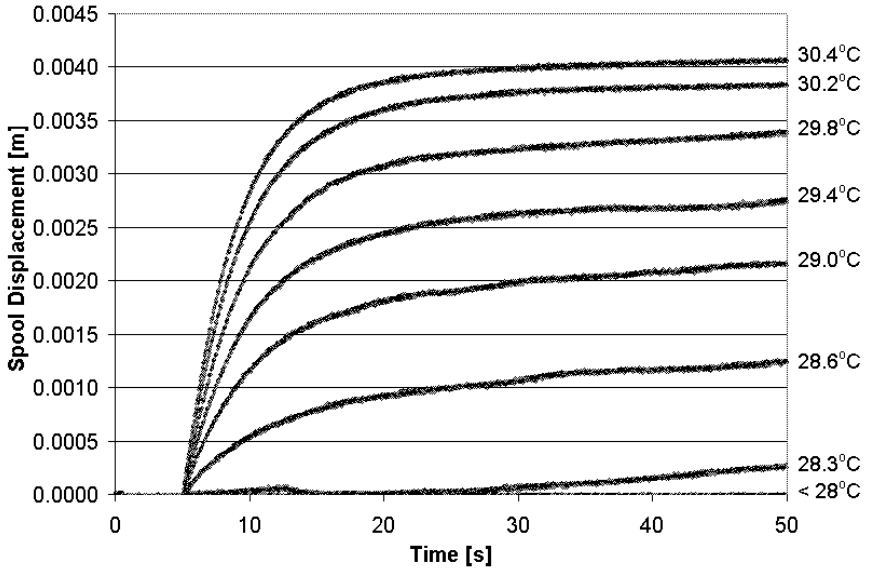

Figure 2.23: Main stage spool displacement step responses for fixed input amplitude and varying temperature at a supply pressure of 4.48 MPa.

It is evident from Figure 2.23 that there was no system response for temperatures less than 28°C. Also, the spool displacement amplitude increased with temperature for a constant input voltage for step responses above 28°C. These observations had two implications from the standpoint of modelling the main stage dynamics.

a) The open loop gain changed with temperature.

b) The open loop gain must reach a threshold value before the system will respond.

The temperature "dead-zone" behaviour exhibited by the system was consistent with

stiction behaviour. In a stiction dominated system, the displacement remains locked at a fixed value until some input force threshold is exceeded. At this point, the static friction is overcome and the system will begin to move under the influence of viscous and coulomb friction. The implication of this with respect to the results shown in Figure 2.23 is that the input force acting on the spool increased with temperature and that below 28^0C there was insufficient force to overcome stiction.

An increasing activation force with temperature was also the explanation for the apparent change in the open loop gain illustrated by the increasing output amplitude of the various tests when compared at 50 s in Figure 2.23. This drift in the steady-state amplitude was evidence of an increasing differential activation pressure. This meant that the gain of the primary, which was assumed constant in an earlier section, was in fact temperature dependent.

The changing value of the differential activation pressure from the primary stage and the consequent activation force on the main stage was not identified in the previous section on primary stage modelling due to the nature of the experimental apparatus and the procedure used in the primary stage study. In the previous section a temperature control system and warm up procedure were employed to ensure consistency in measurement when determining the primary stage dynamics. In the tests performed on the main stage, a different hydraulic supply was used which did not have temperature compensation capability and thus the temperature effects in the open loop became obvious and dramatic.

It was shown in Section 2.2.1.3 that the flow through the jets was turbulent for a wide range of temperatures (viscosities) and, as such, the temperature should have little effect on the flow rate and resulting jet velocity and momentum flux. However, mixing and other fluid phenomena were assumed negligible in that analysis. It has been shown by Comparin et al [28] that a variable Reynolds number can effect the manner in which a jet diffracts around the diverter. Reilly and Moynihan [29] also showed that higher viscosities present at lower temperatures can increase the mixing of the jet and thus produce a widened velocity profile. These effects lead to

a lower average velocity impinging on the fixed width receiving port. Both of these factors also lead to a reduction in the effective gain of the primary stage at lower temperature. The effect of temperature is a factor which was taken into account in the design of the valve spool position controller discussed in a later section.

For the purpose of completeness in modelling, the effect of temperature on the activation force of the primary stage was lumped into a gain scaling factor, K_T. This factor was developed by comparing the output amplitude of the simulated system to the measured values plotted in Figure 2.23. The scaling factor was a second order polynomial function whose output was in the range $0 \rightarrow 1$ and took the following form:

$$K_T = -0.055T^2 + 3.466T - 54.091. \tag{2.28}$$

Aside from temperature dependence, another characteristic of the main stage performance which was evaluated from the results in Figure 2.23 was the settling time exhibited by the system. It was clear from the responses in Figure 2.23 that the system was heavily overdamped which, employing a second order linear model, resulted in two real poles. The slower of these poles could be approximated by the time constant exhibited by the system. The experimental data were used to evaluate the data generated by Rosa [26] in which the dominant open-loop pole was located at $s = -2.72\ \frac{rad}{s}$. That pole corresponded to a time constant, $\tau_R = 0.37\ s$ and a settling time of $T_{sR} = 1.83\ s$ using the 99% criterion when the system was assumed to be of first order. As shown in Figure 2.23, the system clearly had not settled within 2 s. The true settling time was found to be approximately 25 s rather than the 2 s determined by the physical model.

The large difference between the predicted settling time and that exhibited by the system indicated that the dominant pole was not at $s = -2.72\ \frac{rad}{s}$ as calculated from Rosa's data. Rather, the data indicated a time constant of $\tau_m = 5\ s$, corresponding to a pole at $s = -0.2\ \frac{rad}{s}$. As the spring constants and spool mass were directly measured quantities, the large time constant was determined to be due to

a larger damping coefficient. There is an upper limit on the effect viscous friction on the spool can have on the damping leading to the investigation of other potential sources of damping in this system. Thus, the configuration of the pilot lines which connected the main stage to the primary were examined. Rather than treating the pilot lines as lossless signal transmission lines, the effect of the hydraulic resistance, QR, created by the receiving port was taken into account. A schematic of this system interpretation is shown in Figure 2.24.

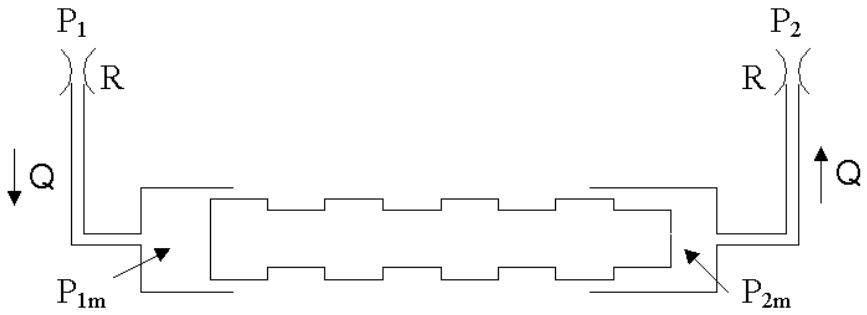

Figure 2.24: Schematic of the spool with restricting orifices.

In this model the differential activation pressure was redefined as the difference in spool end pressures, P_{1m} and P_{2m},

$$\Delta P = P_{1m} - P_{2m}. \tag{2.29}$$

The direction of motion and thus flow was completely arbitrary so the following notations were chosen to address directionality:

$$P_{1m} = P_1 + QR, \tag{2.30}$$

and,

$$P_{2m} = P_2 - QR. \tag{2.31}$$

The effects of compressibility were ignored and, as such, the flow through the restricting orifices, Q, was a function of the spool velocity only,

$$Q = A_p \dot{x_v}. \tag{2.32}$$

Equations 2.29, 2.30, 2.31, and 2.32 were combined to yield a new description for the differential activation pressure including the effects of the restricting orifices:

$$\Delta P = P_1 - P_2 + 2RA_p\dot{x}_v. \tag{2.33}$$

The product of the differential activation pressure and the spool area were taken to be the input force in Equation 2.20 which was rewritten as:

$$m\frac{d^2x_v}{dt^2} + \left(\beta + 2RA_p^2\right)\frac{dx_v}{dt} + kx_v = A_p\left(P_1 - P_2\right). \tag{2.34}$$

It was clear by inspection of Equation 2.34 that the restriction created by the primary stage receiving ports added directly to the damping of the system and it was concluded to account for the discrepancy between the calculated and experimentally determined time constants (slowest dominant pole). Preliminary calculations indicated that the hydraulic resistance created by the pilot lines would be of the same order as that required to generate the experimentally determined transfer function (Appendix B). It was clear that the experimental system would have to be assumed correct and the model made to fit the acquired data. The valve spool displacement was therefore modelled with a second order transfer function with a damping coefficient which reflected the experimentally determined poles:

$$\frac{X_v}{\Delta F} = \frac{1}{0.2174s^2 + 18165s + 3720}. \tag{2.35}$$

Verification of this model required the combination of the primary and secondary stage models. This is the subject of the next section.

2.2.4 Model of the Dynamics of the Two-Stage Valve

In the previous sections physical models of the primary and main stages of the two-stage proportional valve were developed. Experimental results were used to determine the required parameters used in these models. The combination of the two models (representing the two stages) and the testing of their validity is described

in this section. The complete valve model was obtained by combining Equations 2.19 and 2.35 with the result,

$$\frac{X_v}{V} = \frac{K_p K_T}{(s+200)(0.2174s^2 + 18165s + 3720)}. \tag{2.36}$$

Equation 2.36 was simulated using Matlab/Simulink®as shown in Figure 2.25. The results of step responses for 0.5 V input at final temperatures of 28.6°C, 29.4°C, and 30.2°C with a gradient of $0.004\frac{^\circ C}{s}$ are shown in Figure 2.26.

2.3 Spool Position Control

The purpose of the in depth system identification undertaken with regard to the valve was to determine its dynamic behaviour such that a controller could be designed which would ensure repeatable and accurate position of a valve spool. The control of the spool position was integral to the flow control strategy applied by the author. In fact, since the flow control technique was an open loop technique, aside from the mapping of the pressure/flow relationship discussed in the next chapter, spool displacement error was the largest source of error in the implementation. The goal of maintaining portability of the velocity control method (allowing for simple realization of the approach with different hardware) also played a critical role in the design of the controller.

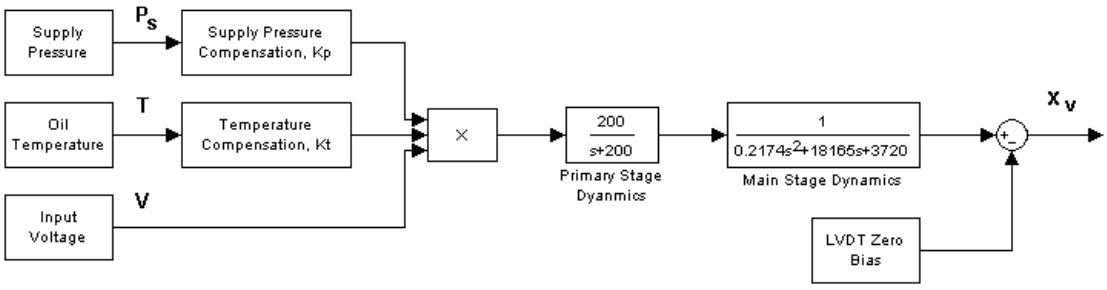

Figure 2.25: Block diagram of the two-stage proportional valve dynamics.

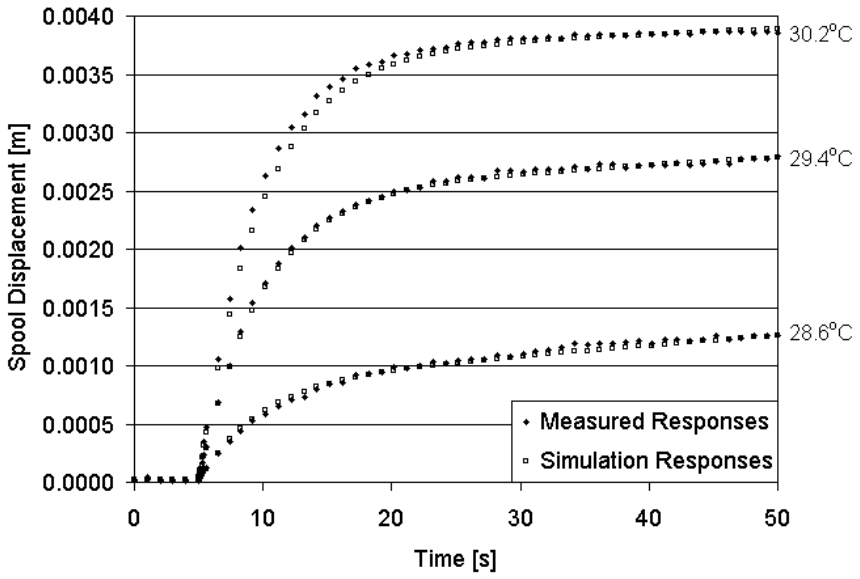

Figure 2.26: Measured and simulated spool displacement step responses for an input of 0.5 V at final temperatures of 28.6°C, 29.4°C, and 30.2°C.

The first step in development of the valve controller was to outline the performance criteria. In operation, it was desirable that the valve be essentially transparent with respect to the overall dynamics. This was considered to be the case when the valve dynamics were an order of magnitude faster than the overall system dynamics. This would imply a dominant closed loop pole no less than -2 $\frac{rad}{s}$.

A further criterion for the valve controller was the need for "smooth" operation. Large acceleration terms can be introduced in hydraulic systems when a large load that is being held against gravity is suddenly "dropped" through the rapid opening of a valve on the holding side of a cylinder and the simultaneous application of pressure to the opposite side. In these cases it is often advantageous to *slow* the response of the valve.

The criterion requiring smooth performance is related to another requirement: repeatability. As introduced in the first chapter of this thesis, the flow control method employed by the author was a predictive method; therefore, it was necessary that the behaviour of the system be, at all times, predictable. The variable open loop

primary stage gain identified in the previous sections would have resulted in variable closed loop poles in the displacement transfer function. This would have resulted in a variable transient behaviour unless these factors were compensated for using feedback. As it was never the intent to directly feed back temperature or pressure information to the valve position controller, a different approach was taken. The development of a spool position controller which satisfied these opposing goals is the subject of the next section.

2.3.0.1 Development of the Model Reference Spool Position Control Loop

The system identification performed on the valve indicated that the valve exhibited linear behaviour with two notable exceptions:

a) A temperature dependent primary stage gain.

b) A pressure dependent primary stage gain.

These items are "soft" nonlinearities. Their effects on the system were not discontinuous and filtered to some degree by the mechanical behaviour of the valve spool, given that both were internal to the valve.

The first step in the investigation was to linearize the dynamic equations for the valve. This was done by developing a "fastest" and a "slowest" dynamic case for corresponding fixed operating conditions. In the fastest case, the supply pressure and temperature would be high, thereby maximizing the internal gain dependent on these factors. The slowest case is under the opposite conditions. Operating ranges were chosen somewhat arbitrarily, but they reflected the realities of the working environment in the laboratory. High and low supply pressures were chosen to be $10.3 \times 10^6\ Pa$ and $3.4 \times 10^6\ Pa$ respectively. Temperatures were chosen to vary from 36°C to 29°C which were the maxximum and minimum values under which testing

was performed. Application of these values to the complete valve model resulted in two transfer functions,

$$G_{high} = \frac{15730}{0.2174s^3 + 1.821 \times 10^4 s^2 + 3.637 \times 10^6 s + 7.44 \times 10^5}, \tag{2.37}$$

and,

$$G_{low} = \frac{3003}{0.2174s^3 + 1.821 \times 10^4 s^2 + 3.637 \times 10^6 s + 7.44 \times 10^5}. \tag{2.38}$$

The short comings of a conventional linear controller in the presence of variable gain were illustrated by placing these two transfer functions in a feedback control loop with the addition of a proportional controller as shown in Figure 2.27.

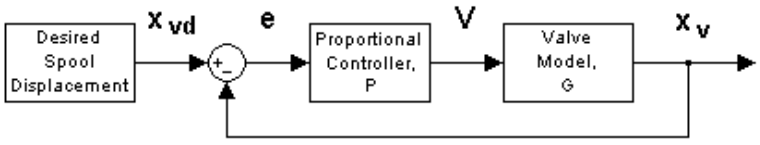

Figure 2.27: Valve spool displacement simulation control loop with proportional feedback control.

In this configuration, in order to achieve the dominant closed loop pole $s > -2 \quad \frac{rad}{s}$ for the loop including G_{low}, a proportional gain, P, of 6000 was required. The step responses for the two transfer functions subject to this same controller are shown in Figure 2.28.

The variation in the rise time of the two responses was troublesome, especially with respect to the lower gain case. The settling time for the step response was on the order of one second, but the gain could not be increased without making the fast closed loop transfer function underdamped. Introducing an adaptive proportional gain was briefly considered, but this would have required direct feedback of the temperature and the supply pressure.

Developing a model reference controller of the type employed by Pietola and Vilenius [5] was considered a better option. A variation on this type of controller, called an

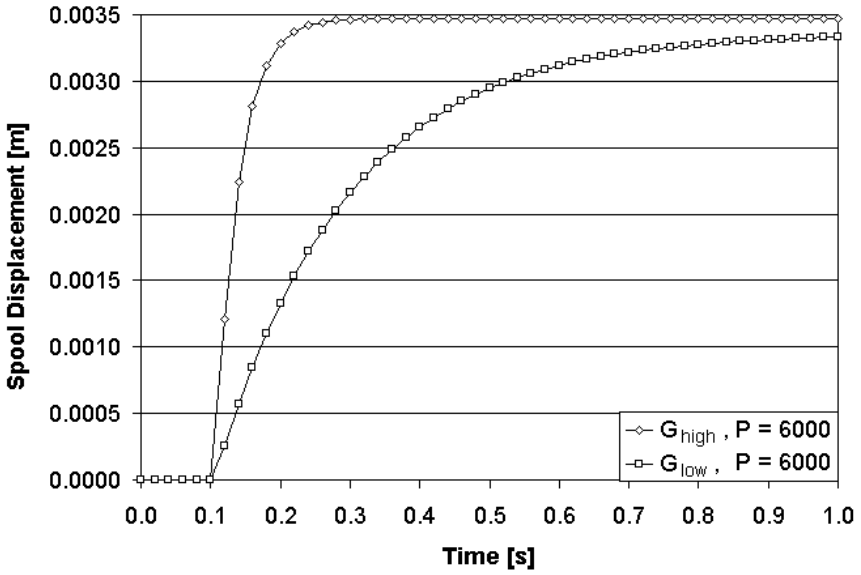

Figure 2.28: Results of a simulated step response for a fast and slow linearized valve transfer function.

explicit model reference controller, is described by Landau [23] and was used as a model for the controller design discussed here.

The reference model was chosen to reflect the dynamics of the actual valve and, as such, a proportional control system of the type shown in Figure 2.27 was employed. An open loop gain of 6000 was mid-range between those in Equation 2.37 and 2.38 and was chosen as a compromise between stability and response time. The proportional gain was set at 10000 which met quantitative requirements for the dominant closed loop pole location ($s = -18.4\ \frac{rad}{s}$) and settling time ($Ts = 0.218\ s$).

It was determined during initial testing that the model reference transfer function contained a pole which exceeded the maximum sample rate of the the hardware and software used to implement the system. For this reason, an order reduction was performed on the system. The simplest method was to eliminate the fastest pole and adjust the closed loop gain. The new transfer function took the following form:

$$G_{reduced} = \frac{3003}{s^2 + 200.36s + 3341.52}. \tag{2.39}$$

To ensure that this order reduction would not affect the dynamics of the system, the reduced and original transfer functions were compared in both the frequency and the time domains using a Bode plot and a step response respectively. The results are shown in Figure 2.29.

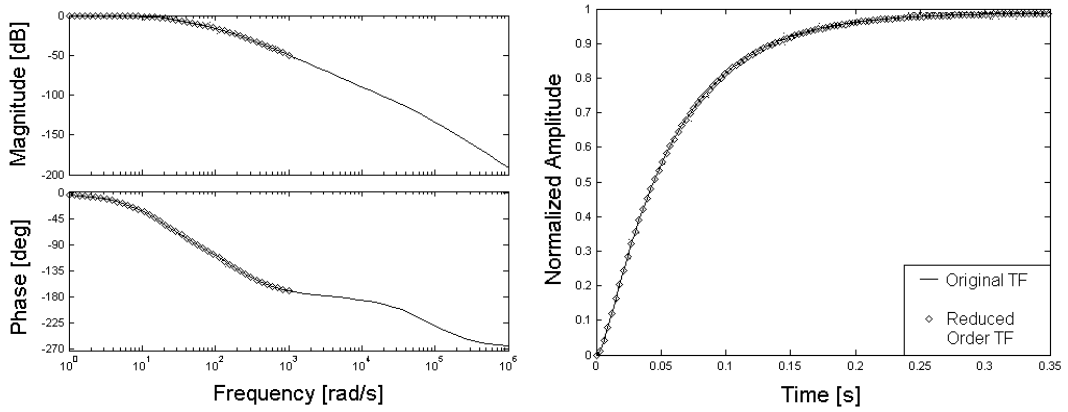

Figure 2.29: Responses of the reduced order and original valve reference models.

There was no difference in the frequency responses up to 1000 $\frac{rad}{s}$ which was outside the operating range of the system. The step responses showed virtually no variation.

The reduced order model was used to construct a model reference controller (MRC) as shown in the block diagram in Figure 2.30.

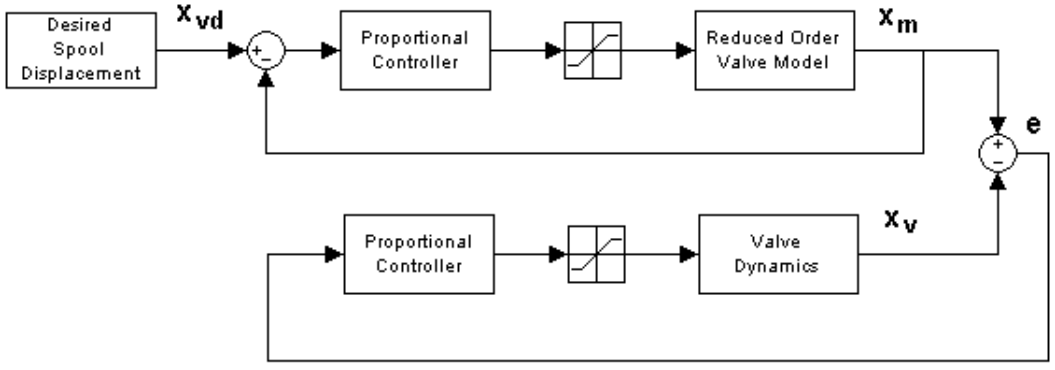

Figure 2.30: Block diagram of the model reference controller.

In this configuration the proportional gain in the valve spool control loop could be increased significantly and the stability of the system not compromised. Step responses for six cases are presented in Figures 2.31, 2.32, and 2.33. The cases considered were small, medium and large valve displacements at low, medium and high supply pressures. At "small" valve displacements, there was sufficient flow through the valve at nominal load to produce motion that was only just visually discernable. "Large" valve displacements were considered those displacements at which the flow rate through the valve approached the maximum pump flow at nominal load pressure. This corresponded to a range between 0.001 and 0.002 m (1 to 2 mm). Low pressure was the smallest steady value attainable with the relief valve in place on the test system or 3.45 MPa (500 psi). The high pressure value was set at 6.89 MPa (1000 psi) for safety reasons.

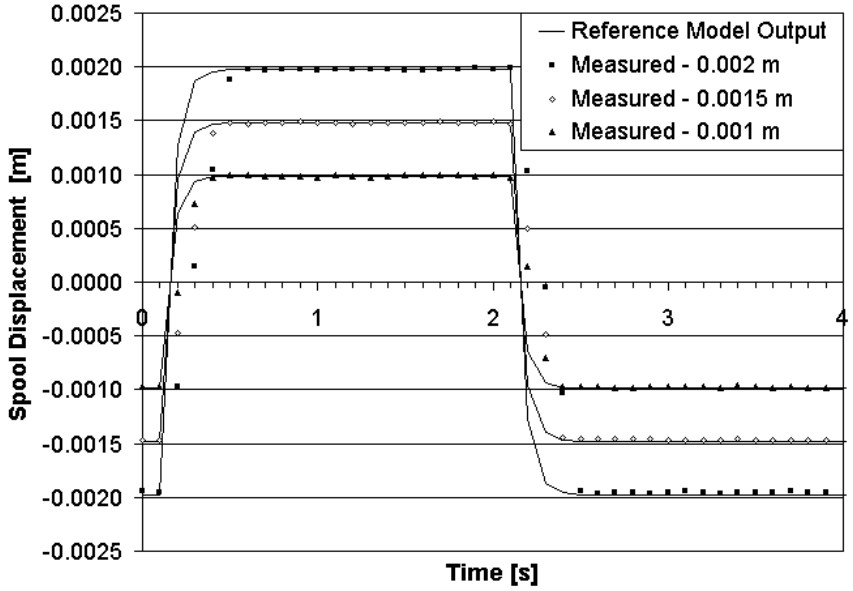

Figure 2.31: Valve spool displacement step responses at $P_s = 3.45\ MPa$.

First and foremost these results showed an improvement in the previously observed discrepancy in the rise time for the high and the low supply pressure cases (these correspond to the step responses shown in Figure 2.28 of the simulated high and low gain transfer functions). The low pressure cases were performed immediately following start up to ensure the oil was as cold as possible (room temperature of 21°C).

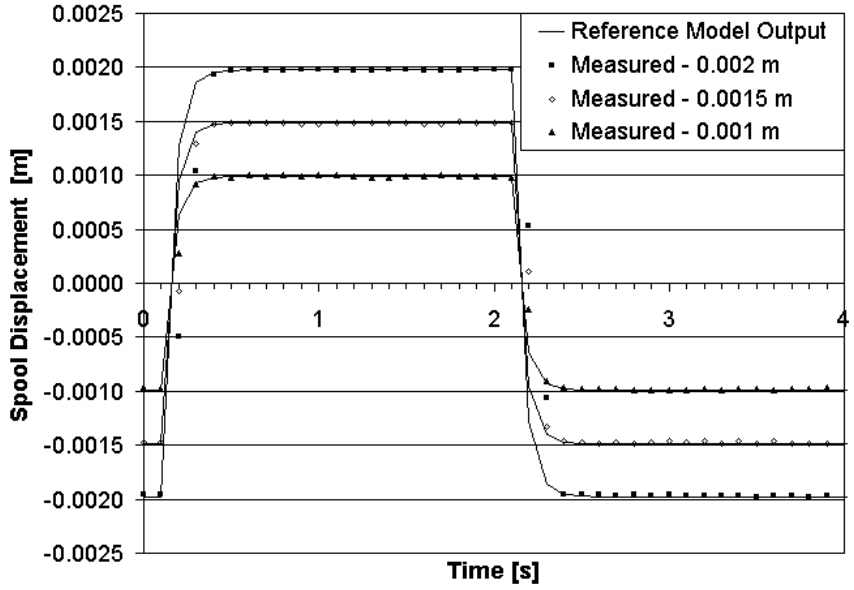

Figure 2.32: Valve spool displacement step responses at $P_s = 5.17\ MPa$.

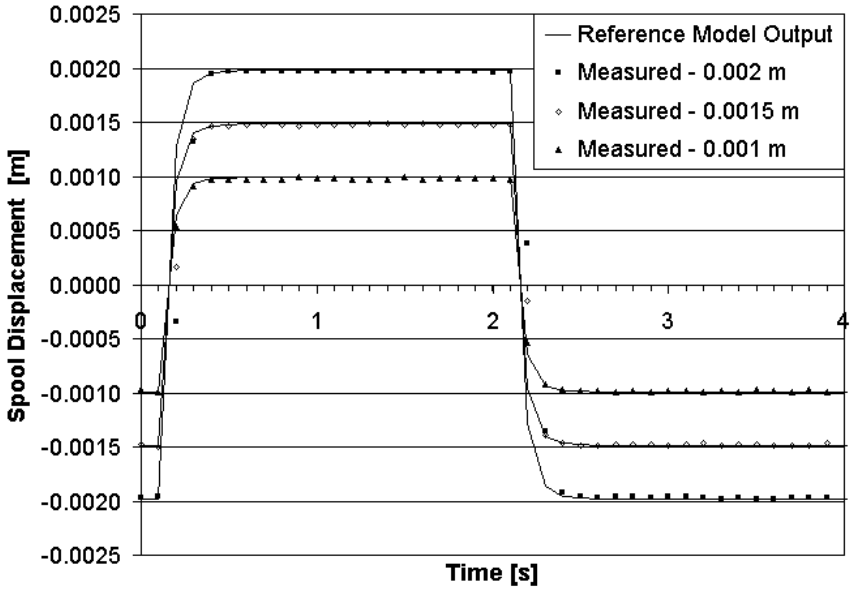

Figure 2.33: Valve spool displacement step responses at $P_s = 6.89\ MPa$.

The combination of low supply pressure and temperature produced a minimum open loop gain in the valve. Despite this small open loop gain, the variation in rise time between this test and the highest gain case was still less than 0.1 s. At very low

open loop gains, amplifier saturation could be playing a role in limiting achievable rise time.

The high supply pressure of 6.89 MPa is in the range more likely to be encountered in a mobile hydraulic application. The controller provides excellent performance under this operating condition. There was no overshoot despite a greater than 5 fold increase in open loop gain.

It should be noted that the explicit reference model was based on proportional control of the valve. Since the valve may be modelled as a second order type 0 system, zero steady state error is not assured by this configuration. With the gains employed, the steady state output was limited to $\sim$ 98 % of the input. This can be seen in the step response results. This error could be removed by including an integrator in the model control loop.

It was also noted that the controller as developed, allowed a large gain in the hardware control loop. This provided a solution to the stiction problem, which was most prevalent at the null position. It was mentioned earlier in this section that the valve contained some deadzone. This influenced the choice of the operating range for the step displacements presented. This was considered to be a pressure/flow relationship issue and is addressed in the next chapter.

Finally, it is to be noted that although this controller was developed for a specific valve, the approach is valid for any valve whose dominant closed loop pole is equal or greater than that of the valve used in this research. Through appropriate choice of feedback gains, any valve which satisfies this criterion could be used in the same fashion [23], thereby maintaining portability of the approach.

2.4 Concluding Comments on the Dynamic Characteristics of the Valve

Through a system identification and modelling procedure, it was shown in this chapter that the electrohydraulic valve used in this study had several operating condition dependent behaviours. This trait is not uncommon amongst electrohydraulic spool valves. Fortunately, it was found that the dynamics of the valve could be made repeatable and approximately linear by the introduction of a model reference controller based on the system identification performed on the valve. This was consistent with Research Goal #2 outlined in the Introduction of this Thesis. Furthermore, the approach that was developed could be applied in a straightforward fashion to any valve whose dynamics are at least as "fast" as those of the valve used in this research.

The underlying purpose behind achieving repeatable and accurate position control of the valve spool is that it is a requirement for the development of the predictive flow control strategy which is the subject of Chapter 3.

Chapter 3

Flow Estimation in a Spool Type Valve

It was stated in the introduction to Chapter 2 that a proportional valve is usually designed to produce a valve spool displacement that is proportional to the input signal. In this research, substantial effort was expended to ensure that this was the case for the valve used. In particular it was of critical importance to control accurately the displacement of the valve spool so that a relationship between valve spool displacement and the flow characteristics of the valve could be determined.

Obtaining velocity or position control in any hydraulic system is a matter of controlling the amount of oil which arrives at the actuator. This is commonly referred to as "flow control". Flow control with a valve is achieved by introducing a restriction in the hydraulic line of appropriate dimension such that the desired flow rate is obtained. This is commonly done with two orifices in series which together create the required equivalent restriction. In this arrangement, one orifice remains fixed and the other varies in response to changing operating conditions. A typical series orifice configuration (referred to as a pressure compensated flow control valve) is shown in Figure 3.1.

The underlying principle is that if a constant pressure drop is maintained across the fixed orifice, A_1, the flow rate will depend only on the open area of this orifice.

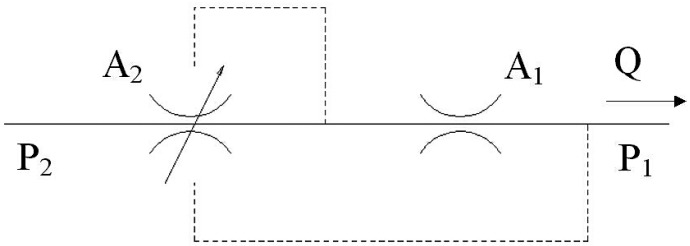

Figure 3.1: A series orifice pressure compensated flow device.

Therefore, the variable orifice, A_2, responding to hydraulic feedback, varies its area to ensure this is the case.

An alternative approach to flow control is presented in this thesis. The series orifice arrangement is replaced with a single orifice (in this case the proportional valve) and electronic pressure feedback is used to adjust the area of the orifice to achieve the desired flow rate. To maintain the generality and portability of this approach, it was assumed that the restrictive orifice could have any geometry. In application of this method the geometry is not necessarily known to the user.

The remainder of this chapter considers the theoretical development and experimental work performed in the development of the single orifice flow controller. First, a new method by which the flow characteristics of a valve of unknown configuration can be determined and expressed in a mathematically compact fashion is introduced. Next, the method by which the mathematical description of the flow characteristics was applied to, and optimized for, the specific valve examined in Chapter 2 is discussed. Finally, an experimental examination of the specific mathematical expression (or "valve map") which resulted is discussed with conclusions on its performance.

3.1 Describing Equations for the Flow Through a Spool Valve

The flow of oil through a spool valve is governed by two factors:

1. The shape of the opening created between the valve spool and the valve body (valve geometry) and,
2. The relationship between pressure and flow given the orifice shape (flow regime).

The effect of these factors on the flow and their mathematical representation in hydraulic analysis are discussed in the remainder of this section.

3.1.1 Valve Geometry

The actual geometry of a spool valve orifice can vary considerably from manufacturer-to-manufacturer. In general, the shape of the orifice in a spool valve is annular as was indicated in Figure 2.3. The area of the orifice is determined by the clearance between the valve spool and the valve body. Some manufacturers modify the edges of the spool in order to obtain desirable effects in terms of valve wear, dynamic range (a larger orifice opening for a smaller spool displacement), or reduced flow forces.

In typical spool valve analysis [21], the orifice area is written as a function of valve spool linear displacement:

$$A_o = w \cdot x_s, \tag{3.1}$$

where:

$$\begin{aligned} w &= \text{orifice gradient} \left[\frac{m^2}{m}\right], \\ x_s &= \text{linear displacement of the valve spool} \left[m\right]. \end{aligned}$$

The bevelling of the valve spool that is evident in Figure 2.3 was designed to created a constant value for the orifice gradient, w, but this is not the rule. In many cases it may not be possible to determine the orifice gradient for a given valve without extensive testing or disassembly. The need for detailed knowledge of the orifice configuration was addressed in this study by eliminating the need for an explicit description of the valve orifice in the expression for the flow through the valve as will be discussed in Section 3.2.

3.1.2 Laminar and Turbulent Pressure/Flow Relationships

In a traditional hydraulic valve analysis, having ascertained the orifice geometry, the flow through a valve is assumed to be either laminar or turbulent, depending on the Reynolds number [24]. The definition of a flow in the laminar regime is one which is dominated by fluid viscous effects. The turbulent regime describes flows where the inertial effects dominate the characteristics. The Reynolds number is the ratio of the inertial effects (based on the density and fluid velocity) and the viscous effects (based on absolute viscosity and geometry).

If a fluid flow is assumed to be fully turbulent, then it can be described by the "turbulent flow equation" which is derived from an analysis based on the conservation of momentum subject to several constraints. The development and experimental confirmation of this relationship is well known and well represented in many texts [21], [24] and therefore presented without proof in this thesis:

$$Q = C_d A_o \sqrt{\frac{2}{\rho}} \sqrt{P_1 - P_2}, \tag{3.2}$$

where:

$$\begin{aligned} P_1 - P_2 &= \text{differential pressure across the orifice} \left[Pa\right]. \\ Q &= \text{volumetric flow rate} \left[\frac{m^3}{s}\right] \\ C_d &= \text{orifice discharge coefficient} \left[unitless\right] \end{aligned}$$

$$
\begin{aligned}
A_o &= \text{orifice area} \left[m^2\right] \\
\rho &= \text{fluid density.} \left[\frac{kg}{m^3}\right]
\end{aligned}
$$

Similarly, if the flow is fully laminar then the relationship between the pressure and the flow, is described by:

$$Q = C_{lam} A_o \left(P_1 - P_2\right), \tag{3.3}$$

where:

$$C_{lam} = \text{generic geometry dependant laminar discharge coefficient} \left[\frac{m^2 s}{kg}\right].$$

Equations 3.2 and 3.3, show respectively, that turbulent flow depends on the square root of the pressure difference while laminar flow directly depends on the pressure difference. It has been suggested by Merritt [21], and more recently by Wu and Burton [22], that the turbulent orifice equation can be mapped to the laminar regime by appropriate shaping of the discharge coefficient. Unfortunately, both studies require *a priori* knowledge of the geometry of the orifice.

The dependence of a traditional analysis on the understanding of the geometry of the valve can not be overstated. The underlying implication is that a flow control strategy using this type of analysis to predict the flow rate based on pressure cannot be undertaken without detailed specifications (manufacturing drawings) or disassembly of the valve itself.

As discussed in Chapter 1, an important goal of the research described in this thesis was to develop a straightforward test procedure and a new empirical mathematical expression which would describe the pressure/flow relationship over the entire operating range of the valve without regard for geometry or flow regime. It was also desirable for this new expression to be continuous to avoid complications associated with switching in a piecewise solution. In the remainder of this chapter a new empirical method of adapting the turbulent orifice equation to describe the pressure/flow characteristics of the valve is presented.

3.2 "Mapping" the Flow Characteristics of a Spool Valve

3.2.1 Single Equation Description of Laminar and Turbulent Flow Regimes

As the turbulent orifice equation is widely used and understood, a modified version of this equation was used to describe the flow through the valve. This was justified in that the turbulent orifice equation, as presented in Equation 3.2, requires modification in application to achieve accuracy [21]. The reason for this is that the discharge coefficient, C_d, can be assumed constant only under a very limited set of constraints which include assumptions about the area of the vena contracta of the orifice and the value of the Reynolds number. Unfortunately, these constraints do not allow for a changing orifice geometry with valve displacement which is impossible to predict if the geometry is unknown from the outset.

Rather than attempting to calculate the flow rate through the valve by estimating a discharge coefficient and an orifice gradient, an experimental apparatus was designed, instrumented and calibrated to measure the flow rate for varying valve spool displacement and differential pressures. The test apparatus is shown schematically in Figure 3.2.

A typical test run consisted of the following steps;

1. The system was warmed up using the procedure discussed earlier in this thesis.
2. At a fixed operating point ($P_s = constant$ and $Temperature = 38°C$), the valve spool was moved to a fixed position, x_v [1].

[1]The LVDT neutral position $x_v = 0$ was determined by increasing the input voltage to the valve until a flow rate was just discernable above the noise of the flow meter. As discussed later in this chapter, the limitations on the resolution of the flow meter led to the introduction of a bias in x_v. This had no effect on this procedure and is corrected later in this section.

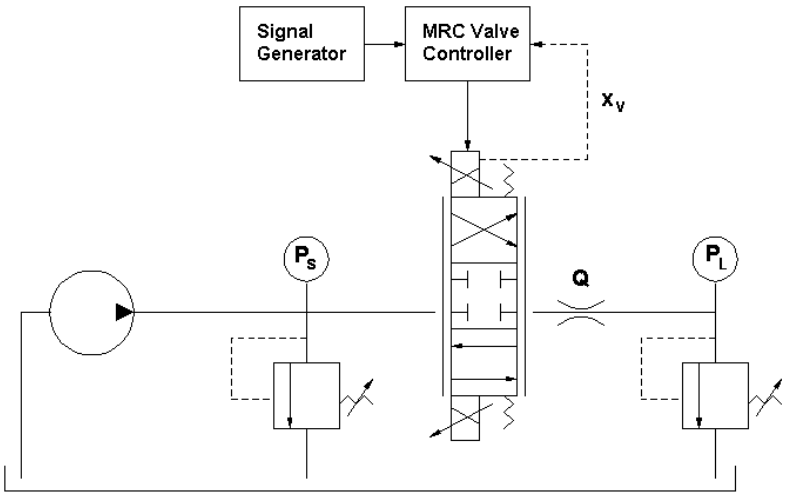

Figure 3.2: Experimental apparatus used to determine the relationship between pressure, flow rate and displacement in the proportional valve.

3. With the spool at position, x_v, the load pressure, P_L, was increased incrementally.

4. At each increment of load pressure, the flow rate, Q, was recorded for a minimum duration of 10 s.

5. The valve spool was moved to a new position and steps 2 and 3 were repeated.

Time averaged results for each operating condition are presented in Figure 3.3.

The results of flow rate as a function of valve displacement and differential pressure over the operating range of the valve were used as a reference data set to determine an empirical function describing the same behaviour. Because this function "maps" differential pressure and valve spool displacement to flow rate, the result is referred to as a "valve map".

At first glance the pressure/flow curves appeared to have a square root profile which would have indicated that the turbulent orifice equation would provide an accurate prediction of the true pressure/flow relationship. However, Figure 3.4 illustrates the short comings of the turbulent orifice equation in predicting flow rate. Flow

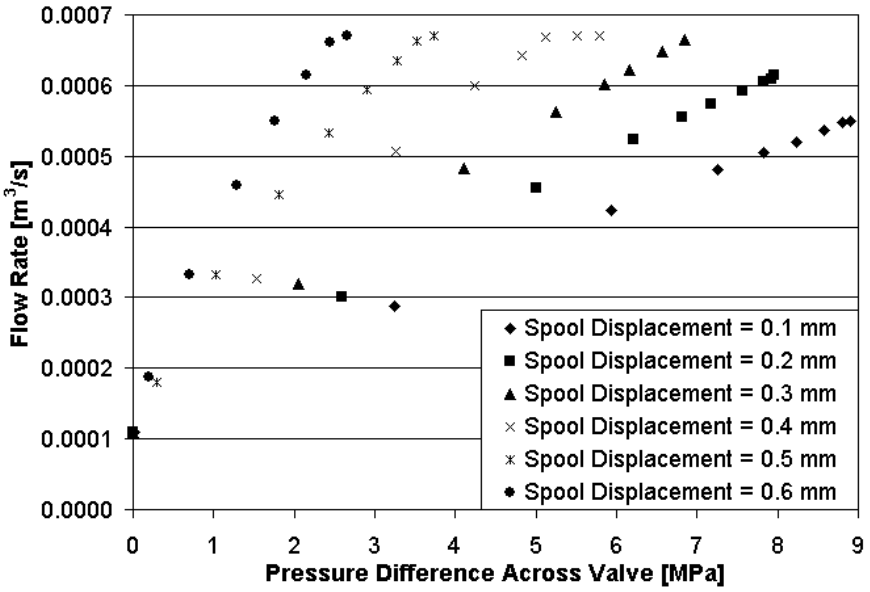

Figure 3.3: Flow rate through a proportional valve for changing valve opening and pressure drop at 38 $^{\circ}C$. (Note: Flow meter resolution placed a lower limit on the flow rates which could be measured.)

rates were calculated using Equation 3.2 and the same valve displacements and pressures as the data points in Figure 3.3. The orifice gradient used was determined experimentally by Rosa [26] for the same valve. Both measured flow rates and the turbulent orifice equation calculations are plotted for comparison in Figure 3.4.

It was concluded that the turbulent orifice equation was relatively effective at predicting the flow rate at large valve openings. The accuracy degraded as the valve opening was reduced. The combination of unknown valve geometry and unknown flow regime made the turbulent orifice equation invalid in the small displacement range.

The initial approach to extending the range of the turbulent orifice equation to accommodate low flow rates was to modify the discharge coefficient in terms of the Reynolds number as suggested by Merritt [21]. This was abandoned as the unknown geometry of the valve would have made for a large number of unverifiable assumptions. Furthermore, the experimental data showed that there was no obvious

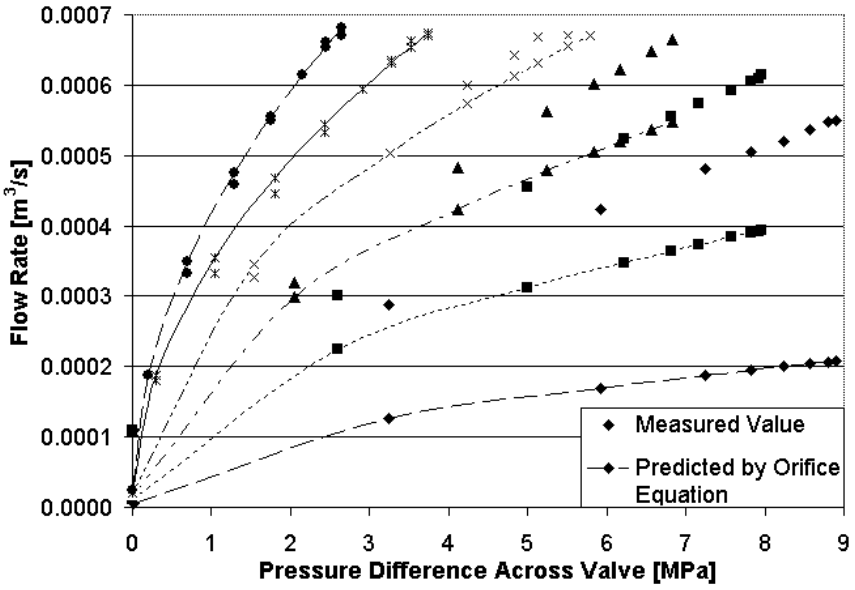

Figure 3.4: Experimental value of flow rate through a proportional valve and the calculations according to the turbulent orifice equation for the valve openings in Figure 3.3.

division between the two regimes; rather, the flow appeared to be fully turbulent at high differential pressures but did not appear to be fully laminar (a straight line in the pressure flow curve) at low differential pressures. Instead, in the valve mapping technique adopted in this study, the experimental data set plotted in Figure 3.3 was fitted to the relationship,

$$Q = Kx_v\sqrt{\Delta P}, \tag{3.4}$$

where $K = f\{x_v, \Delta P\}$. A mathematically simple relationship was sought which related the value of the flow coefficient, K, to the instantaneous operating conditions x_v and ΔP. Therefore, a new empirical analysis technique was employed to determine this coefficient.

3.2.2 Modification of the Turbulent Orifice Equation

Two concerns governed the approach to finding a solution for the modified flow coefficient, K: portability and computational simplicity. In terms of portability, it was paramount to keep the mathematical relationship $K = f\{x_v, \Delta P\}$ as general as possible so that any proportional valve could be used with a minimum of experimental data collection of pressure, flow rate and valve spool displacement.

In terms of computational simplicity, it was envisioned that the valve map should be implementable on a stand-alone micro-controller which might be of limited memory or limited computational power. The issue of limited memory excluded a look-up table of P, Q, and x_v as storage of a large amount of data would be required to capture the entire operating range of the valve. The issue of computational speed meant that a simple continuous mathematical relationship with a minimum of logic and a minimum number of variable parameters was desired. A continuous differentiable relationship was also desirable in the case of future implementation of a self-tuning algorithm, for example.

As a first step, the flow coefficient was determined by applying Equation 3.4 to the data presented in Figure 3.3. The result was a family of curves such as that presented in Figure 3.5.

It is apparent from these curves that the flow coefficient depends both on the valve spool displacement, x_v, and the differential pressure, ΔP. Qualitatively, the results were consistent with the flow equations in that the flow coefficient should tend to a constant value for fully turbulent flow and vary approximately with the square of the pressure for laminar flows.

More specifically, the solution for the flow coefficient formed linear curves, the slope and intercept of which varied with the valve spool displacement. The result of this was a flow coefficient of the form:

$$K\left(x_v, \Delta P\right) = m\left(x_v\right)\Delta P + b\left(x_v\right), \tag{3.5}$$

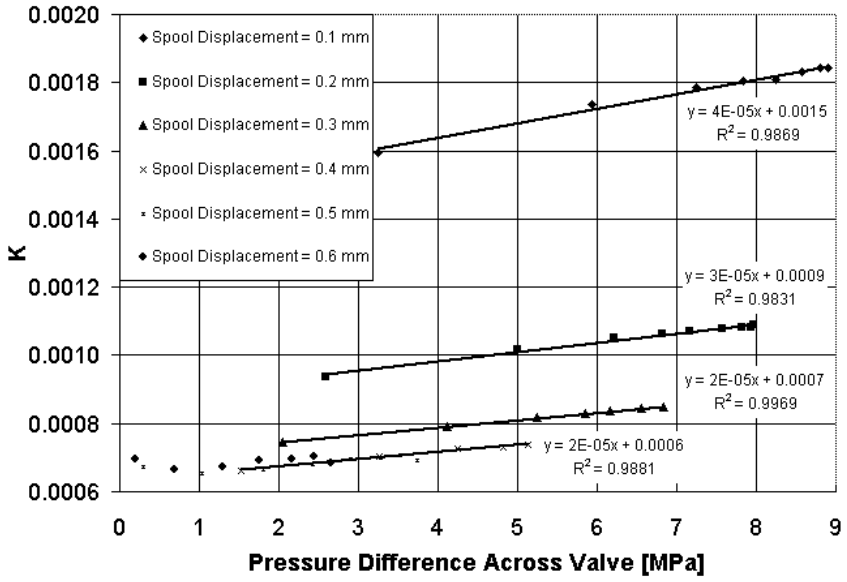

Figure 3.5: Calculated flow coefficient based on experimental values of flow.

To determine the mathematical dependence of the slope and the intercept on the displacement, these two terms were plotted as dependent variables against the valve displacement and fitted with an appropriate curve (in both cases exponential) as shown in Figures 3.6 and 3.7.

The results of the best fit curves gave a slope described mathematically by,

$$m(x_v) = 4 \times 10^{-11} e^{-10762 x_v} + 2.14 \times 10^{-11}, \tag{3.6}$$

and, likewise, the intercept,

$$b(x_v) = 0.0023 e^{-8500 x_v} + 0.00061. \tag{3.7}$$

Equations 3.4, 3.5, 3.6, and 3.7 were combined to give the "modified turbulent orifice equation" and could be written in terms of generic coefficients as:

$$Q = \left[\left(C_1 + C_2 e^{C_3 x_v} \right) \Delta P + C_4 + C_5 e^{C_6 x_v} \right] x_v \sqrt{\Delta P}. \tag{3.8}$$

When Equation 3.8 was applied to the operating conditions presented in Figure 3.3 with the coefficients in Equations 3.6 and 3.7 the results shown in Figure 3.8 were obtained.

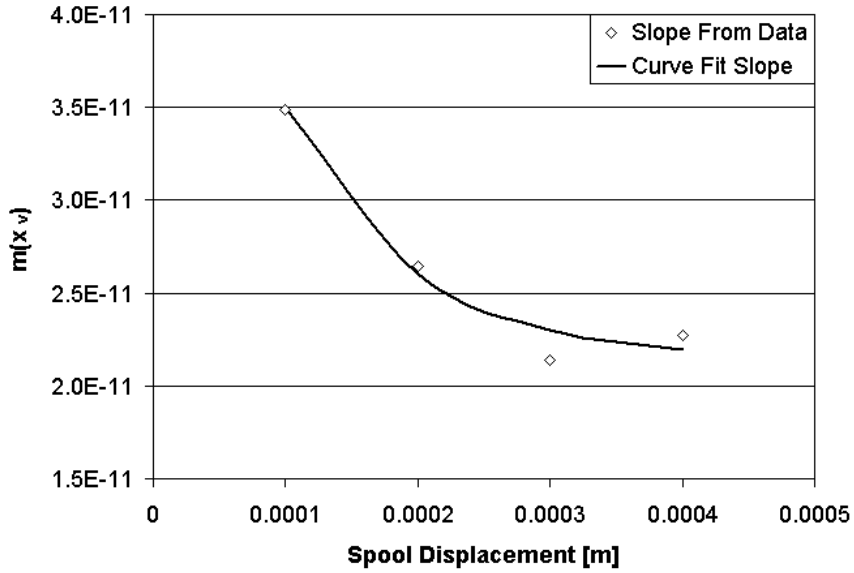

Figure 3.6: Calculated and curve fit slopes of the flow coefficient, K, for various spool displacements.

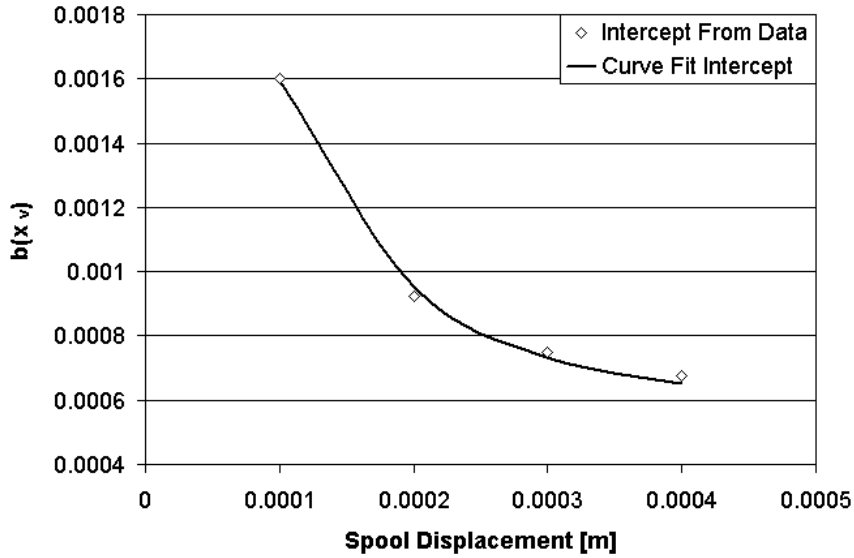

Figure 3.7: Calculated and curve fit intercept of the flow coefficient, K, for various spool displacements.

By comparing the data presented in Figure 3.8 with the data shown in Figure 3.4 it

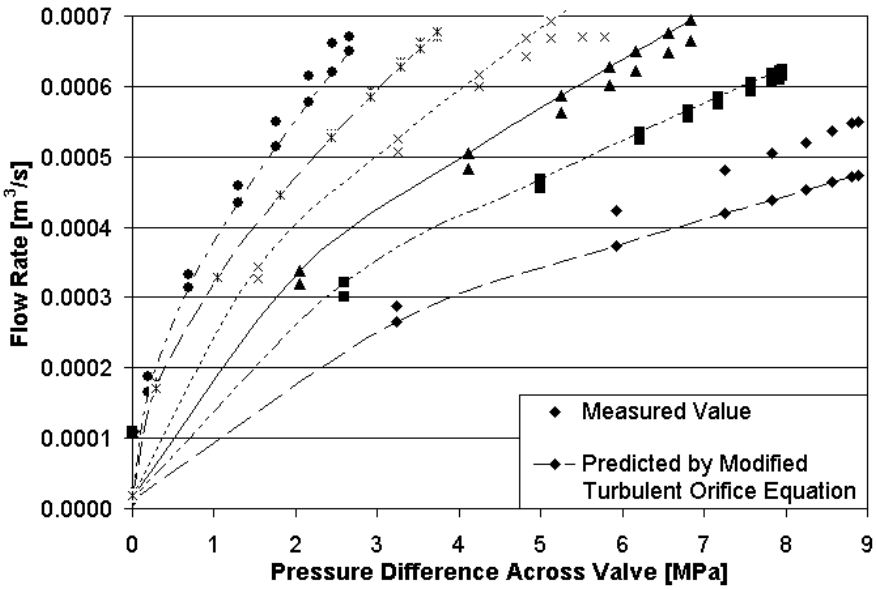

Figure 3.8: Calculated flow rate based on the "modified turbulent orifice equation".

became immediately apparent that the modified orifice equation not only predicted the flow rate for large valve openings (Reynolds numbers) with reasonable accuracy, but that it also provided a good prediction of the flow rate at small valve openings. The accuracy was quantified by the sum of the absolute error between the measured flow rates and those estimated by both the modified and un-modified turbulent orifice equations for the measured differential pressures at each spool position. These results are shown graphically in Figure 3.9.

Of particular importance is the fact that the improvement in the flow rate prediction was achieved with a function that is continuous and differentiable. Furthermore, the data set required was relatively small and was simple to obtain, thus indicating promise of possible adaptation for an online measurement strategy.

The accuracy of the map was limited by the error in the coefficients generated by the series of curve fits. Recall that the data in Figure 3.2 were first reduced to a set of lines by a linear regression (K values). The slope and intercept of these lines were then determined with a second algorithm which fitted the K values to exponential functions. The error in the first regression due to measurement error and outliers

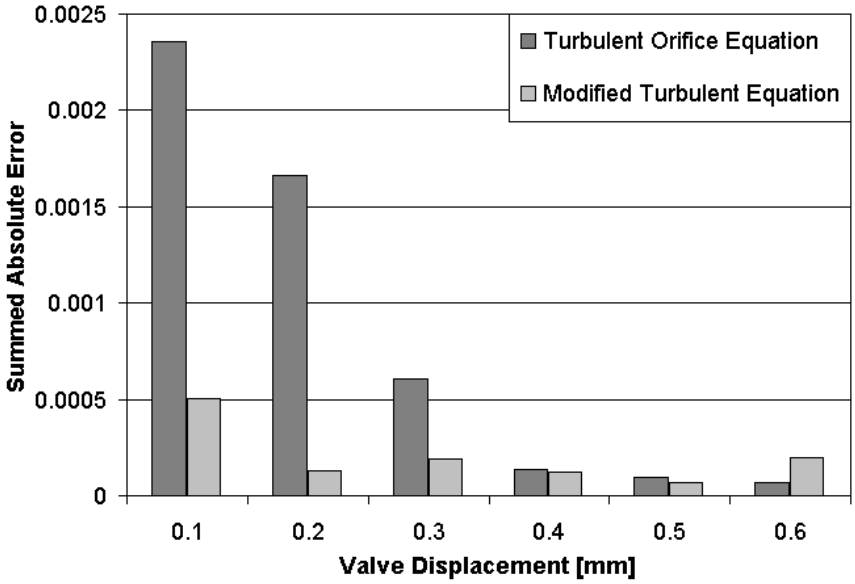

Figure 3.9: Error comparison of the modified and un-modified turbulent orifice equation approximations.

compounded when the slopes and intercepts were then used for the second curve fit. Furthermore, as the technique purposely removed the need for knowledge of the geometry of the valve, the coefficients that were found had no physical counterparts and, as such, could not be analyzed for error sensitivity in any practical sense.

The introduction of these errors did not invalidate the approach as the coefficients produced reasonable flow estimation accuracy and the form of the valve map equation had been verified. It was decided, therefore, that an optimization routine would be employed to refine the coefficients and to determine if an improvement on the curve fitting technique was achievable with an equation of this form. The development and implementation of the optimization routine to the novel valve mapping procedure is the subject of the next section.

3.2.3 Development of the Valve Map Optimization Routine

Mathematically representing the pressure/flow/displacement relationship for a valve over its entire operating range without *a priori* knowledge of its geometry was a

technical challenge as parameters lost their physical significance. This problem was compounded by the desire to show that the function developed in the previous section (Equation 3.5) had the ability to match other orifice configurations.

As an analytical solution for function coefficients was impossible for different flow cases, an optimization routine was developed to generate the best parameter set for the functions in Equations 3.8. This section describes the mathematical details of the optimization routine used and presents relevant results.

The optimization routine employed was the *Downhill Simplex* routine. This routine was a modification of that suggested by Nelder and Mead [30]. This routine is a self-contained method for finding minima in nonlinear problems without requiring the calculation of a gradient. Algorithms of this type were shown to be quite effective when applied to hydraulic systems by Andersson [31].

The advantage of this routine is the reduced number of calculations required as a result of not calculating a gradient in parameter space [31]. The disadvantage is that the routine does not converge as quickly as other methods might. However, these were not deemed crucial to the application as good starting values were always available for the routine and the optimization reached a minima in very few steps as shown later in this section. Furthermore, the compactness of the code relative to other methods (50 lines for the *Downhill Simplex* and over 300 for the *Davidson-Fletcher-Powell*) was deemed a significant advantage in a microcontroller application.

In the optimization process, the *Downhill Simplex Method* manipulates the vertices of a "simplex" to move "down-hill" toward the minima. The simplex is the geometric construct created by $m+1$ parameter sets in coefficient space, where m is the number of parameters in each set. The method approaches the minima based on calculating the instantaneous error of a given data set rather than solving, either explicitly or approximately, for the derivatives of the function to indicate the direction of the minima.

The optimization in this case was a best fit of the flow rate as estimated by the

modified turbulent orifice equation (Equation 3.8) to a measured set of flow rates such as those shown in Figure 3.3. The fitness of a parameter set was evaluated by finding the minimum summed squared error, L, over a set of flows measured at known pressures and spool displacements. Comparing the measured flow to that estimated by Equation 3.8, the function to be minimized was written as,

$$L = \sum_{n=1}^{np} \left\{ Q_n - \left[\left(C_1 + C_2 e^{C_3 x_n} \right) \Delta P_n + \left(C_4 + C_5 e^{C_6 x_n} \right) \right] x_n \sqrt{\Delta P_n} \right\}^2 \qquad (3.9)$$

where:

$$\begin{aligned} n &= \text{current data point,} \\ np &= \text{total number of data points in the data set.} \end{aligned}$$

In order to gain a better understanding of the *Downhill Simplex Method* and evaluate its suitability to minimize Equation 3.9, a function of similar form, but in two-space (C_1, C_2), was considered first:

$$L = \sum_{n=1}^{np} \left\{ Q_n - \left[\left(C_1 + e^{C_2 x_n} \right) \right] x_n \sqrt{\Delta P_n} \right\}^2 \qquad (3.10)$$

In two-space it is possible to plot the error, L, on the vertical axis if a known optimum solution exists. An error surface was therefore generated using Equation 3.10 assuming a global minimum at the coefficients $C_1 = 0.8$ and $C_2 = -1000$, or,

$$\mathbf{S_{opt}} = \begin{bmatrix} C_1 \\ C_2 \end{bmatrix} = \begin{bmatrix} 0.8 \\ -1000 \end{bmatrix},$$

for an arbitrary data set of displacements and pressures. It was then possible to picture how the algorithm moves the simplex through the error space subject to the same displacement and pressure data. A plot of the error space with the location of the global minimum is shown in Figure 3.10.

The principle of the *Downhill Simplex Method* is that given $m + 1$ vertices, a vertex with a smaller error should lie in the direction opposite the vertex exhibiting the

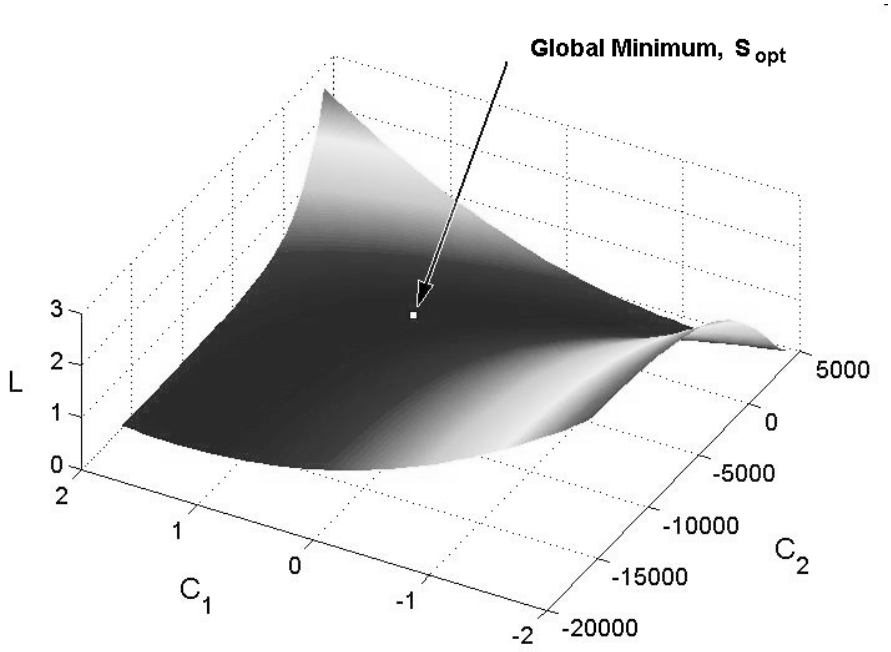

Figure 3.10: Error surface for the contracted function with global minimum indicated.

largest error. Thus, the first step in applying the method is to choose a non-optimal starting set of coefficients (a starting vertex):

$$\mathbf{S_0} = \begin{bmatrix} C_{10} \\ C_{20} \end{bmatrix} = \begin{bmatrix} 1 \\ 3000 \end{bmatrix}.$$

It should be noted that, although this vertex can be chosen arbitrarily, it is useful to consider the length scale of the parameters to avoid lengthy convergence times. As an example, a starting value several magnitudes smaller than the actual value is unadvisable. The starting vertex was then used to generate m additional vertices according to the following mutation routine:

$$\mathbf{S_n} = \left[\lambda_n \lambda_n^T + \mathbf{I}\right] \mathbf{S_0}, \tag{3.11}$$

where λ_n was chosen to be:

$$\lambda_1 = \begin{bmatrix} \sqrt{0.1} \\ 0 \end{bmatrix} \quad \text{and} \quad \lambda_2 = \begin{bmatrix} 0 \\ \sqrt{0.1} \end{bmatrix}$$

to achieve a mutation of 10% for one parameter in each of the two new data sets. The three resulting vertices were plotted on the error surface as shown in Figure 3.11. It is interesting to note that, in two-space, the simplex reduced to a triangle.

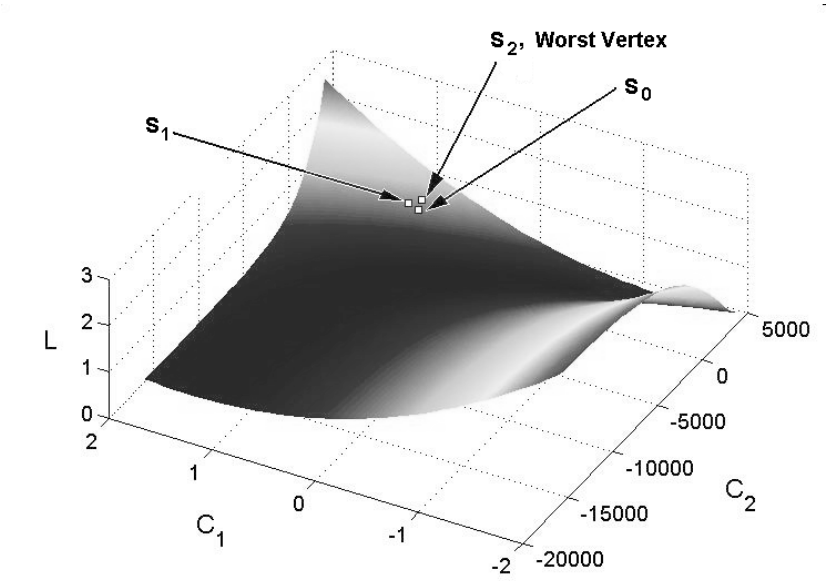

Figure 3.11: Error surface with the initial simplex indicated.

Inspection of the vertex positions relative to the minimum shows that the worst vertex is $\mathbf{S_2}$. Thus, the algorithm found the centroid of the face of the simplex opposite of this worst point.

$$\mathbf{S_{ave}} = \frac{\mathbf{S_0} + \mathbf{S_1}}{m} \tag{3.12}$$

A new set of parameters was then projected along a line from the worst point through the centroid to a new point some factor, k, on the other side of the face, $\mathbf{S_{ave}}$.

$$\mathbf{S_{new}} = \mathbf{S_{ave}} + k(\mathbf{S_{ave}} - \mathbf{S_{worst}}) \tag{3.13}$$

The results of this first iteration are shown in Figure 3.12

The algorithm continued this procedure until it reached a point where the new projected vertex was not an improvement over the worst vertex. At this point the algorithm evaluated two options. First, it tested for an improvement inside the

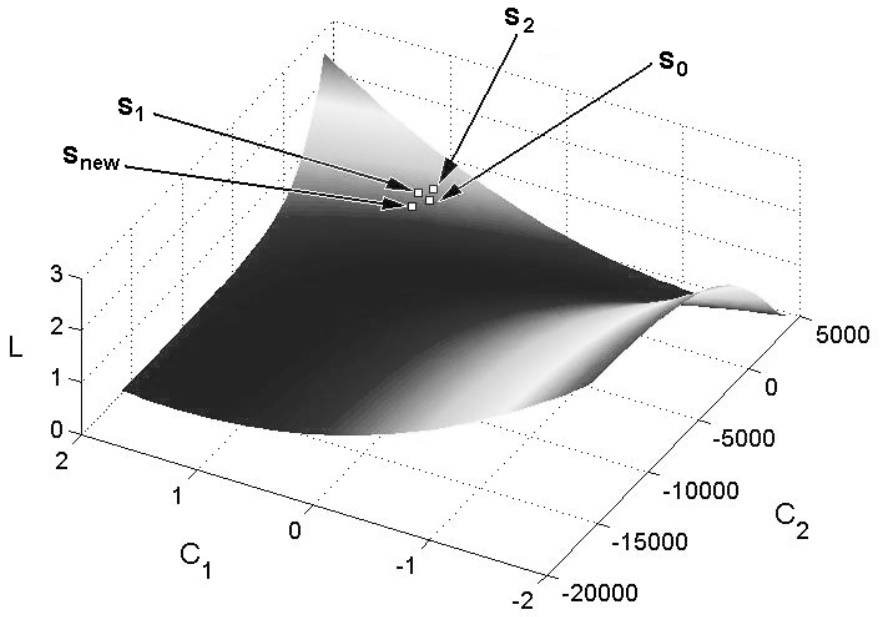

Figure 3.12: Error surface with the initial simplex and first iteration step, $\mathbf{S_{new}}$, indicated.

simplex by making k in Equation 3.13 equal to -0.5. If that failed the algorithm concluded that the minimum lay near the best vertex and contracted around it.

$$\mathbf{S_{m-new}} = \frac{\mathbf{S_m} + \mathbf{S_{best}}}{2} \tag{3.14}$$

The code for the algorithm can be found in Appendix C. The values of the new coefficient vectors are plotted in Figure 3.13 for the first 30 iterations.

Within 30 iterations the algorithm had located the global minimum within 2% for C_1 and 8% for C_2. By 50 iterations this was reduced to 0% for C_1 and 0.01% for C_2. The error was reduced to zero within 60 iterations within the accuracy of MATLAB double precision (16 decimals places). The ability of the routine to locate a minimum in a nonlinear equation of similar form to the modified turbulent orifice equation was verification that the routine was an appropriate choice for tuning the unknown coefficients in Equation 3.8.

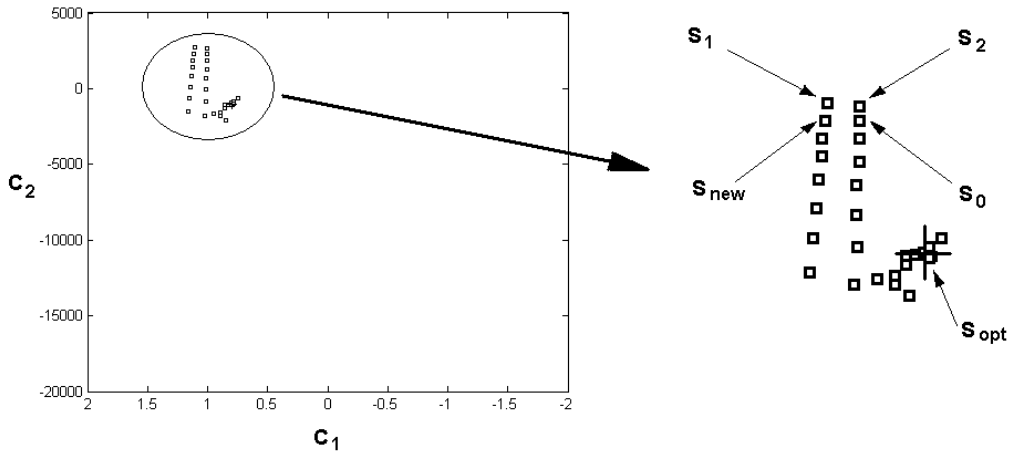

Figure 3.13: Coefficient values for the first 30 steps of the *Downhill Simplex Algorithm* when applied to the example problem. (Left) Full error space. (Right) Exploded view of the area of interest

Unlike the verification tests carried out on the contracted form of the valve map equation, absolute values for the coefficient vector, $\mathbf{S_{opt}}$, for the six-space map were unknown. Thus, a starting point was chosen by examining the length scale of the values determined using the method described in the previous section. Unit values of the same order of magnitude and sign were chosen as starting values. The resulting initialization vector was,

$$\mathbf{S_0} = \begin{bmatrix} 1 \\ 1 \\ -10000 \\ 1 \\ 1 \\ -10000 \end{bmatrix}.$$

The *Downhill Simplex* optimization routine was then employed. Flow rate estimates using the modified turbulent equation with the optimized parameters are shown in Figure 3.14.

Comparisons of errors between the measured and predicted results for the unmod-

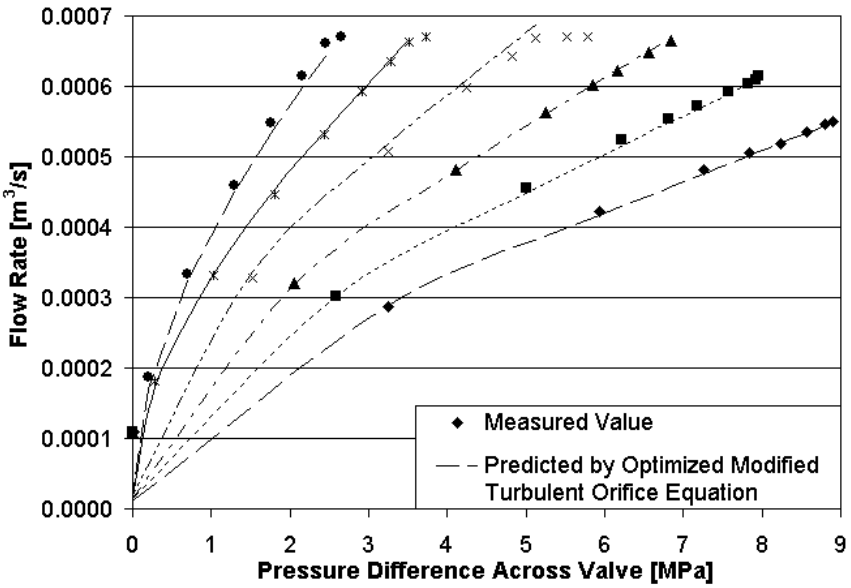

Figure 3.14: Flow rate estimation results using the optimized valve map.

ified turbulent orifice equation, the curve fit modified turbulent equation, and the optimized modified turbulent equation are shown in Figure 3.15.

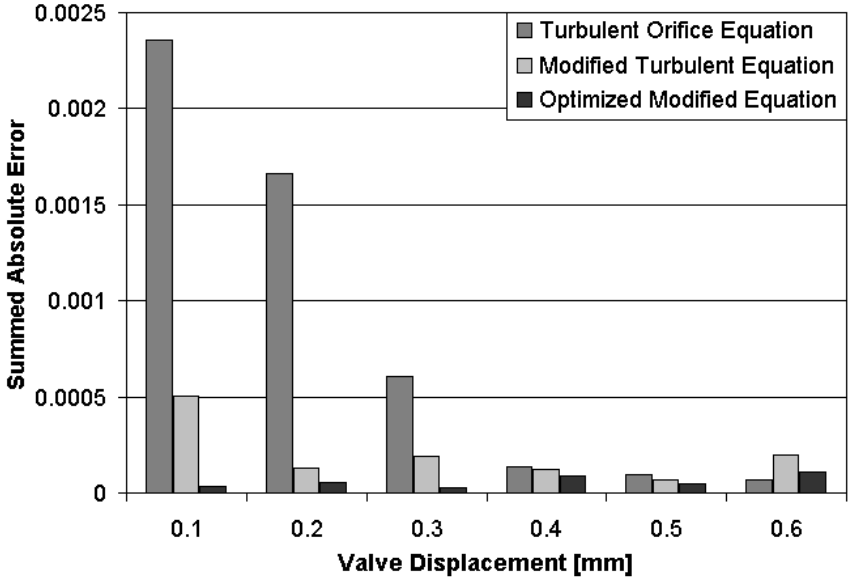

Figure 3.15: Comparison of the error in flow estimation using the unmodified turbulent, the modified turbulent, and the optimized modified turbulent orifice equations.

The results obtained with the optimized modified turbulent equation showed improvement in flow rate estimation over the entire operation range of the valve. Subtle changes in the parameter vector during optimization greatly improved the overall accuracy:

$$\mathbf{S_{curvefit}} = \begin{bmatrix} 2.14 \times 10^{-}11 \\ 4 \times 10^{-}11 \\ -10762 \\ .00061 \\ .0023 \\ -8500 \end{bmatrix} \Longrightarrow \mathbf{S_{optimized}} = \begin{bmatrix} 2.0661 \times 10^{-}11 \\ 6.7309 \times 10^{-}11 \\ -11598 \\ 6.313 \times 10^{-}4 \\ .003 \\ -12785 \end{bmatrix}$$

The optimization discussed thus far concentrated on a range of flows from zero to 6×10^{-4} $\frac{m^3}{s}$ (10 gpm) to meet the flow requirements for the JD 410G loader which was the initial application for this body of research. It was mentioned in Chapter 1, however, that testing and evaluation would be performed first on a robot in the laboratory to provide a more controlled environment. While the robot used had similar geometry to the loader, it was actuated by hydraulic cylinders of significantly smaller diameter. This meant that the maximum acceptable flow rate, as dictated by safe robotic arm velocities, was reduced by more than a half. These small flow rates challenged the sensitivity of the flow meter used in the generation of the original flow rate data set used for the parameter estimation. Therefore, the challenge was to evaluate the flow characteristics of the valve *in situ* in the extreme low flow range.

Detailed flow measurements were performed on the same model of valve in a separate study by Ahlers [32]. These results indicated that abrupt changes in the characteristics occur at low flow rates. The results of the measurements by Ahlers [32] are shown in Figure 3.16. For comparison, the data already presented in Figure 3.3 were reformatted to reflect the units used by Ahlers and are also plotted in Figure 3.16. Note that the valve spool displacement has been adjusted by 1.3 mm to reflect the near-zero flow region evident in Ahlers's map that was beneath the resolution of the flow meter used in the original analysis.

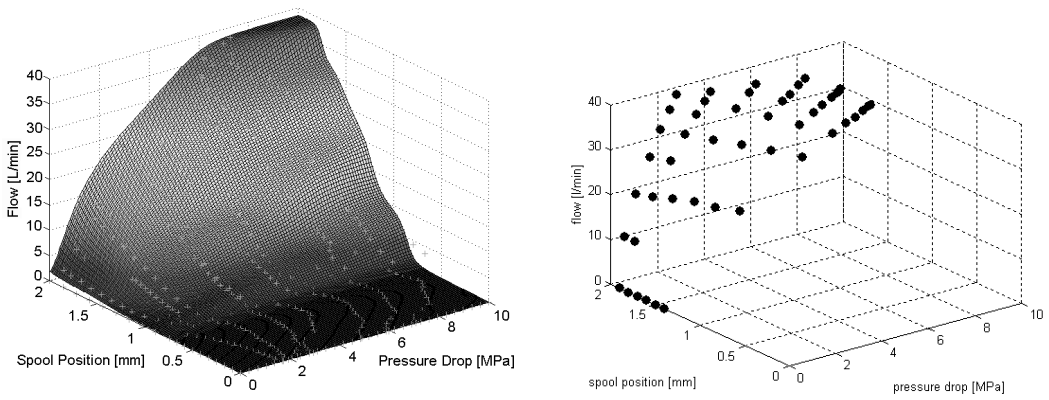

Figure 3.16: (Left) Detailed map of a similar valve generated by Florian Ahlers. Reprinted with permission. (Right) Original flow rate measurements with adjusted units.

Flow rates below $20\frac{L}{min}$ ($0.0003\ \frac{m^3}{s}$) represent the working range required by the robotic arm circuit. This region is below the range of the initial tests and enters a region where the pressure/flow/displacement relationship exhibits some complex behaviour as seen in Figure 3.16 (Left). This change in operating range was taken as an opportunity to show the flexibility of the valve mapping approach and the ability of the modified turbulent orifice equation to estimate a diverse range of flow profiles.

A low flow data set was obtained by replacing the flow meter and downstream relief valve in Figure 3.2 with the hydraulic actuator of the laboratory robot which was equipped with an LVDT for displacement measurement. The output of the LVDT was numerically differentiated and multiplied by the piston area to give a measure of the flow rate. The testing procedure was as follows:

1. The system was forced to dump oil over the relief valve until the temperature measured at the pump outlet stabilized (approximately $36°C$).

2. The valve spool displacement was set at $2.0\times10^{-4}\ m$ and the supply pressure was set to $3.44\ MPa$ ($500\ psi$).

3. The differential pressure, flow rate, and valve spool displacement were recorded for the full range of motion of the robot or $30s$, whichever occurred first.

4. This procedure was repeated at the same valve spool position with the supply pressure increased by 0.69 MPa (100 psi) for each additional run to a maximum supply pressure of 6.9 MPa (1000 psi).

5. The spool displacement was increased by 2.0×10^{-4} m and the process was repeated. The maximum spool displacement considered was 2.6×10^{-3} m.

The measured flow rates were time averaged in the steady state portion of each run and compiled into a valve map representing the low flow characteristics of the valve and are presented in Figure 3.17.

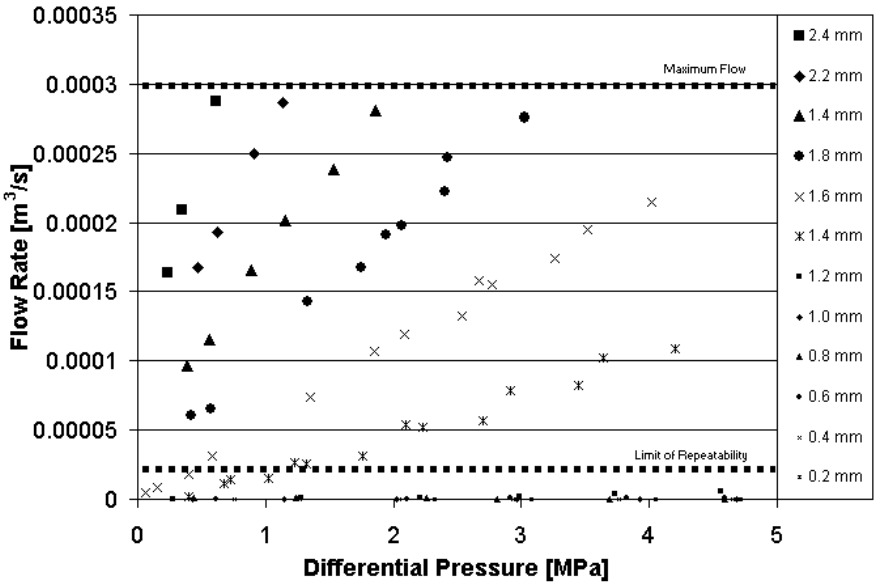

Figure 3.17: Flow rate measurements in the low flow region for variable differential pressure and valve spool displacements.

It was noted that an abrupt change in the flow rate occured between 1.2 mm and 1.4 mm. This is consistent with the measurements made by Ahlers. Furthermore, for spool displacements less than 1.4 mm the flow rates were so small that the resulting motion of the robotic arm was not visually discernable. Also, the motion of the robotic arm for these small valve openings, and hence the measurement of flow rate, was highly influenced by phenomena in the robotic arm such as friction and leakage and the tests in this spool displacement range were not repeatable. For these reasons,

the flow rates for spool displacements less than 1.4 *mm* were not considered in the remaining analysis.

The *Downhill Simplex* optimization routine was applied to the objective function given in Equation 3.9 for the low flow data set excluding values below the limit of repeatability. The measured results and estimates from the optimized equation are presented in Figure 3.18.

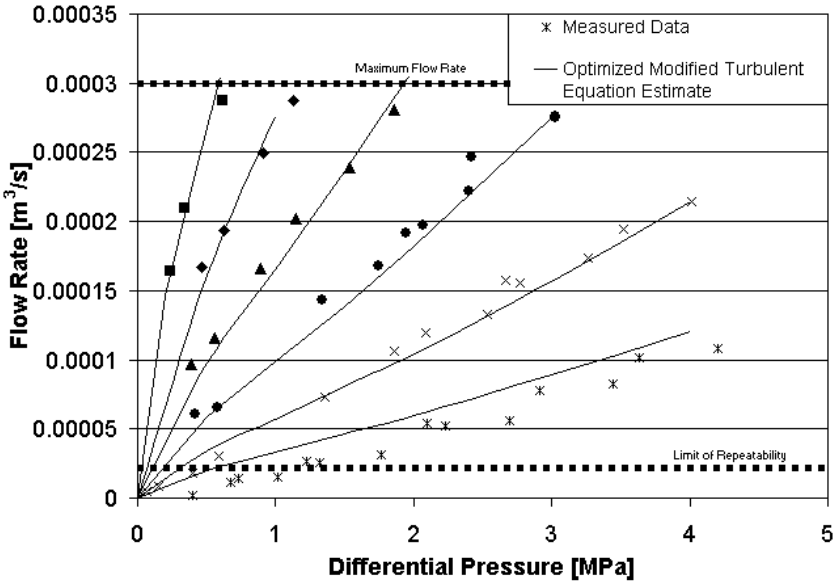

Figure 3.18: Flow rate estimates found using the modified turbulent orifice equation with range specific optimized parameters.

The estimated flow results in Figure 3.18 were obtained using Equation 3.8 with the following optimized coefficients:

$$\mathbf{S_{smallflow}} = \begin{bmatrix} 1.838 \times 10^{-14} \\ 1.346 \times 10^{-12} \\ 27003 \\ 5.911 \times 10^{-8} \\ 6.9249 \times 10^{-6} \\ 22366 \end{bmatrix}$$

The most intriguing difference in the large flow and small flow parameter sets is the

change in sign of the coefficients $S(3)$ and $S(6)$. This is indicative of a discharge coefficient which increased with valve spool displacement as opposed to decreased. This behaviour is consistent with a Reynolds based correction to the discharge coefficient of the turbulent orifice equation put forward by Merritt [21] for extending that equation into the laminar range.

The results achieved in the large and small flow analysis verified that the method for valve mapping introduced in this section is applicable to a wide range of flow characteristics. This was an especially important result as one of the goals of this research was to develop a method which could be easily applied to any given valve whose characteristics may differ from those of the valve used in this study.

3.3 Evaluation of the Accuracy of the Modified Turbulent Orifice Equation

The purpose of developing an accurate valve map strategy was to incorporate this information in an open loop system capable of predicting the velocity of a hydraulically actuated link without direct feedback of either flow rate or velocity. The link between attainable accuracy in velocity control and accuracy of flow estimation was emphasized in the first chapter of this thesis. In this section, the evaluation of the accuracy of the developed modified orifice equation valve map is described.

This evaluation of the accuracy of the flow map was performed in two stages. First recorded data for the flow rate under the conditions of fixed spool displacement and variable pressure were compared to flow rate estimates under the same conditions. This allowed for the determination of a "zone of confidence" which set limits on the allowable range of flows, valve spool displacements, and pressures in which the valve map could be considered an accurate predictor. Next, the valve map was used in conjunction with the model reference controller developed in Chapter 2 to create a pressure compensated flow estimator. The performance of this estimator in estimating flow in real-time was evaluated.

3.3.1 Evaluation for Fixed Spool Displacement

The optimization procedure described in the previous section produced a set of parameters for the modified turbulent orifice equation which produced qualitatively good performance. The purpose of the analysis presented in this section is to quantify that performance. This was done by determining the operating conditions of the pressure and flow in the domain and range shown in Figure 3.18 in which the parameter set and the modified turbulent orifice equation produced estimates within a fixed criteria. This set of operating conditions was termed the "zone of confidence".

The evaluation discussed in this section employed the same recorded values that were time averaged to create the data points in Figure 3.17. The differential pressure and spool displacement time series were used as input values to the modified turbulent orifice equation to generate flow rate estimates. These estimates were then compared to the recorded flow rates at the same operating conditions. Typical results are shown in Figure 3.19.

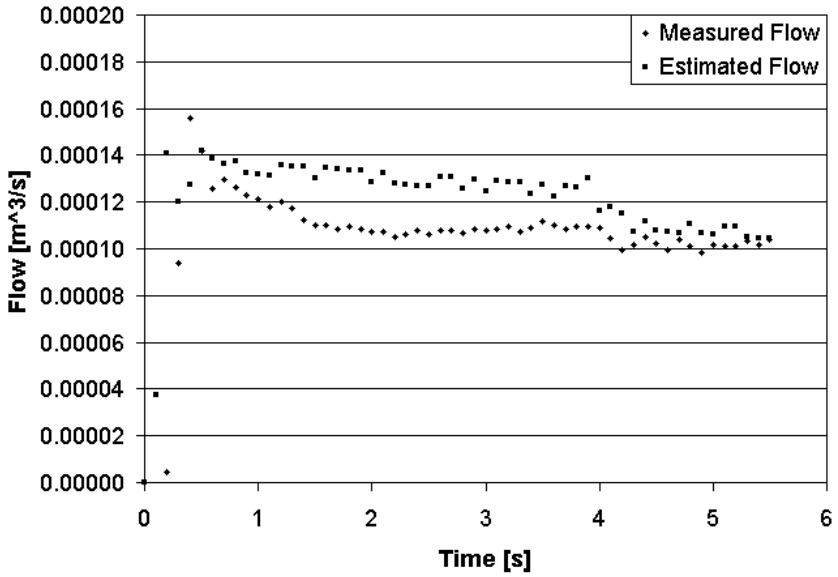

Figure 3.19: Measured and estimated flow rate results for $x_v = 1.6\ mm$ and $Ps = 6.89\ MPa$.

The example shown in Figure 3.19 was chosen for inclusion as it illustrates several

criteria used to determine the valve map zone of confidence. The first step in the analysis was to determine the Percent Root Squared Relative Error (%RSRE) which is defined as:

$$\%RSRE = 100 * \sqrt{\frac{(Measured - Estimated)^2}{Measured^2}}. \tag{3.15}$$

The %RSRE for the series presented in Figure 3.19 is shown in Figure 3.20.

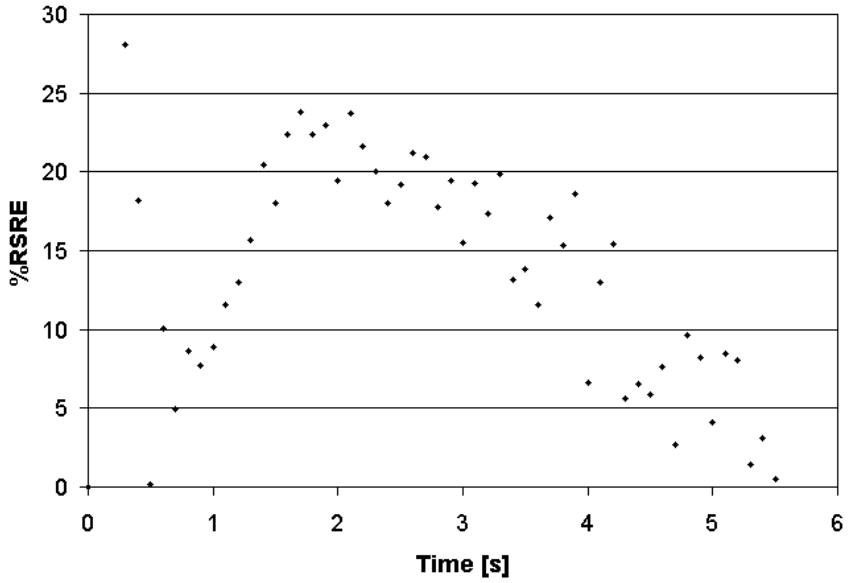

Figure 3.20: Root squared relative error (%RSRE) between measured and estimated flow rate results for $x_v = 1.6mm$ and $Ps = 6.9MPa$.

The results shown in Figure 3.20 confirm a trend which is apparent in Figure 3.19 which is that there are two distinct operating points in this time series following the initial transient phase. These operating points corresponded to a change in the load pressure, and hence the differential pressure, as the robotic arm moved through its trajectory. This is more clearly demonstrated by plotting the same %RSRE against the differential pressure rather than time as shown in Figure 3.21.

Two peaks appear in these results corresponding to two distinct differential pressure operating conditions. At the lower operating condition, the %RSRE is less than 10%, but it exceeds this value for the higher condition. A %RSRE of 10% was

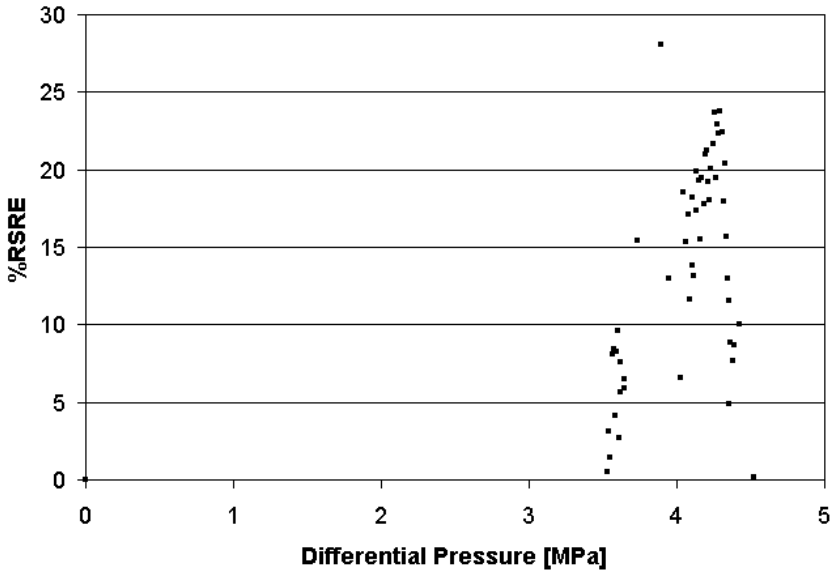

Figure 3.21: Root squared relative error (%RSRE) between measured and estimated flow rate results for $x_v = 1.6mm$ and $Ps = 6.9MPa$ plotted against differential pressure.

chosen to be the maximum acceptable value for the flow estimation error based on what value constitutes a perceivable error to the system operator. Thus, the conclusion in this case was that the modified turbulent orifice equation was valid for spool displacements in the neighbourhood of $x_v = 1.6\ mm$ for differential pressures between $\Delta P = 3.5\ MPa \rightarrow 4\ MPa$. The range of operating conditions covered by this time series is indicated by the rectangular area #1 in Figure 3.22. This procedure was repeated for nine other operating ranges (#2-#10) also indicated in Figure 3.22. The time series and %RSRE plots for these ranges are given in Appendix D.

Examination of the ten operating conditions and application of the 10% root squared relative error criteria allowed the zone of confidence boundary to be determined and this is shown on Figure 3.23. To reiterate, this zone of confidence illustrates the region of flow rates and pressure differentials in which the modified turbulent orifice equation, employing the parameter set determined by the low flow optimization, will

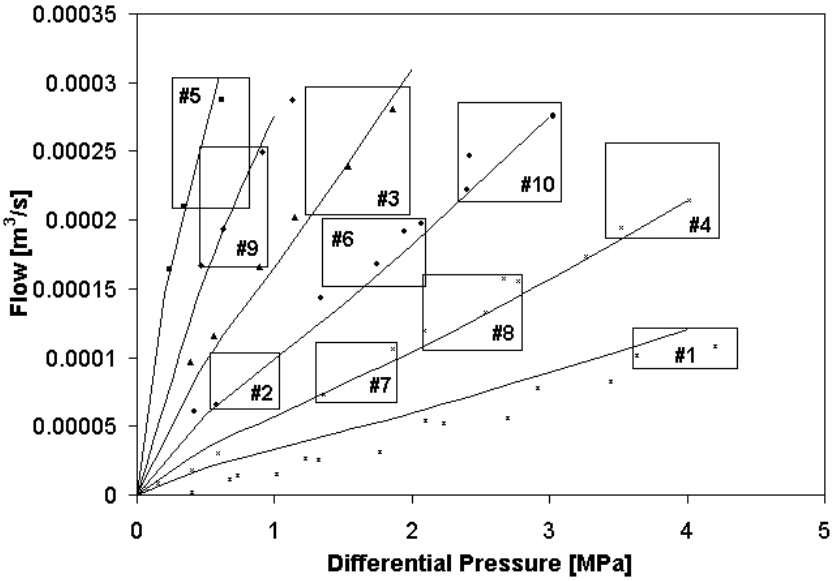

Figure 3.22: Operating ranges encompassed by the tests which were evaluated to determine the zone of confidence.

predict the flow rate within 10% root squared relative error.

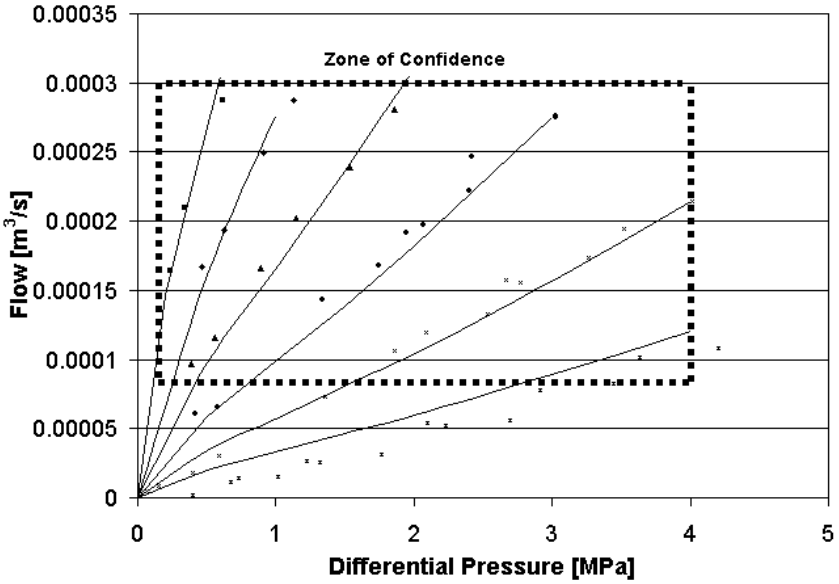

Figure 3.23: Ranges evaluated to determine the zone of confidence.

3.3.2 Evaluation for Dynamically Varying Spool Displacement

In the previous section, the experimental procedure involved setting the spool displacement at a constant value and varying the differential pressure with the flow rate being measured. To evaluate the effectiveness of the modified turbulent orifice equation when subject to dynamically varying spool displacements, a second test apparatus and procedure was developed. In this case, the hydraulic actuator of the robotic arm was made to track a velocity input which varied sinusoidally while being subject to variable differential pressure. The spool position was made to adjust accordingly by a feedback control system.

The feedback control system involved incorporating the valve in a closed loop PID position control loop. A position control system as opposed to a velocity control system was chosen to avoid drift. The velocity was obtained by numerically differentiating the position measurements. A sinusoidal displacement input with a peak-to-peak amplitude of 18 cm was used to ensure that the actuator, and consequently the robotic arm, moved through the greater part of its trajectory. The frequency of the sinusoidal input was varied to provide a range of maximum velocities, and hence flow rates, within the determined zone of confidence. The feedback control system is shown in the block diagram in Figure 3.24. An example of the desired input velocity and the measured actuator velocity is presented in Figure 3.25.

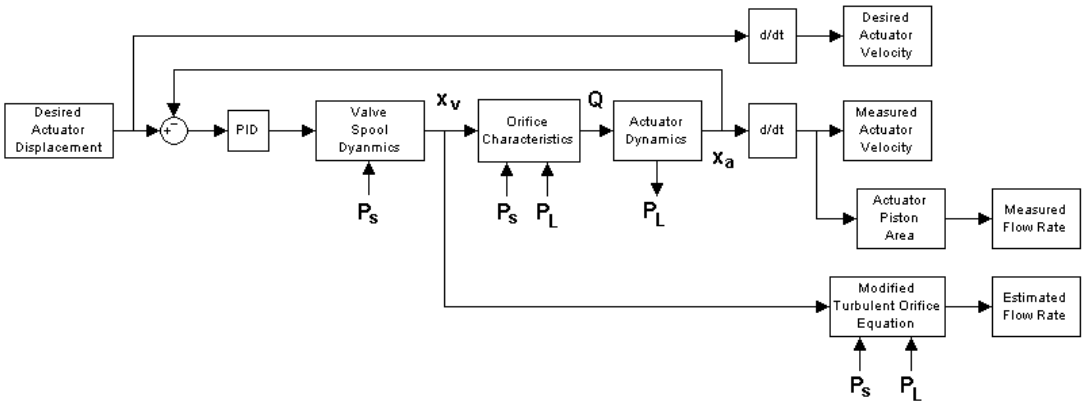

Figure 3.24: Block diagram of the flow estimator.

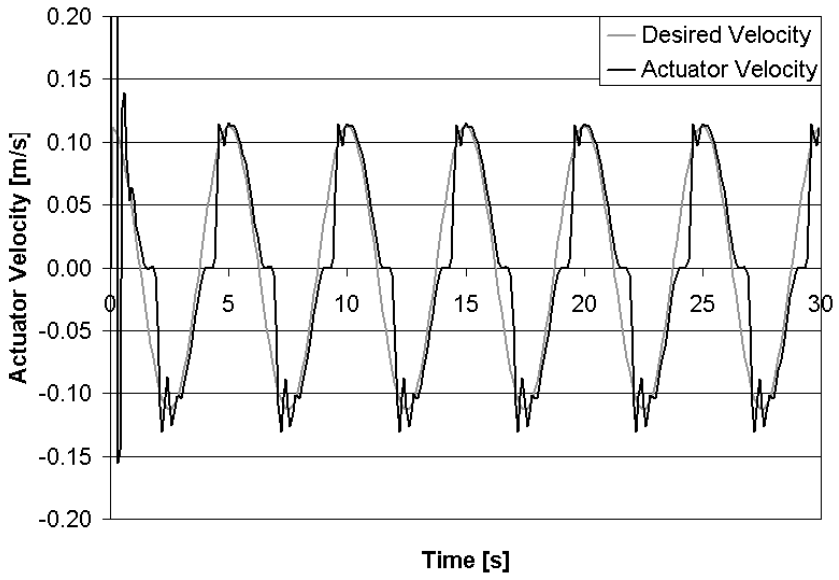

Figure 3.25: Sinusoidal tracking using a linear PID controller and actuator position feedback.

It was evident from data such as those presented in Figure 3.25 that the linear controller was not able to produce accurate tracking control, particularly about the null flow rate. This was not unexpected given the nonlinear nature of the valve and load. This tracking problem is one of the reasons for developing a nonlinear predictive feedforward strategy as will be discussed in the final chapter of this thesis. The accuracy of the PID tracking was not the issue, however. It was of interest to

determine if the valve map could predict the flow regardless of the trajectory.

Nine tests were run under changing operating conditions which were chosen to reflect the entire domain and range encompassed by the zone of confidence. Covering the full velocity range of the zone of confidence required three input frequencies of 0.1, 0.16, and 0.2 Hz and spanning the pressure range required supply pressures of 4.13, 5.52, and 6.89 MPa. The same warm up procedure discussed earlier in this chapter was used before the start of testing. Presented in Figure 3.26, as an example, are the measured and estimated results for a half wave of a sinusoidal input with a frequency of 0.16 Hz and a supply pressure of 4.14 MPa (600 psi).

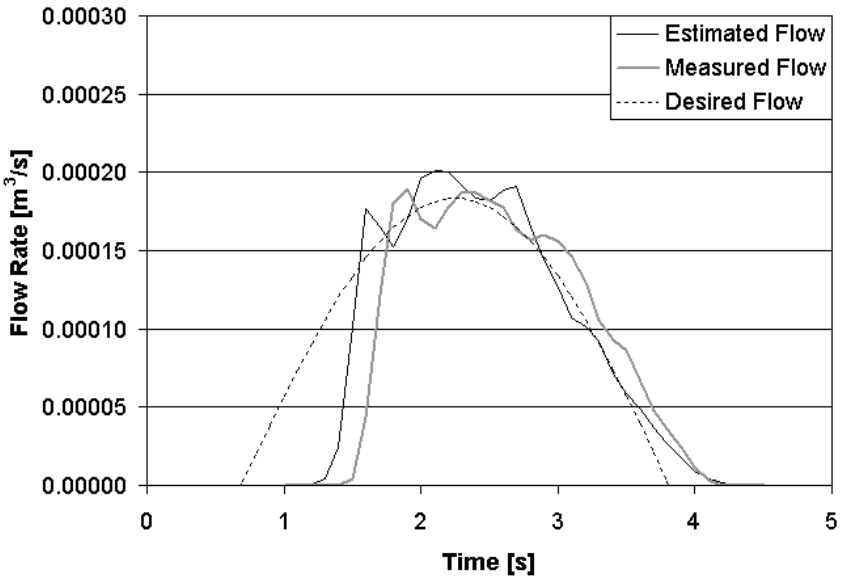

Figure 3.26: Measured and estimated flow results for an input frequency of 0.16 Hz and a supply pressure of 4.14 MPa.

It can be seen in Figure 3.26 that some discrepancy exists between the measured flow rate and that predicted by the valve map. The most obvious difference is that the measured value *lags* the predicted value. This is a result of a transmission delay through the hydraulic lines as the flow estimate is determined at the valve and the measured flow is determined from the cylinder motion. For the purposes of evaluating the accuracy of the modified turbulent orifice equation the delay was

removed by post processing the measured flow rate data. The corrected results with the delay removed are shown in Figure 3.27.

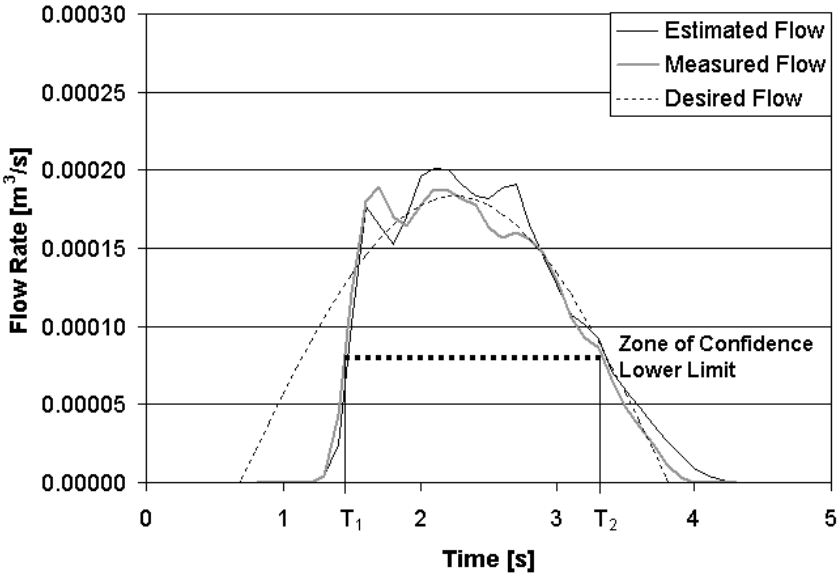

Figure 3.27: Measured and estimated flow results for an input frequency of 0.16 Hz and a supply pressure of 4.14 MPa with time delay removed.

The instantaneous error is shown in Figure 3.28 and quantifies what is visually apparent in Figure 3.27; namely, that at this operating point the valve map estimates are centred about the measured data with pressure transients causing fluctuations and resulting spikes in the error.

The %RSRE was used as the standard measure of flow prediction performance. Recall that a %RSRE of 10% for values within the zone of confidence was considered acceptable estimation performance. A plot of the %RSRE in this region is shown in Figure 3.29.

In the region of interest, T_1 to T_2, the mean %RSRE was 8.7% with a standard deviation of 6.1%. The results were deemed acceptable as the supply pressure used in this run was marginal to operate given the inertia of the robotic arm which lead to large transient values which were difficult to track. This problem diminishes with higher supply pressures as can be seen by comparing the time series (Figure 3.26)

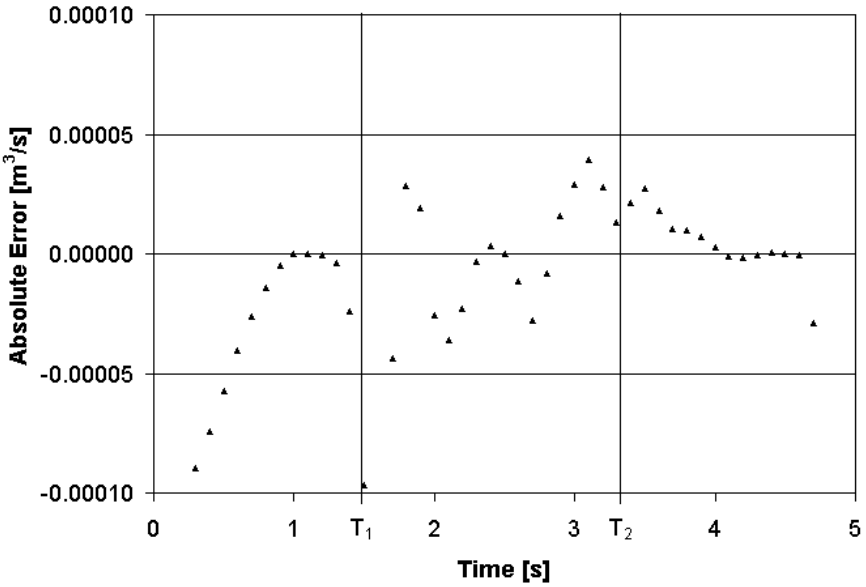

Figure 3.28: Instantaneous error between measured and estimated flow results for an input frequency of 0.16 Hz and a supply pressure of 4.14 MPa with time delay removed.

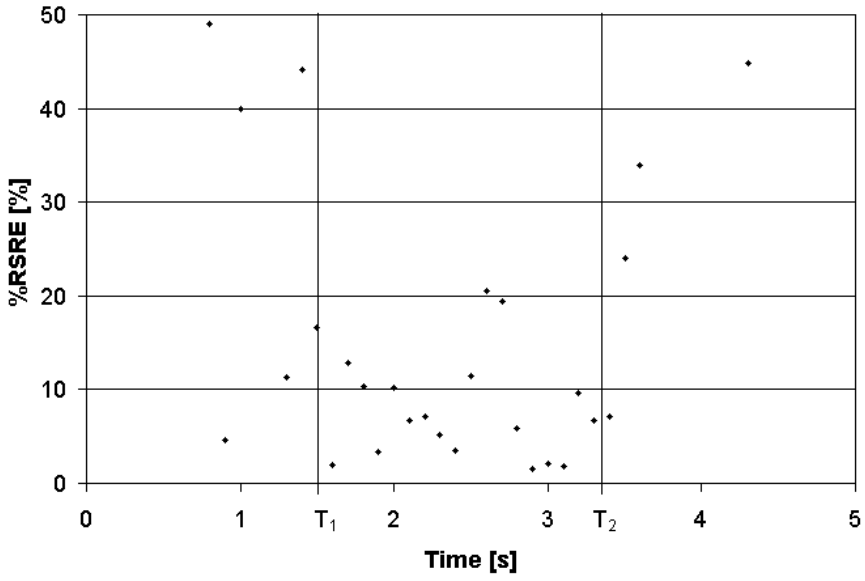

Figure 3.29: The root squared relative error (%RSRE) between measured and estimated flow results for an input frequency of 0.16 Hz and a supply pressure of 4.14 MPa with time delay removed.

and %RSRE (Figure 3.29) for the case just discussed (P_s=4.14 MPa, $f = 0.16Hz$) with the time series and %RSRE for the same input frequency at a significantly higher supply pressure (P_s=6.89 MPa) as shown in Figures 3.30 and 3.31.

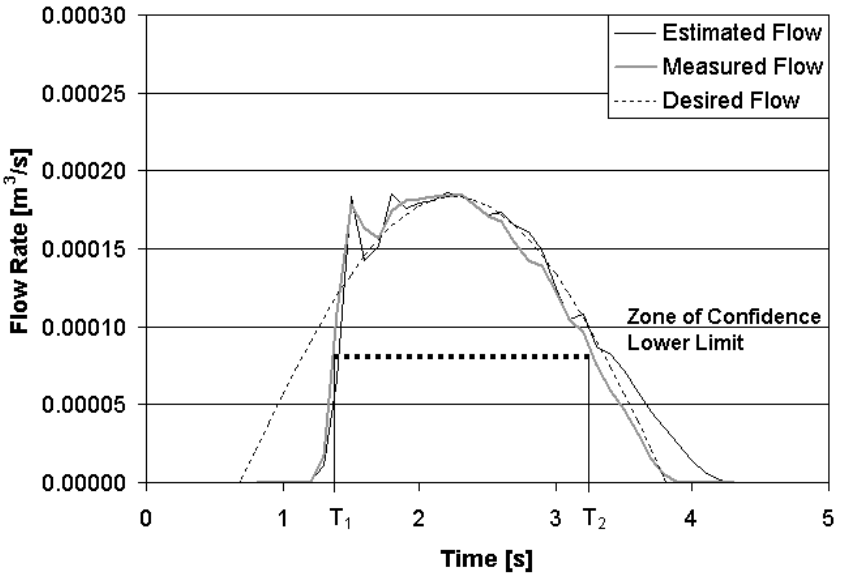

Figure 3.30: Measured and estimated flow results for an input frequency of $0.16Hz$ and a supply pressure of 6.89 MPa.

As mentioned earlier, nine test cases covering the entire zone of confidence were examined and in every case the mean %RSRE for flow rates within the zone of confidence were less than 10%. This was confirmation that the modified turbulent orifice equation provided an accurate real-time estimate of the flow rates for this valve over the prescribed range of operating conditions.

3.4 Concluding Comments on Flow Estimation With a Spool Type Valve

In the introduction to this thesis a velocity control solution for a hydraulically actuated mechanism based on flow control was proposed. Due to practical constraints, it was decided to develop a single component predictive flow controller. This chapter

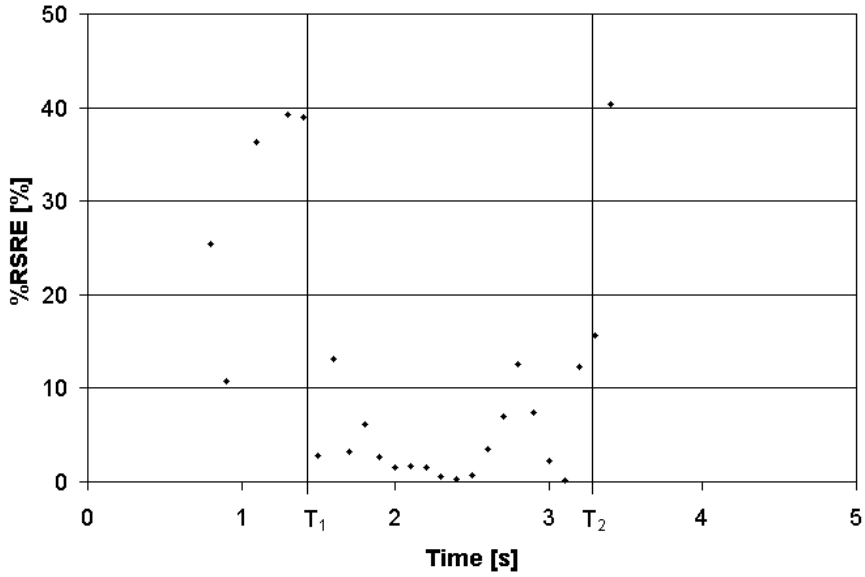

Figure 3.31: The root squared relative error (%RSRE) between measured and estimated flow results for an input frequency of 0.16 Hz and a supply pressure of 6.89 MPa.

outlined the first step in this process, which was to develop a means of characterizing the flow rate through a valve and representing those characteristics in a compact mathematical fashion.

In the course of this, a new empirically determined and optimized form of the turbulent orifice equation was developed. This equation and the experimental approach used to determine its coefficients proved quite versatile as it was used effectively to estimate the flow through a valve which was operating at the low end of its intended operating range with an acceptable accuracy. The material in this chapter was consistent with Research Goal #3 as discussed in Chapter 1.

The next step in developing the predictive velocity controller was to examine the mechanism to be controlled. The kinematics of the mechanism relate the angular velocity of the arm to the linear velocity of the actuator. The linear velocity is related to the flow rate, the control of which will depend on the material developed in this chapter. The kinematics of the robot are the subject of the next chapter.

Chapter 4

Kinematics of the Robot

The operating characteristics of the specific proportional valve used in this study were discussed in Chapter 2. Material presented in Chapter 3 demonstrated the feasibility of using a modified turbulent orifice equation to achieve flow rate estimation with a valve of this type. In this chapter the question of what output a human operator in the control loop wishes to control is addressed. The necessary mathematical relationships between flow rate to the actuator and desired output from the view of the operator are developed. To facilitate this discussion, the application toward which this research was originally oriented will be considered.

As discussed in Chapter 1 this project was based on the "vision" of automating some functions of a front-end loader while still allowing an operator in the loop to provide visual feedback of the angular velocity of the boom arms during manual operation. From the point of view of the operator, it is desirable to obtain one-to-one correspondence between an input signal and the angular velocity of the linkage. As discussed in the introductory chapter, in order to establish the feasibility of the flow prediction approach under controlled conditions, a laboratory robot which functioned in a similar fashion to the loader boom arms was used in this study. This laboratory robot is shown schematically in Figure 4.1.

Consider Figure 4.1. The robot has revolute joints at A, B, and C with the A and C joints fixed in translation. The arm rotates due to flow entering the hydraulic

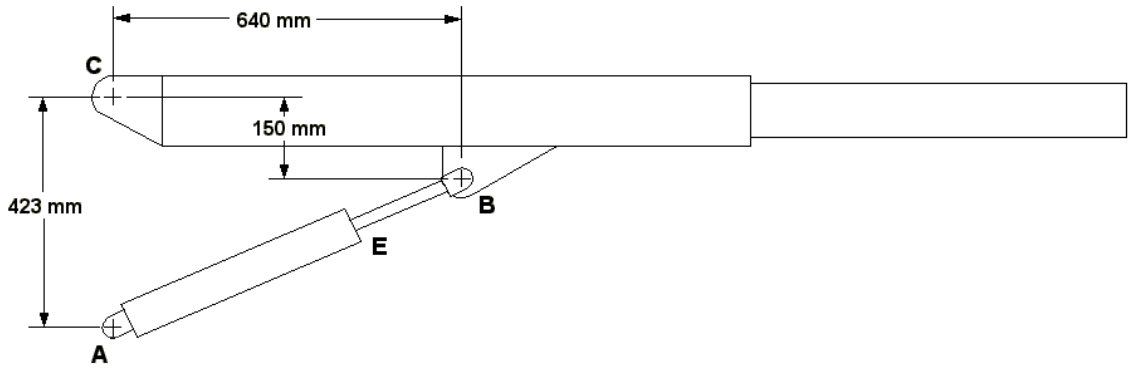

Figure 4.1: Schematic representation of the laboratory robot.

actuator which extends at E. The required mathematical relationship to introduce one-to-one correspondence between operator input and boom angular velocity was that which related the angular velocity of the arm about joint C, and the linear velocity of the hydraulic actuator. It can also been seen from Figure 4.1 that the actuator represents a variable length linkage that can be described in terms of a fixed length (representing a bottomed out cylinder) and a piston extension length.

A notation, θ, was chosen for the angular displacement of the arm about joint C. For the purposes of calibration, the horizontal arm position was chosen as $\theta = 0$. Rotation above the horizontal was considered positive. The range of motion of the robot was thus defined to be in the domain $-18.5^\circ \leq \theta \leq 28.75^\circ$. Consequently, the angular velocity of the robot, $\dot{\theta}$, was positive in the upward direction.

The remainder of this chapter contains the development of the kinematic equations which describe the relative motion of the linkage components and the experimental verification thereof.

4.1 Displacement Analysis

For the kinematic analysis, the nomenclature illustrated in Figure 4.2 was adopted. A vector representation of the mechanism is shown in Figure 4.3.

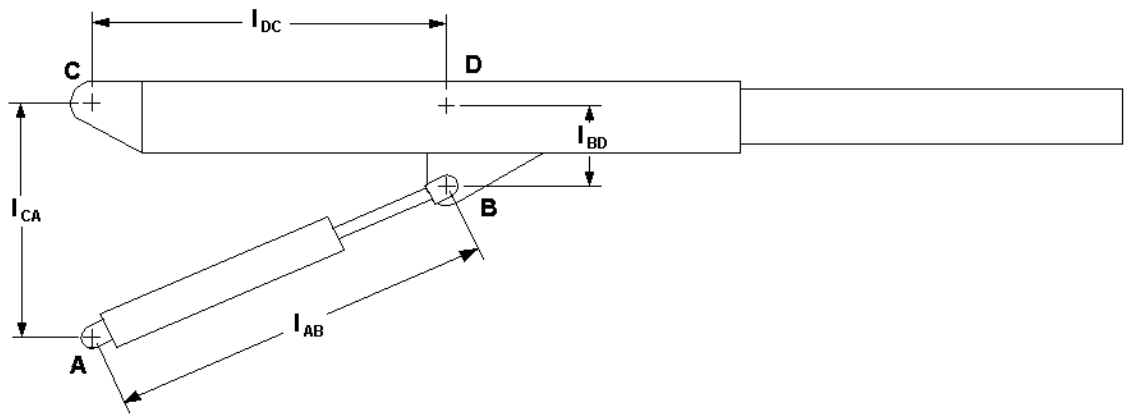

Figure 4.2: Linkage dimensions of consequence for the development of the describing kinematics.

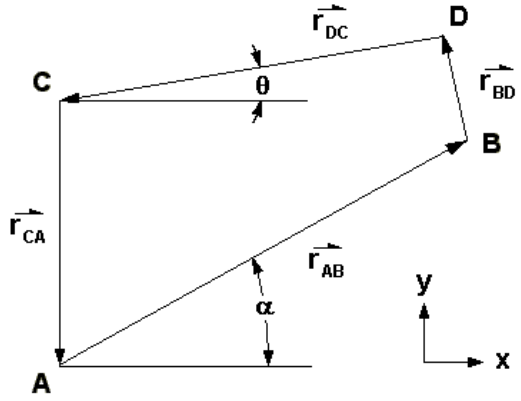

Figure 4.3: Vector representation of the robot linkages.

Since the two vectors, $r_{\vec{DB}}$ and $r_{\vec{CD}}$, were of fixed length and were rigidly connected at point D, they were combined. The reference angle, θ, was adjusted to reflect the orientation of the combined vector and this adjusted value was termed, θ^*. This is shown graphically in Figure 4.4.

The mathematical expressions determined for this combination were:

$$r_{\vec{BD}} + r_{\vec{DC}} = r_{\vec{BC}}, \tag{4.1}$$

and,

$$\theta = \theta^* + atan\frac{|r_{\vec{BD}}|}{|r_{\vec{DC}}|}. \tag{4.2}$$

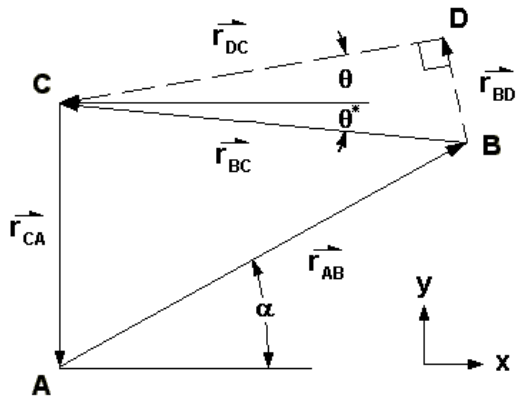

Figure 4.4: Vector representation of the robot linkages with $\vec{r}_{DB}$ and $\vec{r}_{CD}$ combined. Note: the quantity, θ^*, is negative in this case.

Thus, the length of the actuator relative to the angle of the boom was deduced from the following vector sum:

$$0 = \vec{r_{AB}} + \vec{r_{BC}} + \vec{r_{CA}}. \tag{4.3}$$

Application of the coordinate system indicated in Figure 4.4 allowed Equation 4.3 to be written in terms of the two reference angles, α and θ^*,

$$0 = l_{AB}(\hat{i}cos\alpha + \hat{j}sin\alpha) + l_{BC}(-\hat{i}cos\theta^* - \hat{j}sin\theta^*) + l_{CA}(-\hat{j}). \tag{4.4}$$

The terms, $\hat{i}$ and $\hat{j}$, were collected, yielding two equations,

$$\hat{i}: \quad 0 = l_{AB}cos\alpha - l_{BC}cos\theta^*, \tag{4.5}$$

and,

$$\hat{j}: \quad 0 = l_{AB}sin\alpha - l_{BC}sin\theta^* - l_{CA}. \tag{4.6}$$

The unknown quantity, α, was found in terms of the other two unknowns, l_{AB} and θ^*, by first collecting terms containing α on the left hand side,

$$l_{AB}cos\alpha = l_{BC}cos\theta^*, \tag{4.7}$$

and,

$$l_{AB}sin\alpha = l_{BC}sin\theta^* + l_{AC}. \tag{4.8}$$

Equation 4.8 was divided by Equation 4.7, which yielded,

$$tan\alpha = \frac{l_{BC}sin\theta^* + l_{AC}}{l_{BC}cos\theta^*}, \tag{4.9}$$

or,

$$\alpha = atan\left(\frac{l_{BC}sin\theta^* + l_{AC}}{l_{BC}cos\theta^*}\right). \tag{4.10}$$

The length of the actuator, l_{AB}, as a function of the angular displacement of the boom, θ^*, was then found through substitution of Equation 4.10 into Equation 4.7:

$$l_{AB} = \frac{l_{BC}cos\theta^*}{cos\left[atan\left(\frac{l_{BC}sin\theta^* + l_{AC}}{l_{BC}cos\theta^*}\right)\right]}. \tag{4.11}$$

This relationship was verified by instrumenting the laboratory robot. An RVDT was placed on the boom pivot pin and an LVDT was placed on the actuator. The actuator displacement as calculated from the angular displacement by Equation 4.11 was compared to the displacement measured by the LVDT. Typical results are presented in Figure 4.5.

The results were coincidental as expected. A velocity analysis was then performed based on this position analysis.

4.2 Velocity Analysis

A velocity analysis was performed in order that the angular velocity of the robot arm could be related to the velocity of the hydraulic actuator. As a starting point

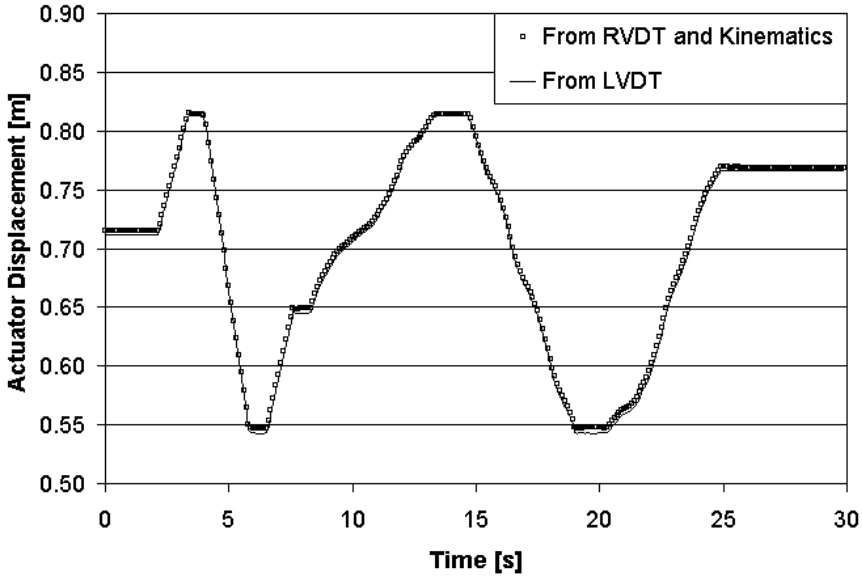

Figure 4.5: Verification of the kinematic position analysis.

the velocity of joint B in Figure 4.2 was considered. Considering the relative velocity of B with respect to C $\vec{v}_B$ is given as,

$$\vec{v_B} = \dot{\theta} l_{BC}(-\hat{i}sin\theta^* + \hat{j}cos\theta^*). \tag{4.12}$$

Also, the velocity of B with respect to A was,

$$\vec{v_B} = \dot{\alpha} l_{AB}(-\hat{i}sin\alpha + \hat{j}cos\alpha) + \dot{l}_{AB}(\hat{i}cos\alpha + \hat{j}sin\alpha). \tag{4.13}$$

The terms, $\hat{i}$ and $\hat{j}$, were collected yielding two equations,

$$\hat{i}: \quad -\dot{\theta} l_{BC} sin\theta^* = -\dot{\alpha} l_{AB} sin\alpha + \dot{l}_{AB} cos\alpha, \tag{4.14}$$

and,

$$\hat{j}: \quad \dot{\theta} l_{BC} cos\theta^* = \dot{\alpha} l_{AB} cos\alpha + \dot{l}_{AB} sin\alpha. \tag{4.15}$$

The link length containing the actuator, l_{AB}, can be calculated from Equation 4.11 and the link length, l_{BC}, was constant. The user input was an angular velocity of the

arm, $\dot{\theta}$, and the desired output was the actuator linear velocity, $\dot{l}_{AB}$. The unknown variable, $\dot{\alpha}$, was isolated from Equation 4.14,

$$\dot{\alpha} = \frac{\dot{l}_{AB} cos\alpha + \dot{\theta} l_{BC} sin\theta^*}{l_{AB} sin\alpha}. \tag{4.16}$$

Substitution of Equation 4.16 into Equation 4.15 and subsequent simplification determined the following expression for the actuator linear velocity,

$$\dot{l}_{AB} = \dot{\theta} l_{BC} sin(\alpha - \theta^*). \tag{4.17}$$

To eliminate the unknown variable, α, the angles which were referenced to the $\hat{i}$-axis (α and θ^*) were converted to interior angles of the triangle ABC through the following two relationships,

$$\alpha^* = \frac{\pi}{2} - \alpha, \tag{4.18}$$

and

$$\theta^{**} = \frac{\pi}{2} + \theta^*. \tag{4.19}$$

The law of sines was then applied to the triangle, ABC, for the purpose of isolating α^*. The expression relating this variable to the robotic arm angular displacement was determined,

$$\alpha^* = sin^{-1}\left(\frac{l_{BC}}{l_{AB}} sin\theta^{**}\right). \tag{4.20}$$

Substitution of Equations 4.18, 4.19 and 4.20 into Equation 4.17 yielded the final expression relating the actuator linear velocity to the robotic arm angular velocity.

$$\dot{l}_{AB} = \dot{\theta} l_{BC} sin\left[\frac{\pi}{2} - sin^{-1}\left(\frac{l_{BC}}{l_{AB} sin(\frac{\pi}{2} + \theta^*)}\right) - \theta^*\right]. \tag{4.21}$$

The validity of Equation 4.21 was tested experimentally. An LVDT attached to the actuator was used to record piston extension, l_{AB}. This value was numerically differentiated to obtain the "measured" actuator velocity data, $\dot{l}_{AB}$. An RVDT was used to measure the angular displacement data, θ^*. This value was numerically differentiated to generate the robotic arm angular velocity, $\dot{\theta}$. The recorded values were used in Equation 4.21 to calculate the actuator velocity as determined by the angular velocity. The input was a random amplitude in valve displacement introduced by an operator. A comparison of measured and computed actuator velocities is presented in Figure 4.6.

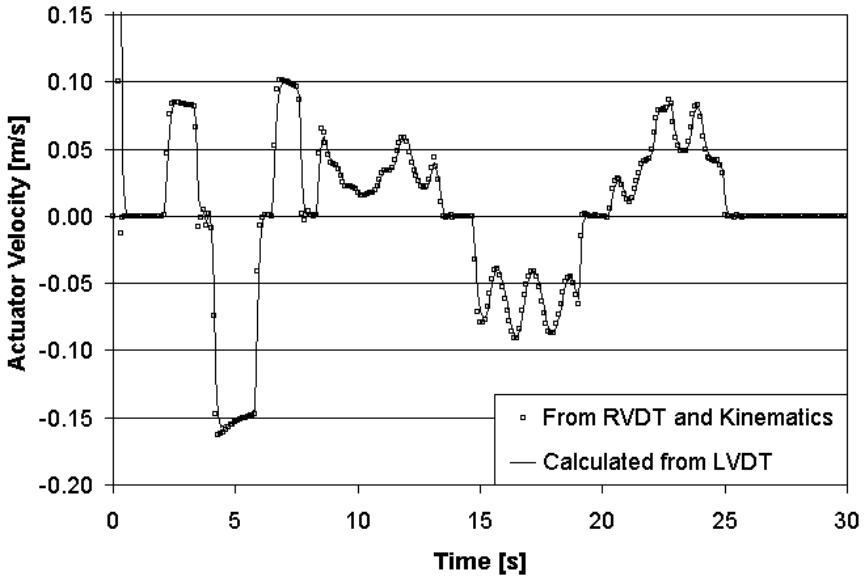

Figure 4.6: Verification of the kinematic velocity analysis.

Again, there was very good agreement between these velocities, which verified the velocity analysis.

4.3 Concluding Comments on the Kinematics of the Robot

The developments in this chapter represent completion of Research Goal #5 presented in the introductory chapter to this thesis. Completion of this goal represents the final component needed in the development of a predictive velocity control scheme. Operator input of desired angular velocity may be transformed to an actuator velocity. The actuator velocity implies a required flow rate. A means has been devised to predict the flow rate through a valve for given operating conditions. A control scheme has also been developed to control one of the valve operating conditions, (valve spool displacement) independent of others (supply and load pressure). The only remaining step is to combine the components to function as a predictive controller which is the subject of the next chapter.

Chapter 5

Velocity Control of the Robot with a Linearizing Feedforward Controller

5.1 Assembling the Linearizing Feedforward Controller

The work presented thus far in this thesis represents the development of individual components which collectively create an open loop velocity control system for a hydraulically actuated linkage. In this chapter, the task of assembling these components into a functioning controller is addressed. For reference it is useful to consider the predictive flow controller as proposed in Chapter 1. A block diagram of that system with annotations indicating areas to be discussed is shown in Figure 5.1.

In the next section, the task of transforming an operator input signal to desired flow rate is examined (A in Figure 5.1). This required application of the kinematic equations developed in Chapter 4. In the third section, the issue of converting the desired flow rate signal to a valve command signal is examined (B in Figure 5.1). This involved finding the inverse solution for the modified turbulent orifice equation

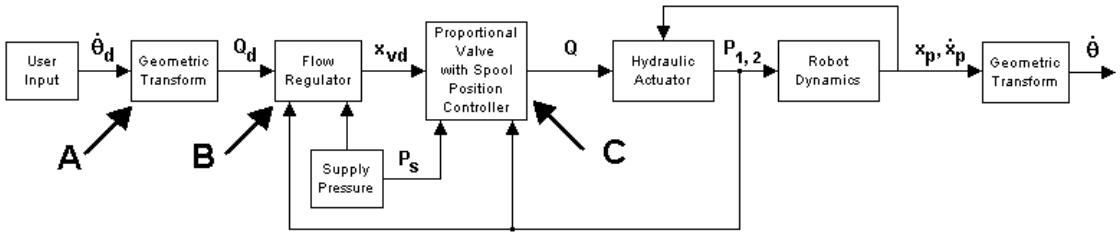

Figure 5.1: Block diagram of the proposed predictive velocity control system.

developed in Chapter 3. In the fourth section interfacing the control algorithm with the physical hydraulic system is addressed (C in Figure 5.1). This relies on the model reference controller for the valve which was developed in Chapter 2. The results of an experimental investigation of the performance of the new controller is described in the fifth section. A brief summary of the material presented is given in the final section.

5.2 User Input to Desired Flow Signal

As discussed earlier in Chapter 1, the operator of a single link rotary mechanism, be it a front-end loader, a backhoe, a crane or a piece of logging equipment, is primarily concerned with the angular velocity of this link and not the velocity of the hydraulic actuator or the flow rate to it. The mathematics to link these system states were solved in Chapter 4 but a few logistical issues remained with the implementation of the hardware in the control loop.

The primary issue involved the use of Equation 4.21. This equation represents the relationship between the actuator velocity, $\dot{l}_{AB}$, and the angular velocity of the boom arm, $\dot{\theta}$. Unfortunately, the relationship also relies on the instantaneous geometry of the boom, (the angular displacement of the boom arm and the actuator displacement are interchangeable according to Equation 4.11) that is,

$$\dot{l}_{AB} = f(\dot{\theta}, l_{AB}). \tag{5.1}$$

This is problematic as the premise of this research project was that applications requiring a predictive velocity control strategy would be "sensor poor". That is, measurement of the states, including the actuator or angular displacement, would be unavailable. Thus, it was important to determine how these values would be estimated and provided as feedback to the kinematic equations.

If the accuracy of the velocity control system approached 0% error, obtaining an estimate of the angular displacement could be achieved by numerically integrating the desired angular velocity. However, the feasibility of using this approach could not be evaluated until the accuracy of the predictive velocity control system in the absence of velocity tracking error was determined. For this reason, in this evaluation, the actuator position and boom angle were presumed known and real-time measurements from the installed RVDT were used as feedback to the kinematic equations.

A second minor issue to be resolved was that of obtaining a desired flow rate from the calculated desired actuator velocity. Leakage across the piston was assumed negligible. If significant leakage was present, this factor would have been compensated for in the valve mapping procedure as flow rate data was not measured directly, but rather inferred from measurements of actuator velocity. Thus, in the absence of leakage, generating a desired flow rate only required the multiplication by the actuator piston area.

5.3 Desired Flow to Valve Control Signal

This section presents the culmination of the most significant contributions of the author in this study. It is shown how the modified turbulent orifice equation developed in Chapter 3 was used to produce a valve control signal with the intent of introducing predictive velocity control.

The modified turbulent orifice equation developed in Chapter 3 was verified through its use as a flow predictor; however, the proposed feedforward linearizing controller

required the use of the *inverse* valve map. The the two approaches are illustrated in Figure 5.2.

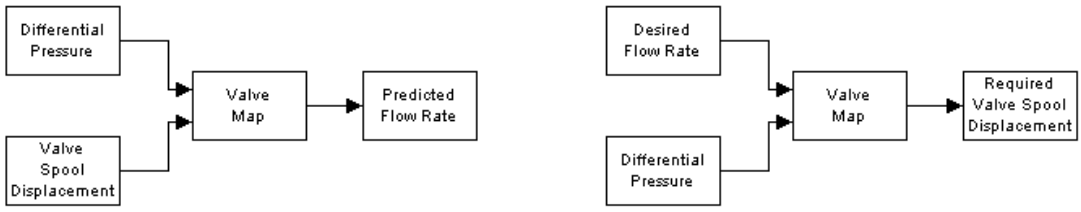

Figure 5.2: (Left) Valve map as a flow predictor. (Right) Inverse valve map generating a control signal.

The desired output of the inverse valve map was a solution for the required valve spool displacement, x_{vd}, which was of the form,

$$x_{vd} = \frac{Q_d}{K\sqrt{\Delta P}}. \tag{5.2}$$

This was not directly achievable as the modified turbulent orifice equation contains the dependent term,

$$K = f(x_{vd}, \Delta P), \tag{5.3}$$

therefore, a method was required to simultaneously solve,

$$Kx_{vd} = \frac{Q_d}{\sqrt{\Delta P}}. \tag{5.4}$$

No straightforward closed form solution to Equation 5.4 was possible. A solution for the required valve spool displacement could be determined through any number of nonlinear root finding techniques. None of the techniques investigated was well suited to implementation in the real-time environment used to implement the control strategy and perform the evaluation of its performance. A series solution was also attempted; however, to achieve 1% accuracy, an 8th order polynomial was required. Rather, the method chosen exploited the capabilities of the MATLAB® software

package to solve differential equations. The function representing K in the modified turbulent orifice equation was placed in a feedback loop of a first order system shown in block diagram form in Figure 5.3. The input was the right hand argument in Equation 5.4.

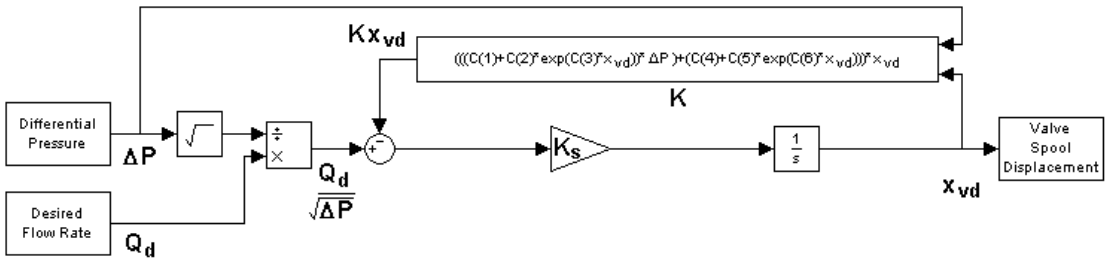

Figure 5.3: Block diagram of the first order solver.

The closed loop transfer function for x_{vd} with respect to $\frac{Q_d}{\sqrt{\Delta P}}$ was found to be,

$$\frac{x_{vd}}{\frac{Q_d}{\sqrt{\Delta P}}} = \frac{K_s}{s + KK_s} = G(s), \tag{5.5}$$

which, at $\lim_{s\to 0} G(s)$, reduced to,

$$\frac{x_{vd}}{\frac{Q_d}{\sqrt{\Delta P}}} = \frac{1}{K}. \tag{5.6}$$

Reordering Equation 5.6 showed that this system tends to the desired valve spool displacement given a differential pressure and a desired flow,

$$x_{vd} = \frac{Q_d}{K\sqrt{\Delta P}}, \tag{5.7}$$

within a settling time determined by the time constant, $\frac{1}{KK_s}$. The closed loop transfer function for this system given in Equation 5.5 is of first order. Thus, the system is stable for all inputs provided that K remains positive, which is true for positive valve spool displacements.

Two additional design considerations affecting the suitability of the first order solver were addressed. First, an appropriate value of K_s was chosen such that the transfer

function remained numerically stable when solved as a sampled data system. Second, the convergence of the solution, as dictated by the root of the characteristic equation of the closed loop system, was evaluated to ensure a solution was found sufficiently fast so as to not interfere with the dynamics of the system.

The risk of numerical instability dictated the maximum allowable gain, K_s, and hence, the minimum time to convergence. The greatest risk of numerical instability occurs in the first two time steps of the numerical integration routine when the operating conditions, P_s and Q_d, create a large value for the feedback, Kx_{vd}. In this scenario, it is possible for the error signal to become large negative resulting in a negative solution for x_{vd}. The nonlinear feedback equation, K, is not valid in the negative domain and the solver is unstable. Consider the first time step for $x_{vd}(0) = 0$. The error signal in this case was:

$$\frac{Q_d}{\sqrt{\Delta P}} - 0 = \frac{Q_d}{\sqrt{\Delta P}}. \tag{5.8}$$

A rectangular numerical integration algorithm provided a solution for the valve spool displacement in its first step,

$$x_{vd} = 0 + \frac{Q_d}{\sqrt{\Delta P}} K_s \Delta T. \tag{5.9}$$

The largest correction in x_{vd} occurs when the ratio of the flow to the differential pressure is maximized. For the zone of confidence developed in Chapter 3, this occurs at $Q_d = 0.0003\ \frac{m^3}{s}$ and $\Delta P = 0.5\ MPa$. The time step in the real-time control implementation was fixed at $\Delta T = 0.001\ s$, therefore, Equation 5.9 reduced to,

$$x_{vd} = 4.2426 \times 10^{-7} K_s. \tag{5.10}$$

As a starting point the maximum allowed correction in x_{vd} was taken to be 0.5 mm which resulted in a the value $K_s = 1.18 \times 10^6$. This value was tested in simulation using the system shown in Figure 5.3 and was found to produce a stable system

response. Trial and error using the same inputs showed that stability was maintained with K_s as high as 2.0×10^6.

The numerical stability analysis placed an upper limit on the gain, K_s, for the scenario when the feedback gain was largest. It was also necessary to evaluate the system performance at operating conditions which resulted in low values of K. This is the case when the ratio of flow to differential pressure is minimized within the zone of confidence, or $Q_d = 0.00008\ \frac{m^3}{s}$ and $\Delta P = 3.5\ MPa$. It should be noted that the time constant for this system is nonlinear as $\tau = \frac{1}{KK_s}$ and $K = f(x)$, and therefore, a single value does not exist. Rather, the critical parameter in this examination was the time to convergence which was taken as the point that the error signal amplitude reaches 95% of its initial value. The time to convergence was expected to be slower in the low K case relative to the high K case. The results for both the high K and low K cases are shown in Figure 5.4.

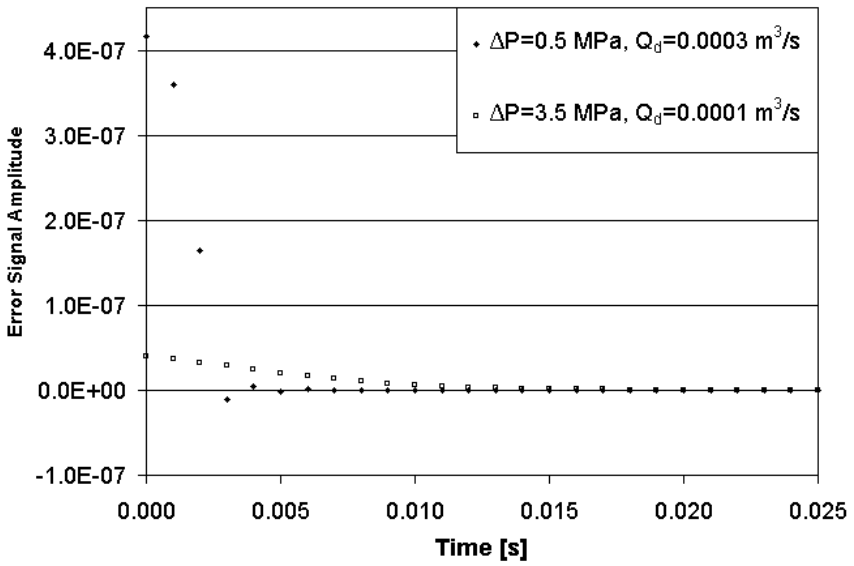

Figure 5.4: Comparison of convergence for high and low K solutions.

The time to convergence for the low K case was found to be 0.012 s which, when the linear time constant relationship in which 3τ=95% of steady state was used as an approximation, indicated a time constant in the neighbourhood of 0.004 s. This

corresponded to a pole at approximately 250 $\frac{rad}{s}$ (40 Hz) for the low gain case. This was sufficiently fast not to interfere with the valve controller which was designed with the dominant closed loop pole at $s = -18.4$.

The first order solver was tested in simulation. Variable differential pressure and valve spool displacements were generated using sine wave generators available in Simulink® . The differential pressure was varied from 2.5 MPa to 1.5 MPa at a frequency of 0.16 Hz. The valve spool displacement was composed of superimposed low and high frequency components and this signal is plotted in Figure 5.6. The differential pressure and spool displacement signals were used as inputs to the modified turbulent orifice equation (Valve Map) where the set of coefficients in that equation were those presented in Chapter 3, $\mathbf{S_{smallflow}}$. The result from the modified turbulent orifice equation was a flow rate. This flow rate and the variable differential pressure signal were then applied to the inverse valve map which employed the first order solver and used the same set of coefficients, $\mathbf{S_{smallflow}}$. The simulation block diagram is shown in Figure 5.5.

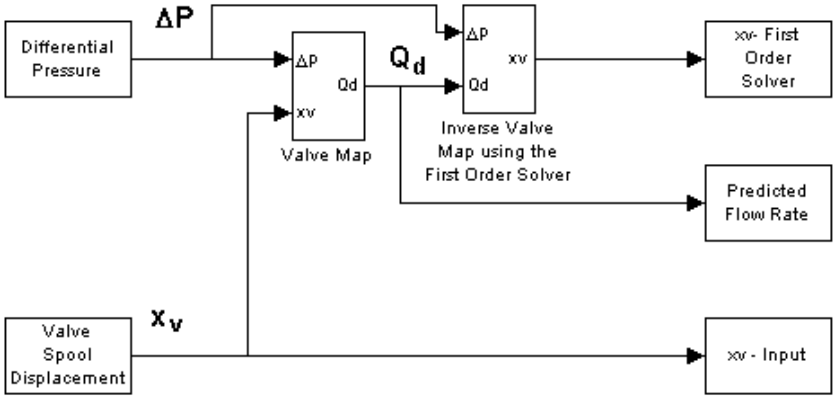

Figure 5.5: System for verification of the first order solver.

The flow rate as calculated by the modified turbulent orifice equation is plotted on one axis in Figure 5.6 with the input spool displacement and that calculated by the first order solver plotted on the other.

It was noted that the input and solved values for the valve spool displacement were

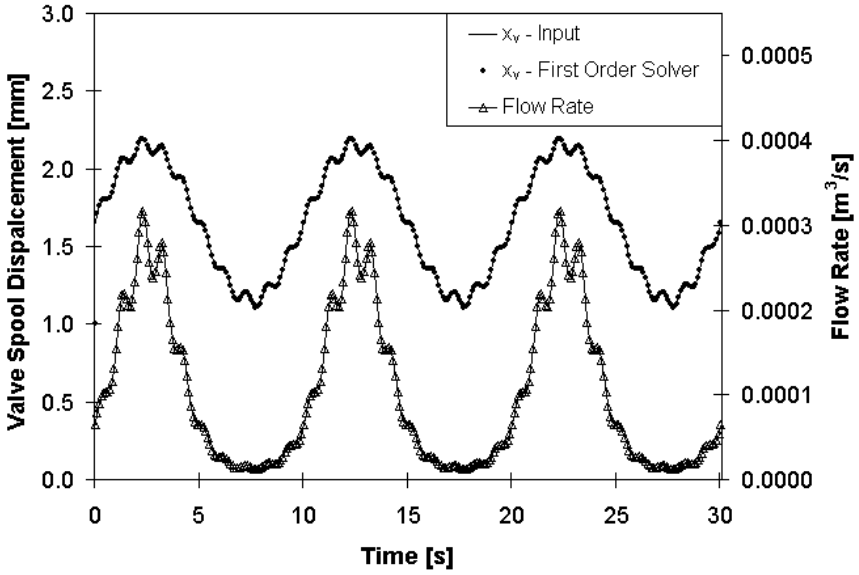

Figure 5.6: First order solver solution. (Note: the x_v - Input and x_v - First Order Solver series are superimposed)

virtually coincident. The only discrepancy, which is not evident in Figure 5.6, was a phase lag of less than 0.002 s. This was considered sufficiently small so as not to be detrimental to the controller performance.

One further consideration was the bi-directional nature of this system. Thus far, developments of the modified turbulent orifice equation and first order solver have assumed that valve spool displacements were always positive. In order to accommodate both up and down actions on the robotic arm, however, the system must be configured as meter-in/meter-out.

In meter-in/meter-out configuration, the valve spool moves in both the positive and negative directions about the null point as discussed in Chapter 2. The sign of the spool direction determines whether supply oil from the pump is directed to the blank side of the actuator (meter-in) or if blank side oil is allowed to return to tank (meter-out). Therefore, switching logic must be introduced to account for the direction of the flow, the direction of the valve spool displacement, and the differential pressure acting across the orifice. The necessary switching to achieve a fully bi-directional valve map is illustrated in Figure 5.7.

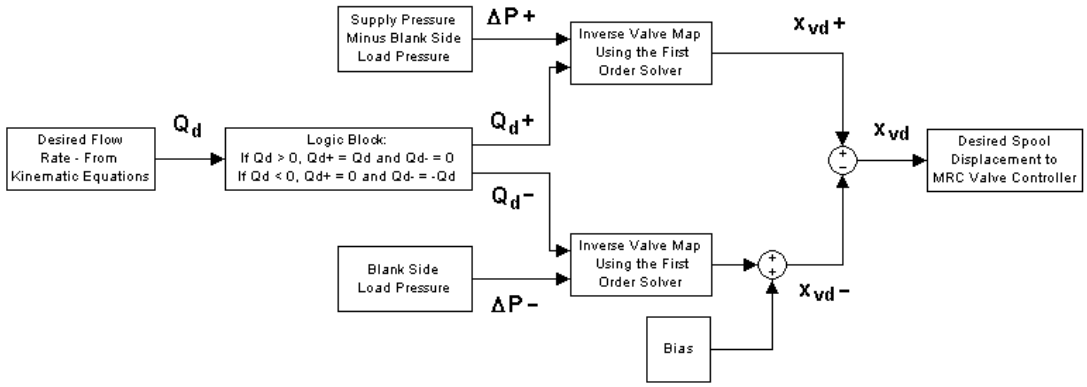

Figure 5.7: Logic switching for the bi-directional valve map.

It was noted that the tank pressure was effectively zero, therefore, the differential pressure in the meter-out operation was the blank side actuator pressure. As well, since all measurements upon which the valve map was based were taken in the positive direction, a positive deadzone was inherent to the valve map as discussed earlier. A small correction was needed to compensate in the negative direction, therefore, a bias was added to the meter-out valve displacement.

Through application of the first order solver and the logic switching to account for directionality, a desired flow rate could be transformed into a desired valve spool displacement signal. Implementation of the real-time controller developed in Chapter 2 to achieve the required valve spool displacement is the subject of the next section.

5.4 Interface With the Hydraulic System

The switching discussed in the previous section (Figure 5.7) produced a bi-polar desired valve spool displacement signal. This became the input to the MRC valve spool displacement controller developed in Chapter 2. The MRC controller produced a control signal that was input to a voltage following operational amplifier circuit. This ensured electrical isolation between the data acquisition equipment and the valve and supplied sufficient current to drive the valve EMA. The complete

block diagram representation of the new linearizing feedforward velocity controller is presented in Figure 5.8.

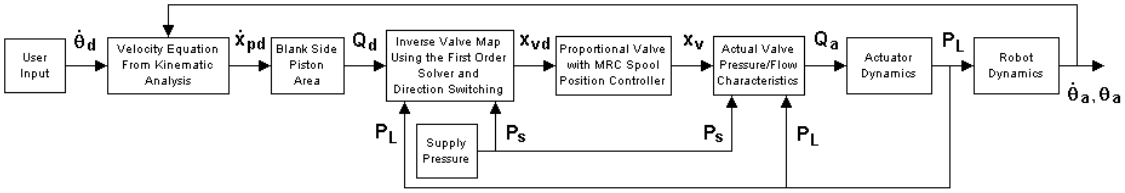

Figure 5.8: The novel linearizing feedforward velocity controller.

5.5 Selected Results of the Linearizing Feedforward Controller

The range of tests which could have been run on the controller is voluminous. The tests conducted in this study support the research goal of this project which was to evaluate the *feasibility* of introducing predictive velocity control on a hydraulically actuated linkage. Evaluation of the controller performance was examined under the following operating conditions:

1. Fixed supply pressure and constant amplitude velocity.
2. Fixed supply pressure and variable amplitude velocity.
3. Variable supply pressure and constant amplitude velocity.

5.5.1 Fixed Supply Pressure - Constant Amplitude Velocity

The goal of the first test was to examine the constant velocity characteristics of the controller subject to a range of supply pressures. These tests do not a imply fixed load pressure as the nonlinear geometry of the robot generated a variable gravitational load as the arm moved through its trajectory. This is analogous to the

problem of variable inertia investigated by Bu and Yao [6] [7] in which those authors used an adaptive controller with full state feedback on a physically similar device.

Twenty four cases encompassing three positive and three negative desired angular velocities at four different supply pressures were examined. The angular velocities were chosen to cover the full range of flow rates within the zone of confidence discussed in Chapter 3. The values used were ± 0.1, ± 0.2, and ± 0.3 $\frac{rad}{s}$ (± 5.7, ± 11.5, and ± 17.2 $\frac{^\circ}{s}$). The robot was operated over its full range of motion for each of the cases. The supply pressures used were also chosen to be representative of the zone of confidence and covered a range from 4.14 MPa to 6.21 MPa.

The testing procedure included a warm up stage as discussed earlier in this thesis. Following the warm up procedure, the arm of the robot was manually moved to the bottom of its trajectory for positive angular velocity tests or to the top for the negative tests. A fixed angular velocity was input to the system shown in Figure 5.8.

The desired and measured velocities for all tests are presented in Figures 5.9 through 5.12. Two points regarding the presentation of results in these figures must be noted. First, the test runs were started and stopped manually, leading to variation in the test durations. Second, for the purposes of visual comparison of the angular velocity tracking for test at different velocities, the time scale of the tests has been normalized by the length of time required for the robot to move from its lower limit to its upper limit at the desired angular velocity, T_{traj}. This corresponds to $T_{traj} = 8.25$ s for the ± 0.1 $\frac{rad}{s}$ tests, $T_{traj} = 4.125$ s for the ± 0.2 $\frac{rad}{s}$ tests, and $T_{traj} = 2.75$ s for the ± 0.3 $\frac{rad}{s}$ tests. This convention is used throughout this discussion and is noted as "Normalized Time" when applied.

The %RSRE for all tests was calculated. For example, the %RSRE as a function of time is shown for the tests performed with a supply pressure of 4.14 MPa in Figure 5.13.

To obtain a measure of performance, the mean of the %RSRE series (such as those in Figure 5.13) were calculated excluding the transient region. The results for all

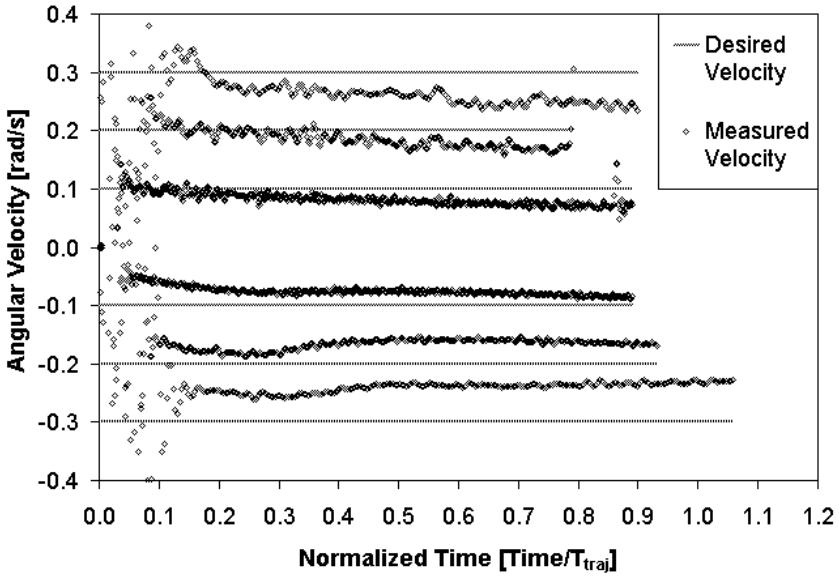

Figure 5.9: Velocity tracking results with a supply pressure of 4.14 MPa. T_{traj} = 8.25, 4.125, and 2.75 s for $\dot{\theta}_d = \pm 0.1$, ± 0.2, and ± 0.3 $\frac{rad}{s}$, respectively.

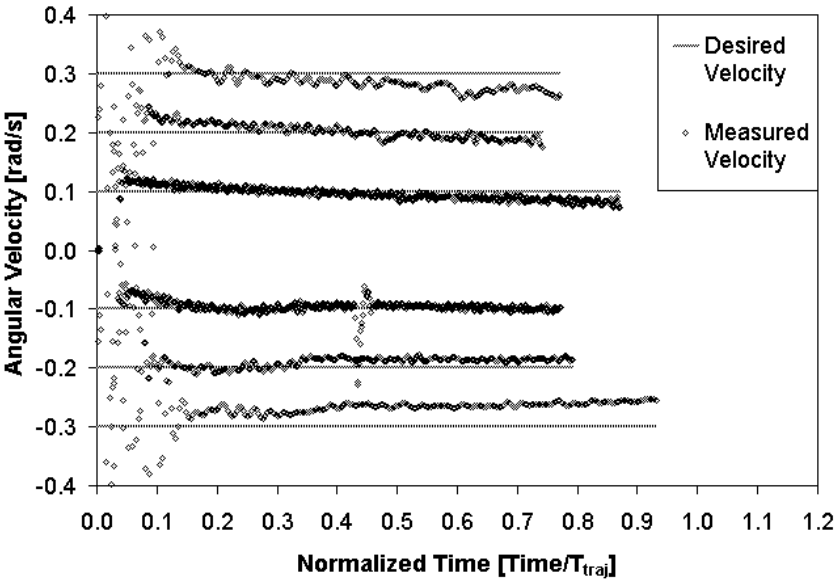

Figure 5.10: Velocity tracking results with a supply pressure of 4.83 MPa. T_{traj} = 8.25, 4.125, and 2.75 s for $\dot{\theta}_d = \pm 0.1$, ± 0.2, and ± 0.3 $\frac{rad}{s}$, respectively.

tests are summarized in Figure 5.14.

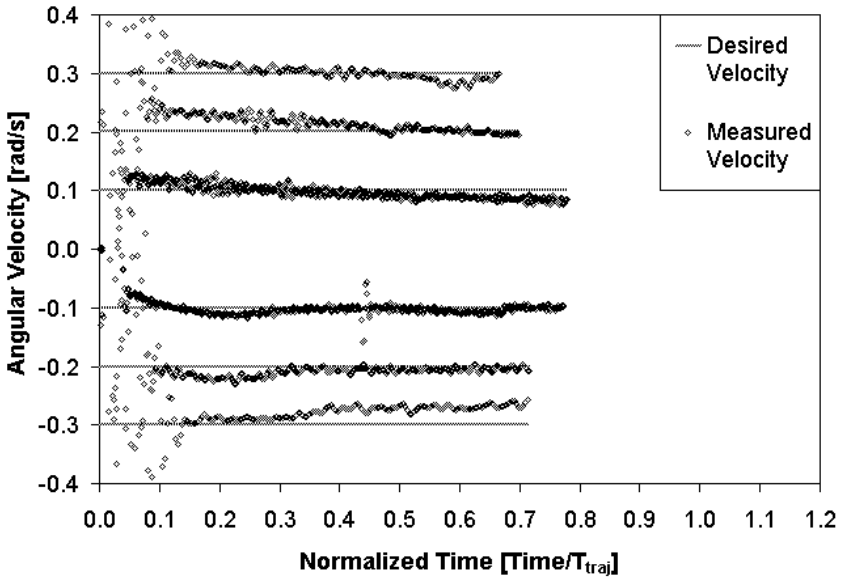

Figure 5.11: Velocity tracking results with a supply pressure of 5.52 MPa. T_{traj} = 8.25, 4.125, and 2.75 s for $\dot{\theta}_d = \pm 0.1$, ± 0.2, and ± 0.3 $\frac{rad}{s}$, respectively.

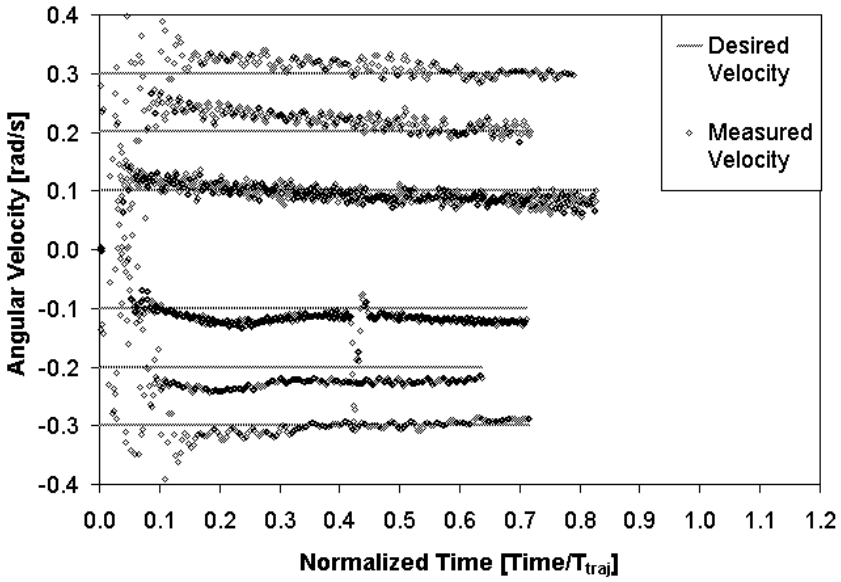

Figure 5.12: Velocity tracking results with a supply pressure of 6.21 MPa. T_{traj} = 8.25, 4.125, and 2.75 s for $\dot{\theta}_d = \pm 0.1$, ± 0.2, and ± 0.3 $\frac{rad}{s}$, respectively.

These results indicate that the velocity was being controlled within 10% of the desired value for operating conditions that are well within the zone of confidence.

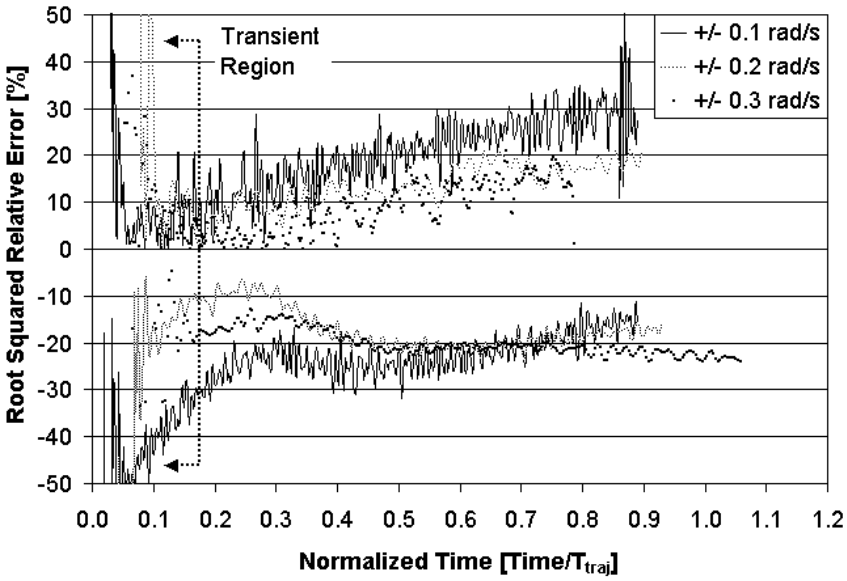

Figure 5.13: Root squared relative error (%RSRE) for tests conducted with P_s=4.14 MPa. (Note: The results of the -0.1, -0.2, and -0.3 $\frac{rad}{s}$ tests are shown negative for clarity.)

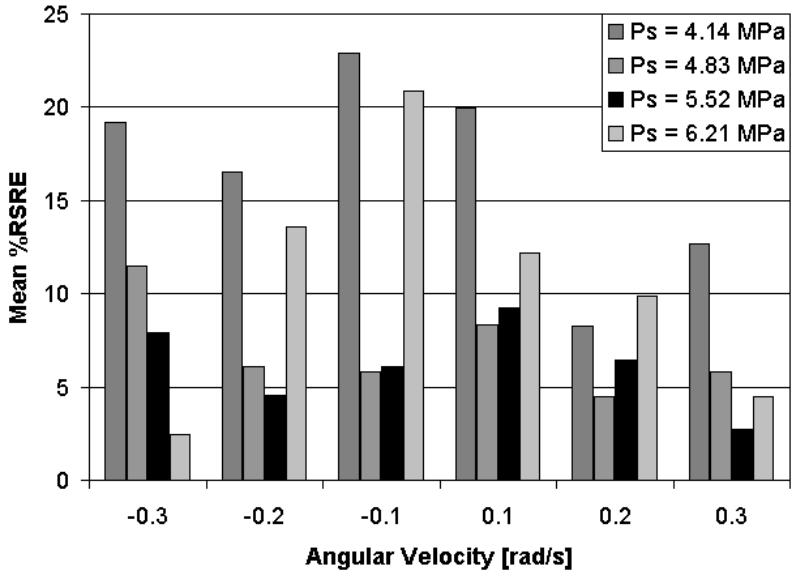

Figure 5.14: A qualitative presentation of the velocity tracking accuracy as shown by the mean root squared relative error (%RSRE) for all constant velocity tests.

Performance of the controller degraded for values that were on the periphery of this zone particularly the tests performed with a supply pressure of 4.14 MPa and desired velocities of ± 0.1 $\frac{rad}{s}$. Examination of the flow rate data for these cases indicated that the differential pressure or required flow rate drifted outside the zone of confidence as the arm moved through its trajectory. This is best illustrated by examining a plot of the flow rate against differential pressure for the case of $P_s = 4.14$ MPa and $\dot{\theta}_d = 0.2$ $\frac{rad}{s}$ shown in Figure 5.15.

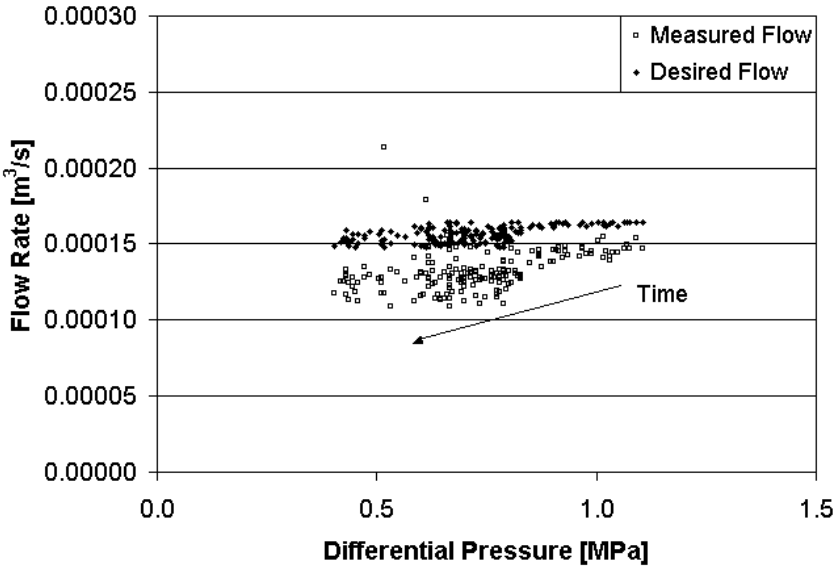

Figure 5.15: Flow rate as a function of differential pressure for P_s=4.14 MPa and $\dot{\theta}_d = 0.2$ $\frac{rad}{s}$.

During this test, at higher differential pressures (>0.75 MPa) the modified turbulent orifice equation estimated the required flow rate within acceptable error. However, as the arm moved through its trajectory the differential pressure dropped outside the zone of confidence and the estimation was correspondingly poor. This was common among the tests performed at this supply pressure. Similarly, the required flow rate, as dictated by the kinematics, dropped outside the zone of confidence for portions of the tests performed at low velocities.

It was determined that the linearizing feedforward controller was capable of main-

taining steady state control of angular velocity within 10% error for operating conditions within the zone of confidence. It was of further interest to determine the repeatability of the control technique subject to a cyclic duty cycle. This is the subject of the next section.

5.5.2 Fixed Supply Pressure - Variable Amplitude Velocity

The second test to be discussed was a variation on the tests presented in the previous section. Rather than a fixed desired velocity, the input was a sinusoidal desired velocity. The purpose of this test was to evaluate the effect of compounding error on repeated motion. This test case proved quite interesting as transient behaviours were found to play a significant role in the potential accuracy for implementing predictive position control of the robot for repeated motions. Sinusoidal velocity plots were developed by supplying a velocity input signal to the linearizing feedforward controller. The velocity signal was generated by numerically differentiating a desired position signal. This was done so that the range of motion could be determined explicitly to ensure that the robot did not exceed the actuator stroke during the test. The amplitude of the position signal was 0.15 rad (8.6 °) and the frequency was varied to adjust the velocity range of the test. A supply pressure of 5.17 MPa was chosen as the best results for the steady state velocity tests were obtained in this range. This value was held constant for all tests. The results for frequencies of 0.1, 0.2, and 0.3 Hz are shown in Figures 5.16 to 5.18.

It was noted that the robot exhibits static friction lockup (stiction) characteristics in the neighbourhood of velocity direction changes. This was due in part to the friction characteristics in the actuator but was also affected by the flow estimation which was outside the zone of confidence near null. If this phenomenon is to be minimized, the low flow characteristics of the valve must be captured in more detail. Alternatively, a "kicker" circuit such as that proposed by [33] may be useful in improved accuracy for zero-crossing motions.

Qualitatively, the results for these tests were excellent as the controller delivered

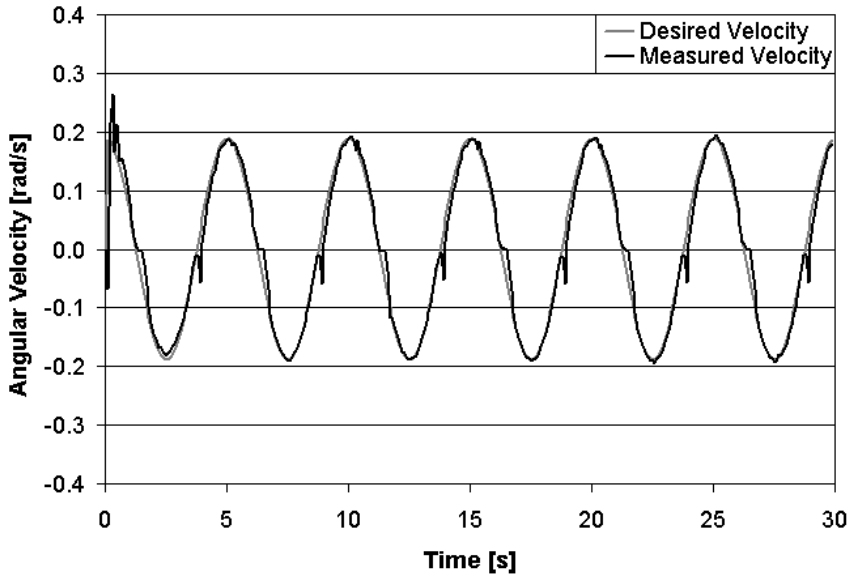

Figure 5.16: Sinusoidal velocity tracking with the LFFC. $P_s = 5.17\ MPa$ and $f = 0.1\ Hz$.

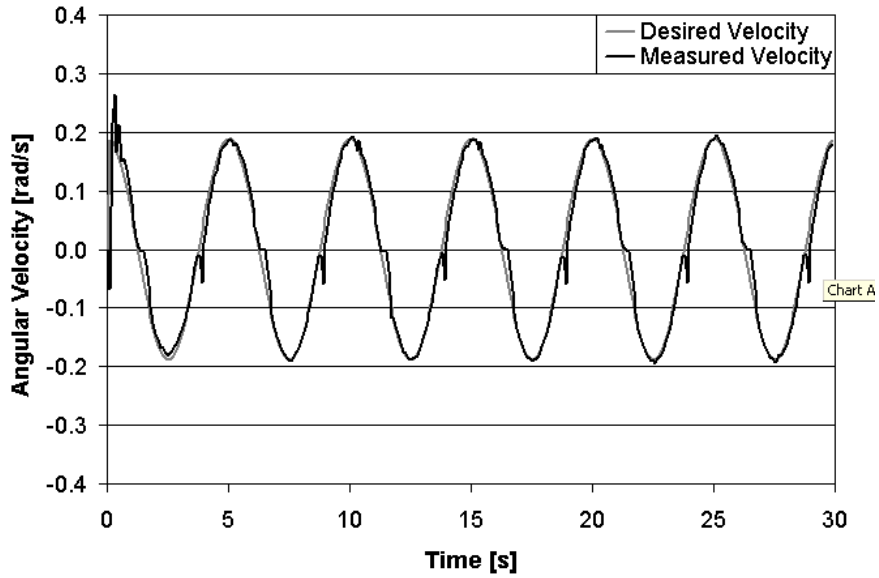

Figure 5.17: Sinusoidal velocity tracking with the LFFC. $P_s = 5.17\ MPa$ and $f = 0.2\ Hz$.

smooth performance and compensated for the variable load pressure that arose from changes in gravitational loading as the arm cycled through its range of motion. The

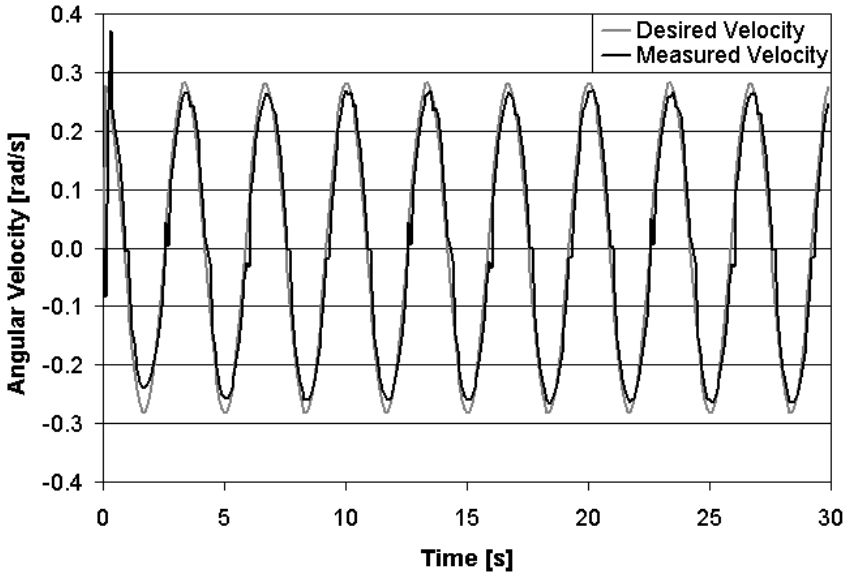

Figure 5.18: Sinusoidal velocity tracking with the LFFC. $P_s = 5.17\ MPa$ and $f = 0.3$ Hz.

least accurate performance was measured at 0.1 Hz which was not surprising as the resulting desired flow rate at this frequency was below the lower limit of the zone of confidence. The calculated %RSRE values for the data presented in Figures 5.16 to 5.18 are shown in Figures 5.19 to 5.21. For the purposes of presentation, the values in the near null region were set to zero as small desired flows, which were substantially outside the zone of confidence, resulted in large relative errors for very small absolute error.

The mean %RSRE (not including zeroed values or the initial transient) for the three cases shown were 13.93%, 3.67%, and 8.40% , respectively. The low velocity results shown in Figure 5.16 highlight the need for improvement in the pressure/flow mathematical relationship for small valve spool displacements. The high velocity results, such as those in Figure 5.18 show the potential for this technique. In fact, when operated for a 30 s run for a sinusoidal input, the cumulative errors in angular position only amounted to 1° as shown by the difference between the desired and measured position values at 30 s in Figure 5.22.

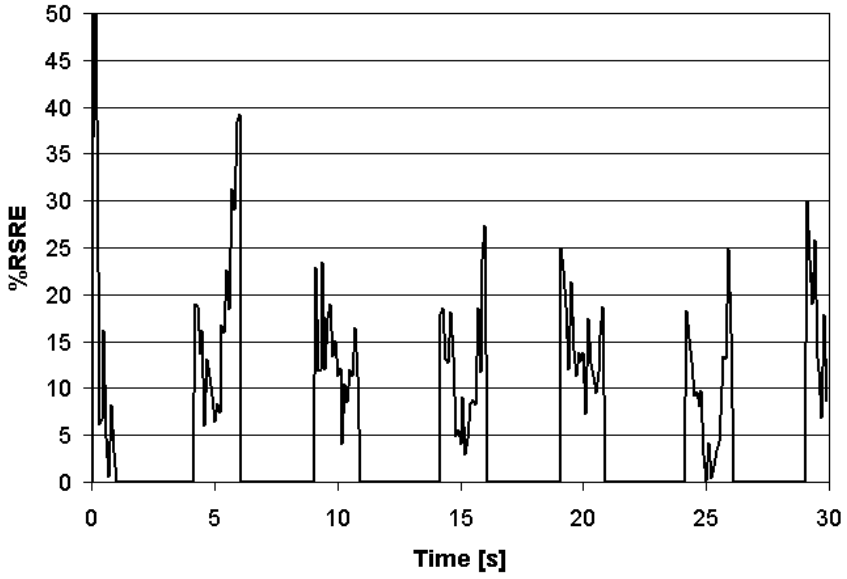

Figure 5.19: Root squared relative error (%RSRE) for sinusoidal velocity tracking with $P_s = 5.17\ MPa$ and $f = 0.1\ Hz$.

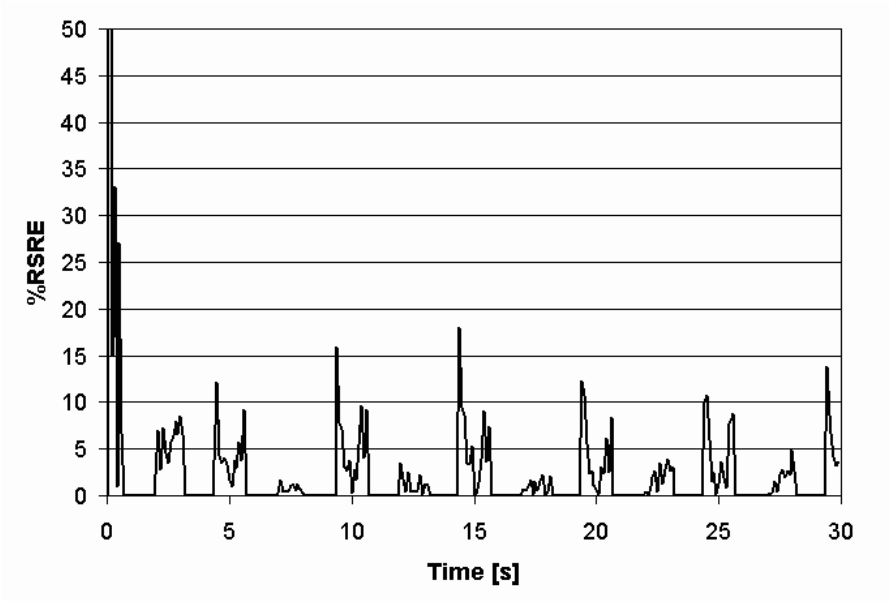

Figure 5.20: Root squared relative error (%RSRE) for sinusoidal velocity tracking with $P_s = 5.17\ MPa$ and $f = 0.2\ Hz$.

The error in the vertical displacement of the tip of the robotic arm was determined from the angular displacement error for the data presented in Figure 5.22. This

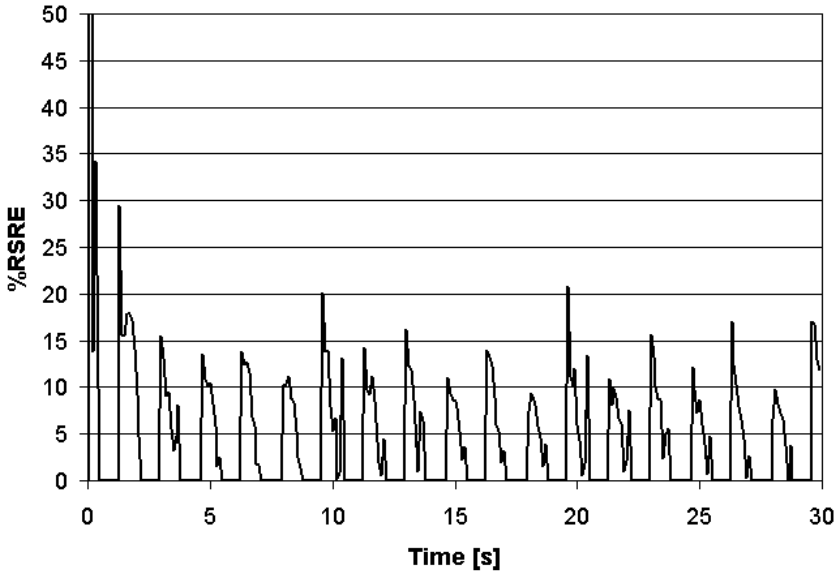

Figure 5.21: Root squared relative error (%RSRE) for sinusoidal velocity tracking with $P_s = 5.17\ MPa$ and $f = 0.3\ Hz$.

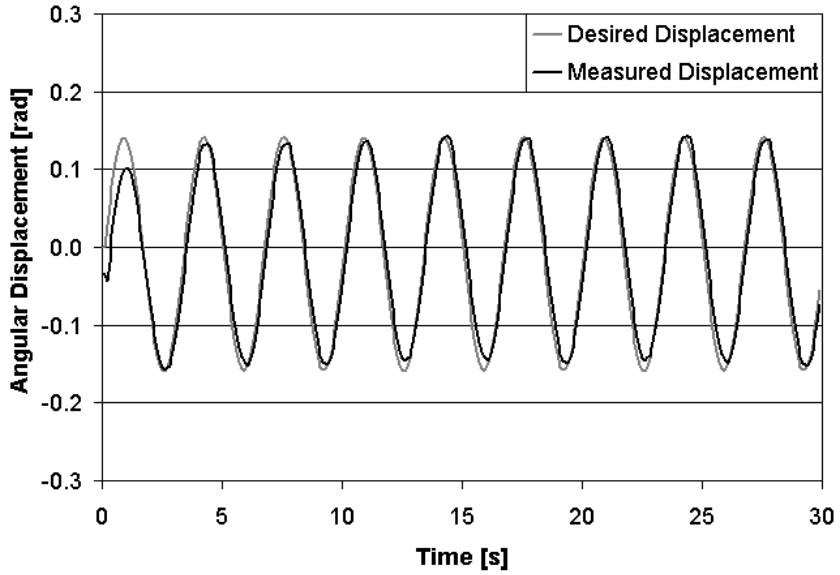

Figure 5.22: Sinusoidal position tracking with $P_s = 5.17\ MPa$ and $f = 0.3\ Hz$.

value was of interest as vertical position is a critical parameter for an operator of offhighway equipment. It is shown in Figure 5.23 that this value did not exceed 6 cm for the duration of the 30 s test. This was comparable to the position tracking error experienced by Guenther et al. [8] using their "variable structure - adaptive

cascade control" algorithm which operated with full state feedback.

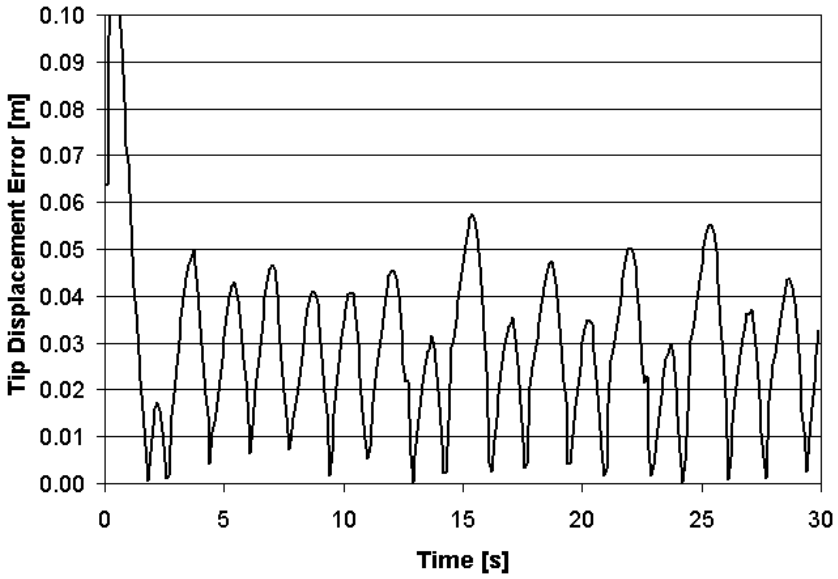

Figure 5.23: Robotic arm tip vertical displacement error with $P_s = 5.17\ MPa$ and $f = 0.3\ Hz$.

The constant supply pressure results presented in this section indicate that this method holds promise for controlling the velocity of a hydraulic link with variable load unsupervised (in the sense that there is no direct feedback) for durations up to and possibly beyond 30 s with only a few percent degradation in position tracking.

5.5.3 Variable Supply Pressure - Constant Amplitude Velocity

One of the constraints for this project, discussed in Chapter 1, was that any velocity control solution must not only accommodate variable load, but also compensate for variable supply pressure. Variable supply pressures arise in load sensing systems often employed in mobile hydraulic equipment. The ability of the system to compensate for supply pressure was examined for the static supply pressure case earlier in this chapter. In this section, the ability of the controller to maintain a fixed desired velocity in the presence of a dynamically variable supply pressure is examined. If the

supply pressure is considered a random non-controllable input to the system then this analysis may be considered a measure of the disturbance rejection capabilities of the linear feedforward controller approach.

The experimental procedure for this set of tests was similar to that used in Section 5.5.1 with the exception that the supply pressure was varied manually over the course of the test by opening and closing the relief valve on the supply pressure line. Because of time restraints imposed by the range of motion of the robot and the need to manually adjust the pressure, only 0.1 $\frac{rad}{s}$ and 0.2 $\frac{rad}{s}$ velocity cases were examined. The desired and measured angular velocities for these two cases are shown in Figure 5.24 with the corresponding supply pressures given in Figure 5.25.

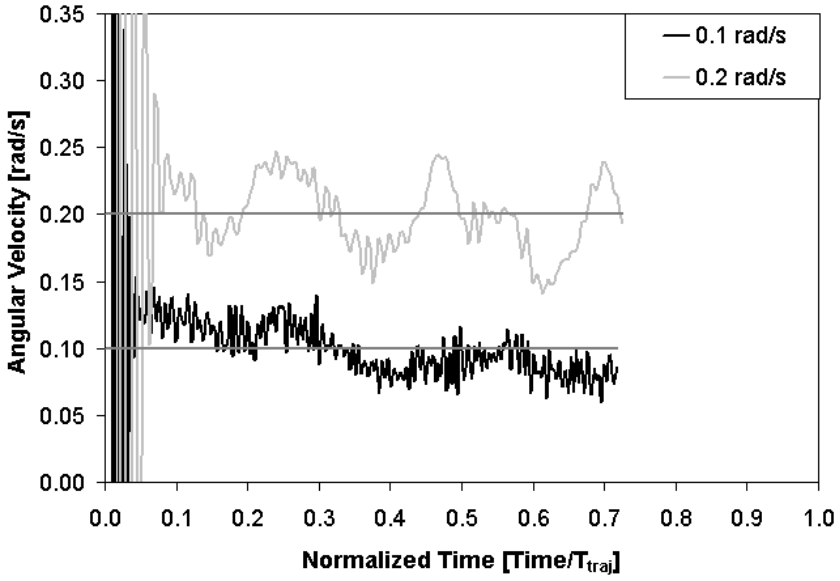

Figure 5.24: Constant angular velocity tracking subject to variable supply pressure. $T_{traj} = 8.25$ and 4.125 s for $\dot{\theta}_d = 0.1$ and 0.2 $\frac{rad}{s}$, respectively.

Initially, the velocity tracking results were regarded as poor. Rather than the 10% tracking accuracy seen in the static tests, the error was now as high as 50% at some points during both tests. It was determined that the modified turbulent orifice equation was not in error and to blame for these poor results. Rather, the relatively fast variation in pressure highlighted the shortcomings of the reference model used in

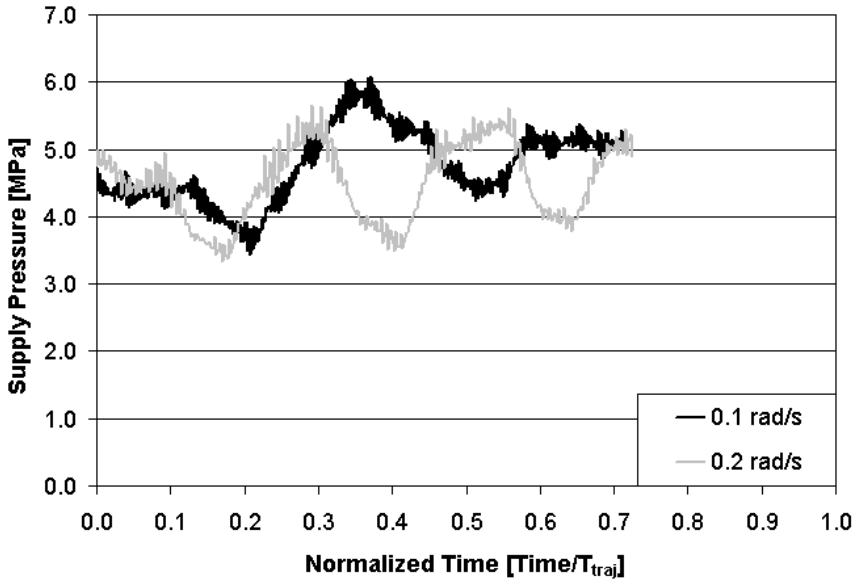

Figure 5.25: Supply pressure for the tests in Figure 5.24. $T_{traj} = 8.25$ and 4.125 s for $\dot{\theta}_d = 0.1$ and 0.2 $\frac{rad}{s}$, respectively.

the model reference valve spool position controller. The valve was not following the desired flow rate as calculated by the modified turbulent orifice equation sufficiently fast to completely negate the effects of the variable supply pressure. This is illustrated in Figure 5.26 which shows the error in the angular velocity tracking on the same plot as the valve spool displacement tracking error for the 0.2 $\frac{rad}{s}$ case.

The solution to this problem lies not in the valve map, but in the design of the valve spool position controller developed in Chapter 2. The model reference controller design was made as general as possible to provide consistent control over a wide range of temperature and supply pressure operating conditions. As a result, the controller was not optimized for response time and, hence, disturbance rejection. An in-depth analysis of the controller capabilities and optimization for a specific operating point may provide improved performance. In support of this, the 0.2 $\frac{rad}{s}$ test was repeated using a modified reference model transfer function in which the dominant closed loop pole was pushed closer to the imaginary axis,

$$G_{ref} = \frac{7840}{s^2 + 200.36s + 8000}. \tag{5.11}$$

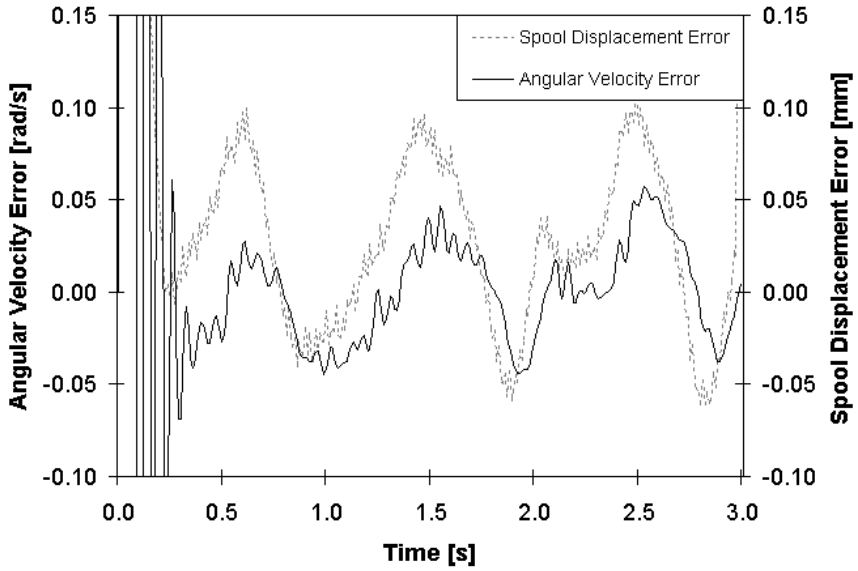

Figure 5.26: Comparison of the angular velocity error and valve spool displacement error for the 0.2 $\frac{rad}{s}$ results in Figure 5.24.

The improvement in the response is evident in the angular velocity error tracking shown in Figure 5.27.

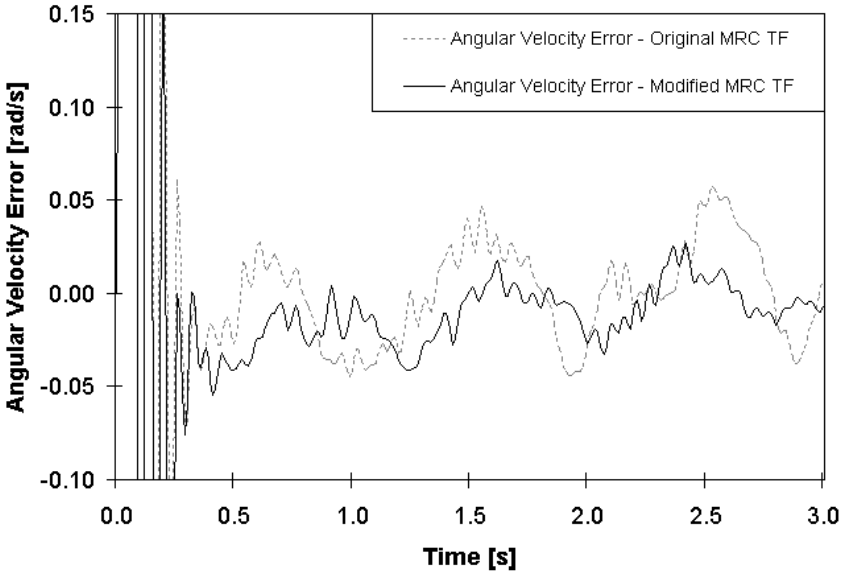

Figure 5.27: Comparison of the angular velocity tracking error with a modified reference model transfer function.

A complete analysis for stability and optimization for response was deemed to be outside the scope of this research. However, because of the approach to the design of the controller, it would be possible to test a new reference model in simulation for faster performance and verify the improvement using the test performed in this section. It was noted that in its original configuration, the algorithm was stable and also able to attenuate the disturbance caused by fluctuations in supply pressure.

5.6 Concluding Comments on Flow Control with the Novel Linearizing Feedforward Controller (LFFC)

Several important contributions were introduced in this chapter. The first of these is that an inverse solution for a nonlinear pressure/flow/displacement relationship can be solved in a stable manner in a real-time application through implementation of a first order solver. Finding an inverse solution for this relationship allowed for the creation of a single component pressure compensated flow control device. This is an important step as it alleviates the requirement for using the modified turbulent orifice equation as a flow rate "observer" whose flow rate estimate must be compared to a desired value in order to calculate a valve control signal.

Second, it was shown that mapping a single orifice can provide accurate directional flow when applied to a gravitationally loaded system in a meter-in/meter-out configuration in conjunction with differential pressure measurements.

Third, it was found that the LFFC could provide acceptable velocity tracking results in regions where the pressure/flow characteristics were known to be accurately captured. The velocity tracking was within 10% of the desired velocity for the majority of the test cases. The LFFC was also found to have some disturbance rejection capability with respect to changes in supply pressure. This function was compromised by an insufficiently fast valve response. The system was also found to be insensitive to

the magnitude of the supply and load pressures, provided that differential pressure remained within the region in which accuracy in flow estimation was determined to exist.

Finally, it was determined that the LFFC has the potential to control position unsupervised (in the sense that there is no direct position feedback) for durations up to 30 s. It may be possible to extend the range of operating conditions and/or the duration for which this is true with a valve which is more closely matched to the intended application.

The material presented in this chapter satisfied Research Goals #4 and #6 introduced in Chapter 1. The inverse solution of the valve map allowed for the creation of a single component pressure compensated flow control device. Integration of this component and the hydraulically actuated link created a predictive velocity control system. The limitations of this system were evaluated.

Chapter 6

Conclusions and Suggestions for Future Work

6.1 Discussion and Review of Research Sub-goals

The "vision" for this research project arose from discussion with industry representatives indicating that automation of repetitive operations for lower cost off-highway equipment using electrohydraulic valves was desirable. These same discussions outlined some of the practical constraints on implementing such a system. The most prominent of these constraints were the cost of components and the working environment which limits the possibilities for feedback instrumentation.

This research vision led to the development of the first goal which was to conduct a comprehensive review of published material in the areas off-highway equipment automation and electrohydraulic motion control. Through the process of completing this goal the scope of the research was defined and the originality of the research was verified.

The literature review showed that an approach for controlling the velocity of a hydraulically actuated mechanism without "closing the loop" using direct displacement, velocity, or flow rate measurements had not been adequately addressed. Sev-

eral works had been published on the use of inexpensive proportional valves for velocity control; however, they retained the requirement of an external loop using displacement feedback.

It was determined that the "linearizing feedforward" approach employed in a number of these publications showed promise, however, the relationships governing the input/output characteristics of each component would need to be known with suitable precision if an approach of this type was to be feasible. Thus, the general configuration of the system was decided upon which achieved Research Goal #1. The remaining research goals addressed specific unknowns in its implementation and evaluation.

It was determined that a proportional valve would be used as the hydraulic control device to limit cost. This raised two challenges. The first was that the position of the valve must be controlled. The second was that the spool position is not necessarily proportional to the flow through the valve for all operating conditions.

With regard to the first challenge, the controller design of a particular valve is usually proprietary and the design of the primary stage and spool configuration varies with manufacturer. Therefore, the first step was to develop a controller for the valve spool which provided repeatable and predictable performance while maintaining portability for a range of valves. Extensive system identification was performed on a particular valve and the information gathered was used to develop a linear model of the valve which provided acceptable performance. This model was then used as the basis for a model reference controller which could be applied to any valve with sufficiently fast dynamics. This arrangement allowed for repeatable performance (within 2%) regardless of operating condition. This was considered to have achieved Research Goal #2.

Addressing the second challenge, experimental measurements for the pressure/flow characteristics of the valve allowed for the development of a novel modified turbulent orifice equation capable of "mapping" pressure and flow to valve displacement for a generic orifice. Being based on empirical measurements, the use of the modified

turbulent orifice equation eliminated the requirement for *a priori* knowledge of the valve geometry. However, it was necessary to develop a method by which the coefficients of the valve map could be altered to "fit" the equation to a given situation. This was done by implementing a nonlinear *Downhill Simplex Method* optimization routine.

The optimization routine was found to accurately fit the coefficients to the data within a small number of iterations. This allows for possible on-line adaptive updating that was not considered in this thesis. The development of the simplex routine combined with the modified turbulent orifice equation created a straightforward method of determining the pressure/flow relationship for a given valve which was considered to achieve Research Goal #3.

A first order solving routine was developed to find the inverse solution for the modified turbulent orifice equation. The use of this equation enabled the determination of the required valve spool displacement given a desired flow rate and an instantaneous differential pressure across the valve. The inverse modified turbulent orifice equation was combined with the valve spool model reference controller to create a single component pressure compensated flow controller. This accomplishment achieved Research Goal #4.

The kinematics of the robot were also solved. The analysis was verified experimentally, thereby achieving Research Goal #5.

Finally, the kinematics, model reference valve spool controller, and the modified turbulent orifice equation were combined to create the open loop linearizing feedforward velocity controller. The performance of the LFFC was evaluated. This controller was found to track a desired velocity within 10% for a range of velocities under variable load and supply conditions. It was also determined that, in ranges where the valve map was particularly accurate, the algorithm could maintain positional accuracy within a few percent for repeated motions over durations up to 30 seconds. This satisfied Research Goal #6.

6.2 Original Contributions

The original contributions of this research are summarized as follows.

The first contribution was the development and implementation of an empirical method for determining pressure/flow relationships for a generic valve. This included several key aspects. First, the general form of an equation capable of describing flows with variable flow regimes and orifice gradients which are nonlinear was developed. Second, this equation was coupled with a nonlinear optimization routine to tune the parameters based solely on system measurements. This approach is novel in that it is applicable to a wide range of valve spool configurations and requires no knowledge of the geometry of the orifice. It also has the advantage of describing a wide flow range with a single continuous differentiable equation which lends itself to online optimization to account for changes in valve characteristics with time.

The second contribution was the integration of a model reference controller and a feedforward linearizing function to create a single component flow control device. The inverse solution to the modified turbulent orifice equation using the first order solver made this approach simpler to implement in a real-time environment by using an ordinary differential equation solution rather than relying on variable step size root finding techniques. Furthermore, this approach may be implemented in any system using traditional velocity or position feedback to improve system repeatability and, potentially, performance.

The third contribution of this work was the integration of the flow controller with the kinematic equations to create a predictive velocity control system capable of operating in a load sensing environment in the presence of variable loading. This approach uses implicit feedback through the differential pressure measurements to account for both variations in load, changes in geometry and changes in supply pressure brought about by interaction with the load sensing system.

6.3 Conclusions

The research presented in this thesis was performed to answer the question of whether or not it is feasible to use a novel linearizing feedforward controller for the velocity control of a single link hydraulically actuated mechanism in the absence of direct feedback.

While the linearizing feedforward controller produced excellent velocity tracking characteristics for specific operating conditions, the performance was less than acceptable for others. Thus, it was concluded that this method is a feasible approach to velocity control only if:

1. The operating system on which it is to be applied has a very narrow range of operating conditions.
2. The system contains no nonlinear geometric transformations, or, a method by which the instantaneous position of the link can be measured for use by the velocity kinematic equations.
3. The pressure/flow characteristics of the valve over the operating range conform to the mathematical relationship described by the modified turbulent orifice equation with greater accuracy.

That having been said, it was also concluded that the linearizing feedforward approach has the potential for excellent response, disturbance rejection and repeatability when used as a single component pressure compensated flow control device.

6.4 Suggestions for Future Work

Several avenues for future study were revealed by the research contained in this thesis. Those avenues are discussed here.

The first avenue involves the control of the proportional valve. The method developed in this thesis overcame the nonlinearities inherent to the primary stage to provide repeatable control over a wide range of operating conditions. Improvements could be made to this method to reduce the steady state error brought about by the exclusion of an integrator in the reference model. The transient performance of the controller could also be improved to enhance the disturbance rejection characteristics of the overall system.

A second avenue for further study involves the valve mapping function. This function proved flexible in its ability to model a range of flows with one inflection. For more complex flows, however, there is insufficient mathematical capability to capture the pressure/flow/displacement characteristics. In many cases, it would be useful to have a more general function which would include more detail in the low flow regions.

A third avenue involves the optimization routine. As developed, optimization of the parameters used in the map occurs off-line. This does not need to be the case. Development and integration of an online parameter optimization routine would allow for real-time compensation for valve wear, component leakage, or temperature.

A fourth avenue is the integration of deadzone compensation to the motion of the spool. This would increase the potential positional accuracy of the control system.

A fifth avenue for study is the development of an indirect displacement measurement technique that could be utilized to compensate for drift present in any velocity control system. A technique which used the propagation time of reflected pressure pulses was investigated early in this research project. The method showed promise but it was determined to be outside the scope of this project and was not fully developed.

Finally, integration and *in situ* testing on a piece of mobile equipment should be conducted. As part of this study, performance comparison with full state feedback techniques should be performed.

References

[1] Cobo, M., Ingram, R., and Centikunt, S.. *Modeling, Identification, and Real-Time Control of a Bucket Hydraulic System for a Wheel Type Loader Earth Moving Equipment*, Mechatronics, 1998, pg. 863-885.

[2] Chen, P., Sun, Z., Mehlschau, T.T., Smith, N., and Frank, A.. *Development of a Remote Control System for a Front-End Loader*, Applied Engineering in Agriculture, 1996, pg. 623-631.

[3] Sepehri, N., Lawrence, P. D., Sassani, F., and Frenette, R.. *Resolved-Mode Teleoperation Control of Heavy-Duty Hydaulic Machines* , ASME Journal of Dynamic Systems, Measurement, and Control, V116, N2, 1994, pg. 232-240.

[4] Gholamreza, V., and Donath, M.. *Dynamic Feedback Linearization of Electro-hydraulically Actuated Control Systems*, ASME Journal of Dynamic Systems, Measurement, and Control, V117, 1995, pg. 468-477.

[5] Pietola, M.T. and Vilenius, M.J.. *Theoretical and Experimental Study of the Effect of Varying Load on the Dynamics of P, MRC, or P+PID/$\dot{x}$ Controlled Electrohydraulic Servosystem*, Proceedings of the IMECHE -Part C-, V203, 1989, pg. 267.

[6] Bu, F. and Yao, B.. *Adaptive Robust Precision Motion Control of Single-Rod Hydraulic Actuators with Time-Varying Unknown Inertia: A Case Study*, FPST, V6, 1999, pg. 131-138.

[7] Bu, F. and Yao, B.. *Nonlinear Adaptive Robust Control of Hydraulic Actuators Regulated by Proportional Directional Control Valves with Deadband and Nonlinear Flow Gains*, Proceedings of the ACC, V5, 2000, pg. 4129.

[8] Guenther, R., Cunha, M.A.B., Pieri, E.R., Negri, V.J.. *VS-ACC Applied to a Hydraulic Actuator*, Proceedings of the ACC, V6, 2000, pg. 4124-4128.

[9] Tafazoli, S., de Silva, C.W., and Lawrence, P.D.. *Tracking Control of an Electrohydraulic Manipulator in the Presence of Friction*, IEEE Transactions on Control Systems Technology, V6, N3, 1998, pg. 401.

[10] Edge, K. and de Almeida, G.. *Decentralized Adaptive Control of a Directly Driven Hydraulic Manipulator: Parts I and II, Theory and Experiment*, Proceedings of the IMECHE -Part I-, V209, 1995, pg. 191-206.

[11] Wang Qingfen, Gu Linyi, and Lu Yongxiang. *Research on Digital Control of Meter-in and Meter-out Independant Regulating for High Inertial Loads*, FPST, V6, 1999, pg. 109.

[12] Yang Cheng. *Application Study of the Electrohydaulic System for Hot Press of Wood-Based Panels*, Proceedings of the 3^{rd} International Symposium on Fluid Power, 1999, pg. 327.

[13] Dobchuk, J.W., Burton, R.T., Ukrainetz, P.R, Nikiforuk, P.N., and Huh, J.Y.. *Comparison of Several Flow Control Strategies of Proportional Valves*, Proceedings of the 5^{th} JFPS International Symposium on Fluid Power, 2002, pg. 763-768.

[14] Hu, H. and Zhang, Q.. *Multi-Function Realization Using an Integrated Programmable E/H Control Valve*, Applied Engineering in Agriculture, V19, N3, May 2003, pg. 283.

[15] Hermani, A. and Daneshmend, L.. *Force Analysis for Automation of the Loading Operation in a LHD-Loader*, Proceedings of the IEEE International Conference on Robotics and Automation, 1992, pg. 645.

[16] Jiing-Yih Lai and Yuan-Rong Chen. *Adaptive Flow Rate Control of a Hydraulic Proportional Valve*, JSME International Journal -Series 3-, V135, N4, 1992, pg. 582.

[17] Zavarehi, M. K., Lawrence, P. D., and Sassani, F.. *Nonlinear Modelling and Validation of Solenoid Controlled Pilot-Operated Servovalves*, IEEE/ASME Transactions on Mechatronics, V4, N3, Sept. 1999, pg. 324.

[18] Henri, P.D., Hollerbach, J.M., and Nahvi, A.. *An Analytical and Experimental Investigation of a Jet Pipe Controlled Electropneumatic Actuator*, IEEE Transactions on Robotics and Automation, V14, N4, August 1998, pg. 601.

[19] Prasetiawan, E, Zhang, R, and Alleyne, A.. *Fundamental Performance Limitations for a Class of Electronic Two-Stage Proportional Flow Valves*, Proceedings of the ACC, V6, 2001, pg. 3955.

[20] Viall, E. N., and Zhang, Q.. *Determining the Discharge Coefficient of a Spool Valve*, Proceedings of the ACC, V5, 2000, pg. 3600-3604.

[21] Merritt, H.E.. Hydraulic Control Systems. John Wiley & Sons, Ltd., New York, 1967.

[22] Wu, D., Burton, R.T. and Schoenau, G.. *An Empirical Discharge Coefficient Model for Orifice Flow*, International Journal of Fluid Power, V3, N3, 2002, pg. 13-18.

[23] Landau, Y., Adaptive Control: The Model Reference Approach. Marcel Dekker, Inc., New York, 1979.

[24] White, F.M.. Fluid Mechanics. McGraw-Hill, Inc., Toronto, 1986.

[25] *Product Information - Lubricants and Specialties, 4th Ed.* Imperial Oil Limited, 1980, pg. 117.

[26] Rosa, A.M.. *Internal Documents*, Fluid Power Group, University of Saskatchewan, 2000.

[27] Phillips, C.L. and Harbor, R.D.. Feedback Control Systems, Prentice-Hall Canada Inc., Toronto, 1991.

[28] Comparin, R.A., Glaettli, H.H., Mitchell, A.E. and Mueller, H.R.. *On the Limitations and Special Effects in Fluid Jet Amplifiers*, Symposium on Fluid Jet Control Devices, ASME, 1962, pg. 65.

[29] Reilly, R.J. and Moynihan, F.A.. *Notes on a Proportional Fluid Amplifier*, Symposium on Fluid Jet Control Devices, ASME, 1962, pg. 51.

[30] Nelder, J.A. and Mead, R.. *A Simplex Method for Function Minimization*, The Computer Journal, V7 I4, 1965, pg. 308-313.

[31] Andersson, J.. Multiobjective Optimization In Engineering Design: Applications to Fluid Power Systems, Linkoping University, Linkoping, Sweden, 2001.

[32] Ahlers, F.. *Internal Documents*, Fluid Power Group, University of Saskatchewan, 2004.

[33] Qian, W.. Neural Network Control of Non-linear Hydraulic System, M.Sc. Thesis, University of Saskatchewan, 1999.

Appendix A

Analysis of Forces on a Valve Spool

In the design process of a position control system it is necessary to understand the forces which the controller must overcome. In the analysis presented in this appendix the forces acting on a valve spool were examined. Of particular interest was the magnitude of the flow force relative to the other spool forces and whether they were negligible when considering the valve spool dynamic behaviour. This is a desirable situation as the flow forces depend on the geometry of the valve spool and the operating condition and significantly increases the complexity in modelling system dynamics.

A diagram of the lateral forces acting on the spool is shown in Figure A.1.

The spring force, F_{ks}, is a net reaction force from the return springs which attempt to keep the spool in its neural position. The flow force, F_{ff}, arises due to acceleration of fluid past the valve land. The force, F_{β}, results from viscous friction between the spool and the valve body. The control force, F_c, must compensate for these and the body forces which arise when the spool position is altered. Thus, the equation of motion for the spool can be written as,

$$m\ddot{x_v} + F_{\beta} + F_{ks} + F_{ff} = F_c, \tag{A.1}$$

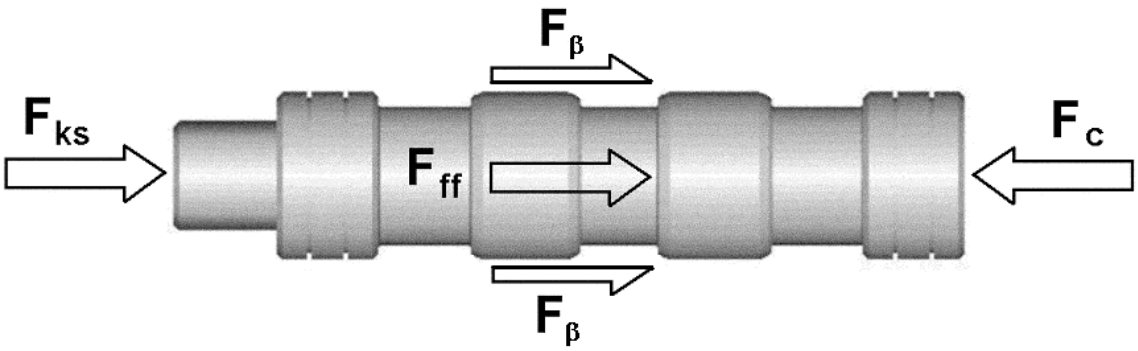

Figure A.1: Lateral forces acting on the valve spool in equilibrium.

where, x_v, is the valve spool displacement. The static forces, F_{ks} and F_β, are discussed first. The valve spool was held in place by a spring at either end. These springs opposed each other and acted to return the valve spool to its neutral position, $x_v = 0$, in the absence of a control signal.

$$F_{ks1} - F_{ks2} = F_{ks}. \tag{A.2}$$

Typically, the return springs are designed such that they operate in a linear manner over the range of motion of the spool and are matched in terms of their spring rates. To ensure the springs stayed in contact with the spool over the entire range of motion of the spool they were pre-compressed by some amount, $x_{precompression}$, thus,

$$F_{ks1} = k(x_{precompression} - x_v), \tag{A.3}$$

and,

$$F_{ks2} = k(x_{precompression} + x_v). \tag{A.4}$$

Combining Equations A.2, A.3 and A.4, yielded the following expression for the spring force:

$$F_{ks} = 2kx_v = k_{eff}x_v. \tag{A.5}$$

The spring constant, k_{eff}, is known from an analysis by Rosa [26] to be 3720 N. The maximum spool displacement is also known to be $x_{vmax} = 4\ mm$. Thus, it can be stated that the spring force varies linearly with spool displacement in the range -14.88 $N < F_{ks} <$ 14.88 N.

The issue of flow forces is discussed next. Fluid flowing from a region of high pressure to a region of low pressure will accelerate. This acceleration results in a localized pressure gradient measured at the valve land near the metering orifice. A graphical representation of this can be found in Merritt [21]. This region of low pressure creates a force imbalance on the spool, which according to Newton's law, must be equal to the mass of the accelerated fluid multiplied by its acceleration. This term was shown by Merritt to be:

$$F_j = \overbrace{\rho V}^{mass} \quad \overbrace{\frac{Q^2}{A_2 V}}^{acceleration} \quad , \tag{A.6}$$

where:

$$\begin{aligned} \rho &= \text{fluid density,} \\ Q &= \text{volumetric flow rate, } and \\ A_2 &= \text{area of the vena contracta.} \end{aligned}$$

This may be simplified to,

$$F_j = \frac{\rho Q^2}{A_2}. \tag{A.7}$$

This force is applied along the long axis of the jet. If the angle between the lateral axis and the long axis of the jet is termed, θ, then the lateral component of this force (which is referred to as simply "the flow force") is,

$$F_{jaxial} = F_{ff} = cos(\theta)\frac{\rho Q^2}{A_2}. \tag{A.8}$$

From Equation A.8 it can be seen that the flow force is maximized when $\frac{Q^2}{A_2}$ is maximized for constant fluid density and jet angle. Since the turbulent orifice equation states that Q is a linear function of A_2, it can be said that the maximum flow forces occurred at the maximum flow rate. For the range of flow rates involved in this study this was 0.0003 $\frac{m^3}{s}$. The minimum spool displacement with which this flow rate was obtained in the differential pressure range examined in this study was $x_v = 1.8\ mm$. If the valve spool is assumed to be sharp edged, then the area of the vena contracta can be roughly approximated by,

$$A_2 = C_c A = C_c \overbrace{2\pi r x_v}^{orifice\ area}, \tag{A.9}$$

where A is the opening area between the valve spool and the valve land, r is the radius of the spool, and C_c is the contraction coefficient for the vena contracta. The contraction coefficient was assumed to be 0.611 [21] and the spool radius was measured to be 9 mm. Thus, the maximum flow force from Equation A.8 is approximately 0.6 N for a jet angle of 63° [21] and a fluid density of 912 $\frac{kg}{m^3}$. Comparing this flow force to the spring force indicated that the flow force was of negligible amplitude.

The dynamic forces are discussed next. These forces dictate the characteristics of the spool motion. Dynamic flow forces were not considered. The mass of the spool was found to be 0.2174 kg and the coefficient of viscous friction was found by Rosa [26] to be 162 $\frac{Ns}{m}$. The relative value of the forces generated from acceleration and viscous friction when a step input in force was applied to the valve spool was studied in simulation. The simulation block diagram as realized in MATLAB/Simulink® is shown in Figure A.2.

A step input in force was applied to the system in Figure A.2 with the resulting step response and component forces shown in Figure A.3.

It is clear from Figure A.3 that the viscous friction dominates the system. In fact, it was found that the value found by Rosa and used in this analysis was less than the

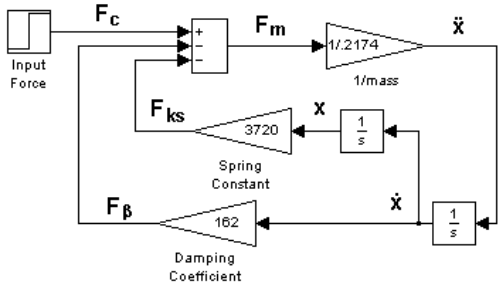

Figure A.2: Simulation used to evaluate dynamic forces.

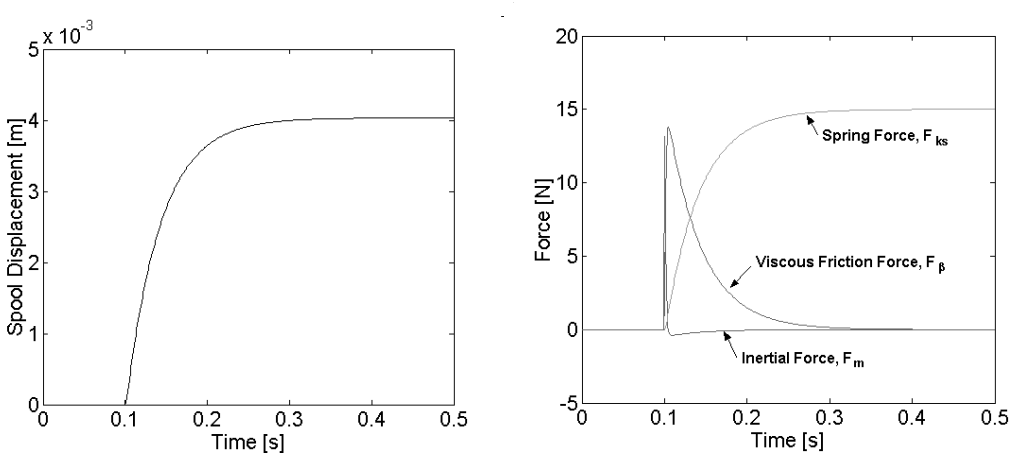

Figure A.3: (Left) Position response to step input in force of 15 N. (Right) Inertial, viscous, and spring forces.

actual value found experimentally. The reasons for this are discussed in Appendix B.

A.1 Concluding Comments

The steady state flow force for the range of flow rates used in this research are comparatively small relative to the spring force. Therefore, in the analysis of the dynamic characteristics of the valve, it could be neglected. Also, it was found that the viscous forces dominate the system dynamics and the determination of the correct value for the damping coefficient is imperative to the accurate modelling of the valve spool motion.

Appendix B

Analysis of Hydraulic Resistance in Pilot Lines

The analysis in this appendix was performed to determine if the pilot lines on the main stage could be the cause of a damping coefficient that was experimentally measured and found to be substantially higher than reported by Rosa [26]. It was postulated that Rosa had accounted for viscous damping of the spool only in his analysis and did not include the effect of pilot lines. Figure B.1 shows the valve spool with the restrictive pilot lines.

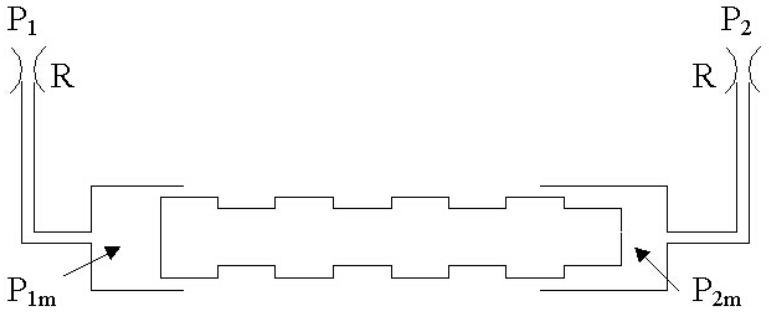

Figure B.1: Schematic of the spool with restricting orifices.

The equation of motion was determined for a system by modelling the pilot lines as

hydraulic restrictions.

$$m\ddot{x_v} + \left(\beta + 2RA_p^2\right)\dot{x_v} + kx_v = A_p\left(P_1 - P_2\right). \tag{B.1}$$

The damping coefficient was redefined as:

$$\beta^* = \beta + 2RA_p^2. \tag{B.2}$$

By combining Equations B.1 and B.2 and performing a Laplace transform on the result, the following was obtained:

$$\frac{X}{P_1 - P_2} = \frac{Ap}{ms^2 + \beta^* s + k}. \tag{B.3}$$

Given that the system appeared heavily overdamped when experimental step responses were examined, a time constant determined from those step responses was a good approximation of the dominant pole. Thus, the combined damping coefficient can be determined from the characteristic equation given in Equation B.3,

$$s_{1,2} = \frac{-\beta^* \pm \sqrt{\beta^{*2} - 4mk}}{2m}. \tag{B.4}$$

Using the experimentally determined values of $\tau = 5\ s$, $m = 0.2174\ kg$, and $k = 3720\ \frac{N}{m}$, Equation B.4 reduced to,

$$-0.08696 = -\beta^* \pm \sqrt{\beta^{*2} - 3235} \tag{B.5}$$

Only the positive case produced a non-imaginary solution with the result $\beta^* = 18600$. Then, the hydraulic resistance component of damping coefficient was determined by subtracting from β^*, the viscous friction found by Rosa,

$$2RA_p^2 = 18600 - 162 = 18438. \tag{B.6}$$

The piston area was calculated to be $2.54 \times 10^{-}4\ m^2$ and thus, from Equation B.6 the restriction was determined to be $R = 14.2 \times 10^{10}\ \frac{Pa\,s}{m^3}$. The laminar flow relationship through an orifice was described by Merritt as,

$$Q = \frac{2\delta^2 D_h A_o}{\mu}\Delta P, \tag{B.7}$$

or,

$$R_m = \frac{\mu}{2\delta^2 D_h A_o}. \tag{B.8}$$

where:

$$\begin{aligned} \delta &= \text{geometry dependant discharge coefficient,} \\ D_h &= \text{hydraulic diameter,} \\ A_o &= \text{orifice diameter,} \, and \\ \mu &= \text{absolute viscosity.} \end{aligned}$$

The restricting orifice was assumed to be the primary stage receiving port which is square with sides 0.5 mm long. This gave values of $D_h = 0.5\ mm$ and $A_o = .25\ mm^2$. The viscosity for the oil used was $\mu = 0.15\ \frac{Ns}{m^2}$ [25]. Substituting these values into Equation B.8 reduced that equation to:

$$R_m = \frac{6 \times 10^8}{\delta^2}. \tag{B.9}$$

Merritt is vague on the appropriate value of δ for a given orifice geometry. A value of $\delta = 0.157$ for a sharp edged slit orifice is listed. From Equation B.9 the hydraulic resistance was calculated to be $R_m = 6 \times 10^10$ at $\delta = 0.1$ and $R_m = 24 \times 10^10$ at $\delta = 0.05$.

B.1 Concluding Comments

The values determined theoretically for the hydraulic resistance bracketed those determined from experimental measurements and indicated that hydraulic resistance in the pilot lines was responsible for the increase in the damping coefficient.

Appendix C

Listing of the Optimization Code

This section contains a listing of the MATLAB® used to implement the simplex optimization routine.

```
%This file optimizes a flow estimate equation
%It was written by Jeff Dobchuk in Sept 2003
%%%%%%%%%%%%%%%%%%%%%%%%%%%%%%%%%%%%%%%%%%%%%%%%%%%%%%%%%%%%%%%%
%Now check for a starting vector in the workspace
%%%%%%%%%%%%%%%%%%%%%%%%%%%%%%%%%%%%%%%%%%%%%%%%%%%%%%%%%%%%%%%%
cexist = input('have you placed a starting vector, C0, in the workspace? [y/n]','s');
cexist = strcmp(cexist,'y');
if cexist == 0
    disp('you should')
    stop
else
    global N
    N=length(C0);
    L=zeros(N+1,1);
    disp(['good, I detect ', num2str(N), ' variables to be optimized'])
end
%%%%%%%%%%%%%%%%%%%%%%%%%%%%%%%%%%%%%%%%%%%%%%%%%%%%%%%%%%%%%%%%
%Now we must load our test data set
%%%%%%%%%%%%%%%%%%%%%%%%%%%%%%%%%%%%%%%%%%%%%%%%%%%%%%%%%%%%%%%%
%LoadData
%%%%%%%%%%%%%%%%%%%%%%%%%%%%%%%%%%%%%%%%%%%%%%%%%%%%%%%%%%%%%%%%
%Now create a matrix which holds the initial starting
%values and N variations on the starting values, where:
%N=the number of parameters.
%%%%%%%%%%%%%%%%%%%%%%%%%%%%%%%%%%%%%%%%%%%%%%%%%%%%%%%%%%%%%%%%
for h=1:300
for q=-3:2
for i=1:N+1
    P(:,i)=C0;
end
```

```
%Now change one value per column vector by Lambda
Lambda=.0005*(q/abs(q));
for i=2:N+1
%
P(i-1,i)=P(i-1,i)+Lambda*P(i-1,i);
%P(i-1,i)=P(i-1,i)+1e-10;
end
%%%%%%%%%%%%%%%%%%%%%%%%%%%%%%%%%%%%%%%%%%%%%%%%%%%%%%%%%%%%%%%%%%%%%%%
%Now find the sum squared error for the initial matrix
%%%%%%%%%%%%%%%%%%%%%%%%%%%%%%%%%%%%%%%%%%%%%%%%%%%%%%%%%%%%%%%%%%%%%%%
for f=1:N+1
    reevalindex=f;
    j=length(Flow);
    L(reevalindex,1)=0;
    for i=1:j
        IE=(Flow(i)-((((P(1,reevalindex)+P(2,reevalindex)*exp(P(3,reevalindex)...
            *Displacement(i)))*Pressure(i))+(P(4,reevalindex)+P(5,reevalindex)...
            *exp(P(6,reevalindex)*Displacement(i))))*(Displacement(i)...
            *sqrt(Pressure(i)))))^2;
        L(reevalindex,1)=L(reevalindex,1)+IE;
    end
end
for d=1:2
%%%%%%%%%%%%%%%%%%%%%%%%%%%%%%%%%%%%%%%%%%%%%%%%%%%%%%%%%%%%%%%%%%%%%%%
%Now find the indices of the highest and lowest
%%%%%%%%%%%%%%%%%%%%%%%%%%%%%%%%%%%%%%%%%%%%%%%%%%%%%%%%%%%%%%%%%%%%%%%
HighIndex=0;
[MaxSSE,HighIndex]=max(L);
[Max2SSE,NextHighIndex]=max([L(1:HighIndex-1);0;L((HighIndex+1):length(L))]);
[MinSSE,LowIndex]=min(L);
%%%%%%%%%%%%%%%%%%%%%%%%%%%%%%%%%%%%%%%%%%%%%%%%%%%%%%%%%%%%%%%%%%%%%%%
%Now find the centroid of the face opposite the highest value
%%%%%%%%%%%%%%%%%%%%%%%%%%%%%%%%%%%%%%%%%%%%%%%%%%%%%%%%%%%%%%%%%%%%%%%
CAve=zeros(N,1);
for x=1:N
        CAve(x)=mean(P(x,:));
end
AveWorst=P(:,HighIndex)/(N+1);
Ccent=CAve-AveWorst;
```

```
%%%%%%%%%%%%%%%%%%%%%%%%%%%%%%%%%%%%%%%%%%%%%%%%%%%%%%%%%%%%%%%%%%%%%%%
%Now find the direction vector from the worst vertex to the
%centroid the extrapolate to the other side of the simplex
%%%%%%%%%%%%%%%%%%%%%%%%%%%%%%%%%%%%%%%%%%%%%%%%%%%%%%%%%%%%%%%%%%%%%%%
DirVec=Ccent-P(:,HighIndex);
alpha=2;
Ctryl=P(:,HighIndex)+alpha*DirVec;
%%%%%%%%%%%%%%%%%%%%%%%%%%%%%%%%%%%%%%%%%%%%%%%%%%%%%%%%%%%%%%%%%%%%%%%
%Now evaluate the error at this new point
%%%%%%%%%%%%%%%%%%%%%%%%%%%%%%%%%%%%%%%%%%%%%%%%%%%%%%%%%%%%%%%%%%%%%%%
j=length(Flow);
Ltryl=0;
reevalindex=1;
for i=1:j
        IE=(Flow(i)-((((Ctryl(1,reevalindex)+Ctryl(2,reevalindex)*exp(Ctryl...
            (3,reevalindex)*Displacement(i)))*Pressure(i))+(Ctryl(4,reevalindex)...
            +Ctryl(5,reevalindex)*exp(Ctryl(6,reevalindex)*Displacement(i))))...
            *(Displacement(i)*sqrt(Pressure(i)))))^2;
        Ltryl=Ltryl+IE;
end
if Ltryl < L(HighIndex)
    P(:,HighIndex)=Ctryl;
    L(HighIndex)=Ltryl;
    disp('keep extrapolation')
elseif Ltryl > L(HighIndex)
    alpha=.5;
    Ctry2=P(:,HighIndex)+alpha*DirVec;
    j=length(Flow);
    Ltry2=0;
    reevalindex=1;
    for i=1:j
        IE=(Flow(i)-((((Ctry2(1,reevalindex)+Ctry2(2,reevalindex)*exp(Ctry2...
            (3,reevalindex)*Displacement(i)))*Pressure(i))+(Ctry2(4,reevalindex)...
            +Ctry2(5,reevalindex)*exp(Ctry2(6,reevalindex)*Displacement(i))))...
            *(Displacement(i)*sqrt(Pressure(i)))))^2;
        Ltry2=Ltry2+IE;
    end
```

```
    if Ltry2 >= L(HighIndex)
        for s=1:N+1
            if s ~= LowIndex
                for r=1:N
                    P(r,s)=(P(r,s)+P(r,LowIndex))/2;
                    for f=1:N+1
                        reevalindex=f;
                        j=length(Flow);
                        L(reevalindex,1)=0;
                        for i=1:j
                            IE=(Flow(i)-((((P(1,reevalindex)+P(2,reevalindex)...
                                *exp(P(3,reevalindex)*Displacement(i)))*Pressure(i))...
                                +(P(4,reevalindex)+P(5,reevalindex)*exp(P(6,reevalindex)...
                                *Displacement(i))))*(Displacement(i)*sqrt(Pressure(i)))))^2;
                            L(reevalindex,1)=L(reevalindex,1)+IE;
                        end
                    end
                end
            end
        end
        disp('contracted around best')
    else
        P(:,HighIndex)=Ctry2;
        L(HighIndex)=Ltry2;
        disp('try 2 was better than the worst')
    end
else
    disp('done')
    break
end
end
[MinSSE,LowIndex]=min(L);
C0=P(:,LowIndex);
L
end
end
```

Appendix D

Times Series and %RSRE for Static Flow Tests

This appendix is a compelation of the time series and %RSRE for the tests used to establish the zone of confidence.

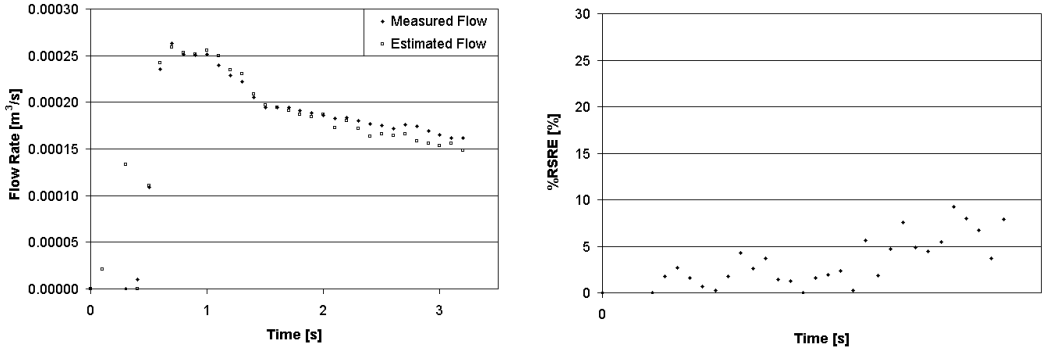

Figure D.1: (Left) Measured and estimated flow rates in zone #1. (Right) %RSRE of the flow rate.

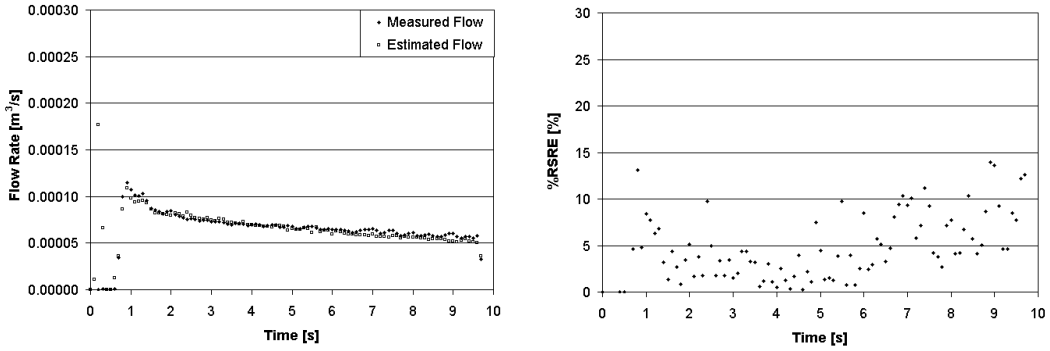

Figure D.2: (Left) Measured and estimated flow rates in zone #2. (Right) %RSRE of the flow rate.

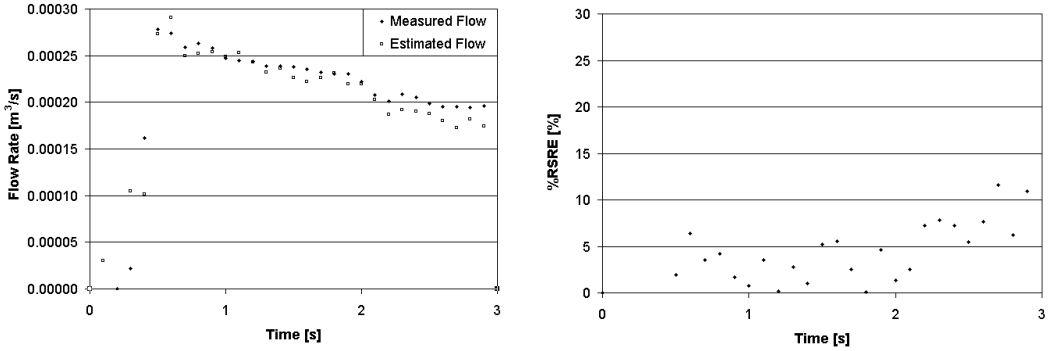

Figure D.3: (Left) Measured and estimated flow rates in zone #3. (Right) %RSRE of the flow rate.

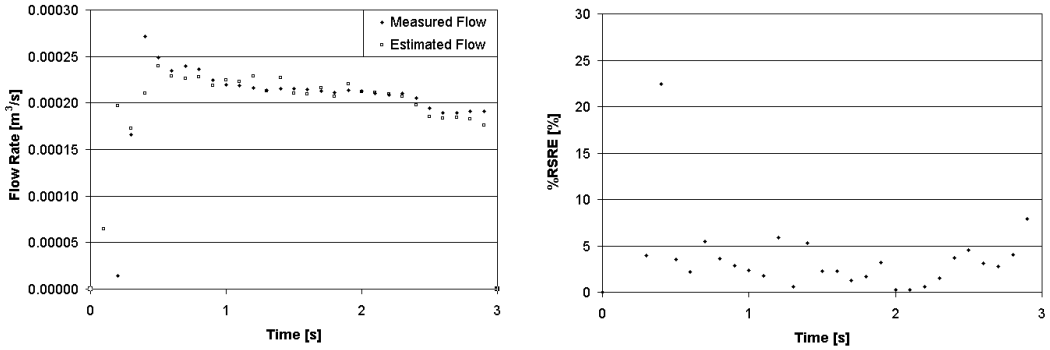

Figure D.4: (Left) Measured and estimated flow rates in zone #4. (Right) %RSRE of the flow rate.

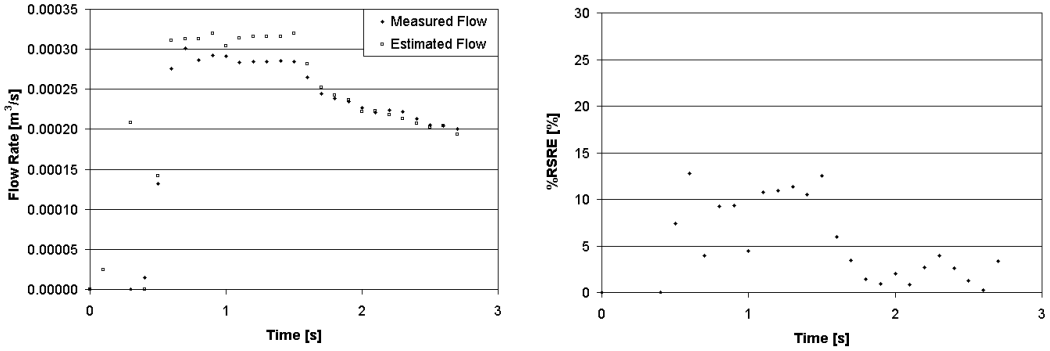

Figure D.5: (Left) Measured and estimated flow rates in zone #5. (Right) %RSRE of the flow rate.

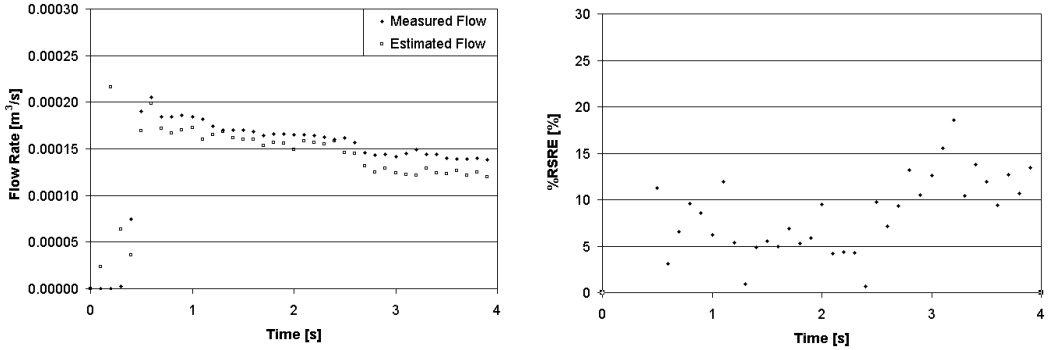

Figure D.6: (Left) Measured and estimated flow rates in zone #6. (Right) %RSRE of the flow rate.

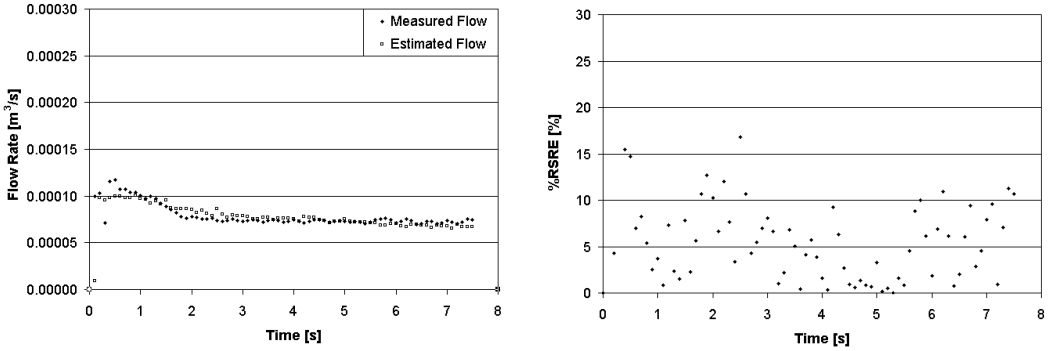

Figure D.7: (Left) Measured and estimated flow rates in zone #7. (Right) %RSRE of the flow rate.

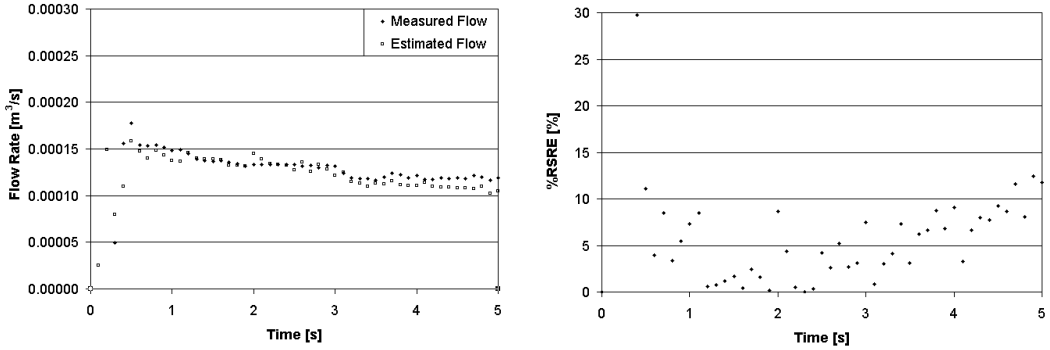

Figure D.8: (Left) Measured and estimated flow rates in zone #8. (Right) %RSRE of the flow rate.

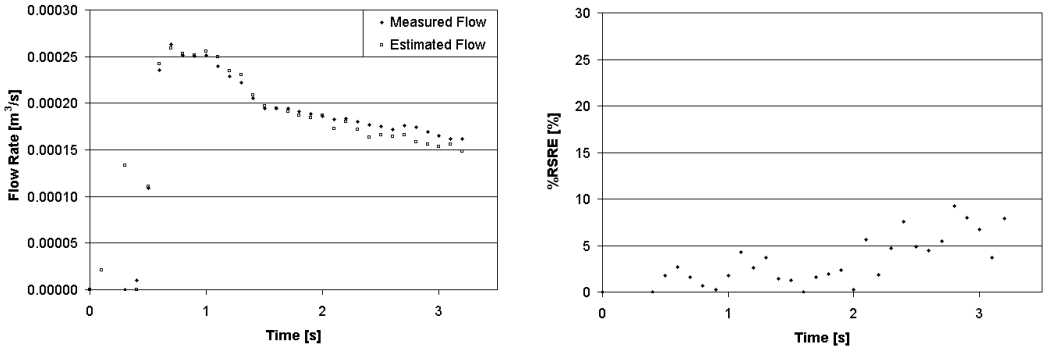

Figure D.9: (Left) Measured and estimated flow rates in zone #9. (Right) %RSRE of the flow rate.